Manganese Clusters with Relevance to Photosystem II

Sumitra Mukhopadhyay,[†] Sanjay K. Mandal,[‡] Sumit Bhaduri,[§] and William H. Armstrong*[,†]

Department of Chemistry, Eugene F. Merkert Chemistry Center, Boston College, 2609 Beacon Street, Chestnut Hill, Massachusetts 02467-3860, Dow Corning Corporation, 2200 West Salzburg Road, Midland, Michigan 48686, and Department of Chemistry and Chemical Biology, Harvard University, 12 Oxford Street, Cambridge, Massachusetts 02138

Received December 10, 2003

Contents

1. Introduction

A tetramanganese cluster (Mn_4) resides at the active site of photosystem II (PSII) in green plants and in certain bacteria and algae. It catalyzes the light-driven water oxidation reaction to generate dioxygen.[1] This is an energetically demanding and complex redox process that holds the key to the survival of life on earth. The proposed catalytic cycle (also known as the Kok cycle) that carries out this four-electron oxidation process is composed of five intermediate states designated as "S_i" states (where $i = 0-4$, see Figure 1).[2,3] This scheme has furnished a seminal scaffold that has stood the test of time. The S_0 to S_3 states can be resolved kinetically while the transient S_4 state is rapidly reduced to the S_0 state with the release of O_2. The S_1 state is thermally most stable in the dark and is thus referred to as the dark-adapted state. However, an understanding of the mechanistic details regarding this catalytic process is greatly hindered due to the absence of precise structural information of the enzyme and the inability to detect any key reaction intermediates. Initially, the structural information on the architecture of the water oxidase (WO) was provided by electron microscopy of active PSII membranes at 15−30 Å resolution[4,5] and by electron crystallography on two- and three-dimensional PSII fragments lacking water oxidizing activity at 8 Å resolution.[6,7] However, very recently, X-ray crystal structures of dark-adapted active PSII membranes have been reported at ∼3.5−3.8 Å resolution.[8−10] The structures are informative regarding the arrangement of protein subunits and the various cofactors but fail to deliver critical insights regarding the exact orientation and structure of the manganese cluster and the immediate ligand environment beyond reasonable doubt. Furthermore, the structures of the less accessible S states (S_2, S_3, and S_0) have not been addressed.

In the absence of sufficient crystallographic information, the Mn_4 structure of WO has been conjectured with the aid of spectroscopic methods, most commonly X-ray absorption (XAS) and electron paramagnetic resonance (EPR) techniques.[11,12] On the basis of findings from these studies and an analysis of manganese oxide mineral structures, several possible arrangements comprised of oxo-bridged dinuclear and trinuclear building blocks have been proposed for the PSII Mn_4 cluster (a few of them are shown in Scheme 1).[13] Many of the current endeavors in obtaining a suitable structural model for the WO active site engage synthesis and characterization of dinuclear, trinuclear, and tetranuclear complexes. Although these synthetic complexes have aided greatly in comprehending the properties of the native Mn_4 cluster, none demonstrates exact structural and/or all spectroscopic features akin to those of the enzyme active site. Nevertheless, achieving a synthetic analogue of the PSII active site that possesses functional activity remains one of the greatest challenges in the field of bioinorganic chemistry. Thus, the synthesis of high-valent oxo-bridged multinuclear manganese clusters with varied nuclearity continues to be the

* To whom correspondence should be addressed. E-mail: armstwi@bc.edu.
[†] Boston College.
[‡] Dow Corning Corporation.
[§] Harvard University.

10.1021/cr0206014 CCC: $48.50
Published on Web 09/08/2004

Sumitra Mukhopadhyay, a native of Calcutta, India, received her B.Sc. (with Honors, in 1995) and M.Sc. (in 1997) degrees in Chemistry from Presidency College, Calcutta, and Indian Institute of Technology, Kanpur, respectively. She completed her Ph.D. in Chemistry from Boston College in 2002 under the supervision of Prof. William H. Armstrong. She is presently pursuing her postdoctoral research with Prof. Stephen J. Lippard at Massachusetts Institute of Technology. Her current work focuses on the design and synthesis of specific platinum-peptide conjugates as anticancer agents to target the angiogenic tumor blood vessels.

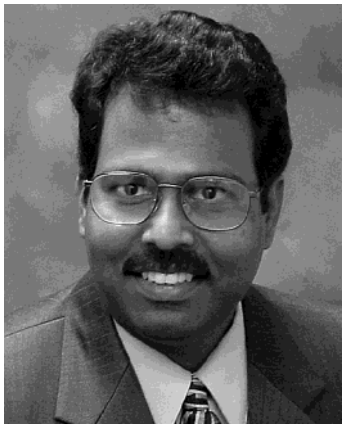

Sanjay K. Mandal currently holds a Technology Leader position in the Electronics Industry of Dow Corning Corporation, Midland, MI. Prior to joining Dow Corning Corporation in 2001, he has worked with Occidental Chemical Corporation, Grand Island, NY, and General Electric Company, Mt. Vernon, IN. He received a B.Sc. (with Honors) in Chemistry from the University of Calcutta, Calcutta, India, in 1986, and a M.Sc. in Chemistry from the Indian Institute of Technology, Kanpur, India, in 1988. He then chose to pursue graduate studies in the United States and earned a Ph.D. in Chemistry (1992) for research work under the direction of Professor F. Albert Cotton at Texas A&M University, College Station, TX. His research interests are broad, extending across inorganic and organic chemistry, with an emphasis on process innovation and improvement and product development for pharmaceutical intermediates, electronic materials, and specialty chemicals. In 1998 he received Occidental Chemical Corporation's Publication of the Year Award. His scholastic achievements included a Robert A. Welch Foundation Pre-doctoral Fellowship by Texas A&M University (1989–1992), a Merit Scholarship by R. K. Mission R. College, India (1984–88), an MCM Scholarship by Indian Institute of Technology, Kanpur, India (1986–1988), and a National Scholarship by the Government of India (1981–1986).

center of activity in this field. This article will review the synthesis and properties of biologically relevant dinuclear, trinuclear, and tetranuclear manganese complexes reported during the period 1975−2003 with emphasis on recently developed systems that have direct and/or indirect implications toward the PSII water oxidase. In addition, this review will provide brief discussions on the spectroscopic properties of the PSII Mn_4 cluster and proposed mechanistic

Sumit Bhaduri was born in Calcutta, India. He did his undergraduate studies in Chemistry (with Honors) at Presidency College, under University of Calcutta, and graduated in 1995. He received his M.Sc. degree from Indian Institute of Technology, Kanpur, in 1997. He then moved on to the United States to do graduate research in Inorganic Chemistry at Indiana University, Bloomington, under the guidance of Prof. George Christou. His doctoral work highlighted the role of manganese in Bioinorganic Chemistry as pertinent to the water oxidase active site. He also was involved in the synthesis of manganese clusters that showed single-molecule magnetism behavior at low temperatures. He is presently a Postdoctoral Associate in the research group of Prof. Richard H. Holm at Harvard University. His current research interests include synthesis of peptide-based ligands for the construction of bridged biological assemblies.

William H. Armstrong was born in Portchester, NY, in 1954 and grew up in the suburbs of New York City and Kansas City. He graduated from Bucknell University in 1976 with a B.S. degree and went on to receive a Ph.D. in Chemistry from Stanford University in 1982 under the guidance of Professor Richard H. Holm. Immediately thereafter he joined the research group of Professor Stephen J. Lippard at Columbia University. Completing his postdoctoral studies at the Massachusetts Institute of Technology, he joined the faculty at the University of California, Berkeley, in 1985. Since 1992, he has been a member of the Chemistry faculty at Boston College in Chestnut Hill, MA. His research efforts have been primarily directed toward the synthesis of inorganic complexes that mimic enzymes that contain two or more active site metal ions.

aspects of oxygen evolution that have been reviewed in detail elsewhere.[1,14−19]

2. Tetramanganese Cluster in Photosystem II

2.1. Composition of Photosystem II

Photosystem II (PSII) is a multi-subunit protein complex embedded in the thylakoid membrane of green plants, cyanobacteria, and algae. This protein is composed of 14 membrane-spanning subunits, three membrane-extrinsic subunits, and more than

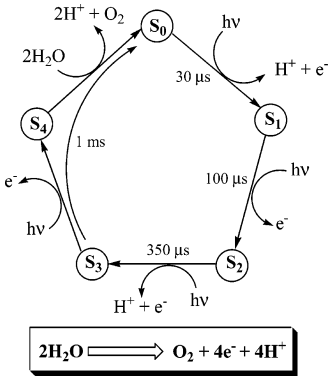

Figure 1. Mechanistic cycle (commonly referred to as the Kok catalytic cycle) for water oxidation in the photosystem II (PSII) active site.[2,3,19]

Scheme 1. Proposed PSII Mn_4 Structures (Adapted from Refs 12 and 13)

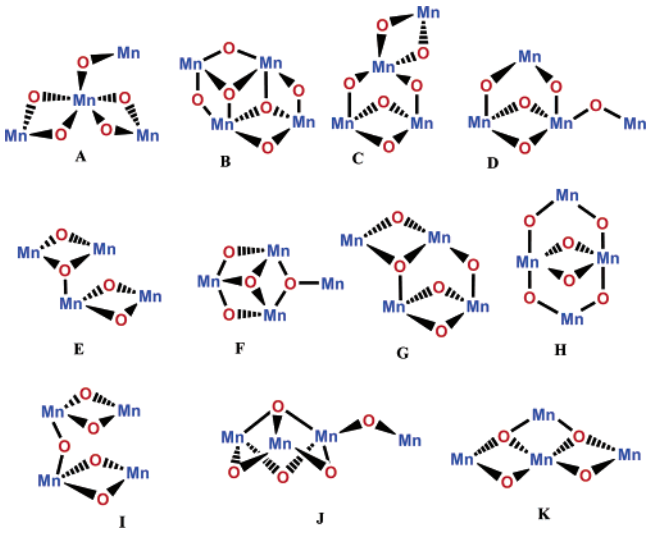

40 cofactors including the Mn_4 cluster, chlorophylls, Fe^{2+}, carotenoids, plastoquinones, and Ca^{2+} and Cl^- ions, with a total mass of about 320 kDa. A schematic diagram of PSII subunits is shown in Figure 2. The membrane-intrinsic part of PSII comprises D1 and D2 reaction center proteins of about 38 kDa each, the chlorophyll-containing inner-antenna subunits CP43 and CP47, α- and *β*-subunits of cytochrome *b*-559, and a few other smaller subunits. The membrane-extrinsic part containing cytochrome *c*-550 and 12-kDa and 33-kDa proteins is located at the lumenal side of the PSII of cyanobacteria and eukaryotic red algae. In higher plants and green algae, two other extrinsic subunits, 24-kDa and 17-kDa polypeptides, are present instead of the 12-kDa subunit and cytochrome *c*-550.[19,20] These subunits have been shown to affect magnetic interactions within the PSII manganese cluster (see below), as illustrated by spectroscopic data.[21,22]

In PSII reaction centers electron transfer initiates with the photoexcitation of P680, a special chlorophyll *a* (Chl *a*), coordinated to D1-His-198, forming P680*, which then undergoes charge-separation by transferring an electron to plastoquinones Q_A and Q_B via pheophytin (Pheo). A non-heme Fe^{2+} is located between Q_A and Q_B. These components are collectively referred to as the acceptor side of PSII. The

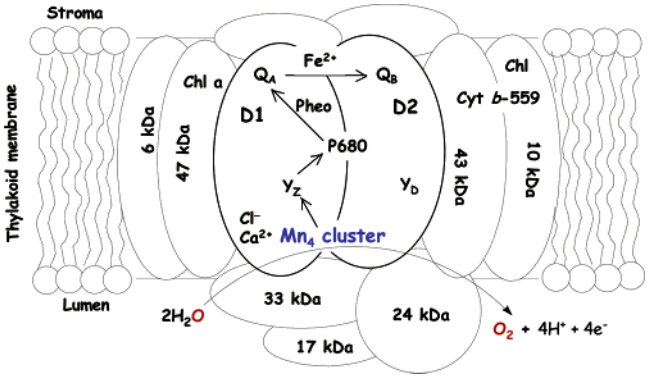

Figure 2. Composition of photosystem II (PSII) in the thylakoid membranes of higher plants and green algae (Adapted from refs 14 and 15). The arrows indicate the direction of the electron transfer that occurs in PSII. The electrons are transferred from P680 to the primary and secondary quinones, Q_A and Q_B, through pheophytin (Pheo). Electrons are then transferred from the Mn_4 cluster to P680 via the redox-active tyrosine, Y_Z. D1 and D2 polypeptides are the reaction center proteins that provide ligations to the Mn_4 cluster and the Ca^{2+} cofactor. CP43 and CP47 are the chlorophyll-containing inner-antenna subunits, and the cytochrome b-559 polypeptide is a heterodimer consisting of α- and *β*-subunits. The 17-, 24-, and 33-kDa extrinsic polypeptides are at the lumenal side of the membrane and critical for the stabilization of the Mn_4 cluster.

donor side of PSII consists of the Mn_4 cluster and a redox-active tyrosine residue D1-Tyr-161 (Y_Z). $P680^+$ is reduced by extracting electrons from Mn_4 via Y_Z. The resulting oxidized manganese cluster then withdraws electrons from water, generating molecular oxygen in the process. The protons liberated in this process contribute to a proton gradient across the thylakoid membrane, essential for ATP synthesis. Another tyrosine residue Y_D, D2-Tyr-160, symmetrically related to Y_Z, does not take part in this electron-transfer process.[14,23]

The Mn_4 cluster, bound at the lumenal side of PSII, is believed to be protected by the three extrinsic subunits, mainly the 33-kDa polypeptide, which is referred to as the "manganese stabilizing protein" or MSP.[22] Removal of either of the 33-kDa subunit or Ca^{2+} or Cl^- cofactor ions results in the termination of the water oxidation process. Andréasson and co-workers demonstrated that the photosynthetic oxygen evolution could take place in the absence of chloride at significant rates (up to ∼50% of that observed in the presence of Cl^-).[24] On the basis of their results, they proposed that Cl^- together with lysine side chains and other charged amino acids maintains a proton-relay network, which allows the transport and release of protons from the water oxidation reaction. They suggest that different methods of Cl^- depletion can cause a severe perturbation of this network with complete or partial loss of water oxidation activity.

2.2. Recent Crystallographic Studies

The lack of adequate crystallographic data of the PSII reaction center has been a long-standing obstacle in gaining structural and mechanistic insights regarding the oxygen evolving biocatalytic process.[19] However, a recent breakthrough in obtaining suitable

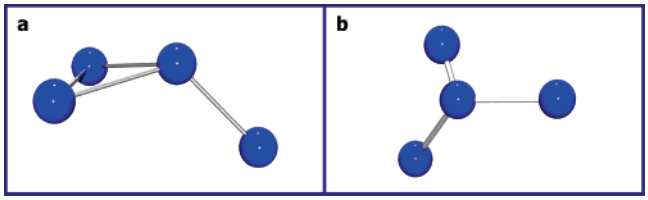

Figure 3. Spatial arrangements of the PSII Mn_4 cluster in *T. elongatus* as shown in the crystal structures (a) at a resolution of 3.8 Å[8] and (b) at a resolution of 3.7 Å.[9]

structural information has been attained from the crystal data by Zouni et al. on *Synechococcus elongates*, also referred to as *Thermosynechococcus elongates*, at a resolution of 3.8 Å and by Kamiya et al. on *Thermosynechococcus vulcanus* at 3.7 Å resolution.[8,9]

The 3.8 Å resolution structure was built as a Cα model. PSII was shown to be a homodimer in the asymmetric unit, with the longest dimensions of the membrane integral part measuring 190 × 100 Å^2. The two monomers in the dimer are related by a C_2 rotational axis perpendicular to the membrane plane. A total of 36 transmembrane helices were found, 22 of which were assigned to CP47, CP43, D1, and D2, and the rest were attributed to smaller subunits including the α- and β-subunits of cytochrome *b*-559. In addition, two of the three extrinsic proteins, the 33-kDa polypeptide and cytochrome *c*-550, were located.

Electron density contoured at 5σ with dimensions of 6.8 × 4.9 × 3.3 Å^3, observed at the lumenal side of the D1 subunit, was assigned to the Mn_4 cluster. Three Mn atoms were positioned roughly at three corners of an isosceles triangle, and the fourth Mn was placed at the center of the triangle, protruding toward the lumenal surface of the membrane (see Figure 3a). The Mn···Mn interatomic distances were deduced to be ∼3.0 Å. Electron density found at ∼7.0 Å away from the manganese cluster was assigned to the redox-active Y_Z residue. A corresponding electron density at helix C in D2, related to Y_Z by the pseudo-C_2 axis, was attributed to the redox-inactive residue Y_D. The essential cofactors Ca^{2+} and Cl^- were not located in this structure, however.

In addition to the above-stated findings, the 12-kDa extrinsic protein subunit was located in the 3.7 Å resolution crystal structure.[9] The shape of the Mn_4 unit was shown to be very similar to that of the previously reported structure; however, in this case, all four Mn ions were found to be roughly coplanar (Figure 3b). These data provide additional information relating to the coordination environment of the Mn centers. At least four to five bonding interactions between the Mn cluster and the D1 polypeptide were established. The C-terminal group of Ala-344 is directly ligated to the cluster, which is in agreement with mutagenesis experiments (see section 2.5). Several other residues, including Asp-170, Glu-333 (or His-332), His-337, and Asp-189 (or His-190), were also identified as possible ligation sites for the Mn cluster. However, neither Ca^{2+} nor Cl^- ions were located in this structure.

After the submission of this review, a crystal structure of *T. elongates* at 3.5 Å resolution by Ferreira et al. was reported.[10] In this case the X-ray resolution is only marginally improved compared to the cases of the aforementioned studies. However, a dramatically different geometry of the active site, involving a Mn_3CaO_4 cubane-like core, has been postulated despite a close resemblance in the location and shape of the electron densities to that obtained in the previous two crystal structures. In this structural model the fourth Mn ion has been proposed to be linked to the Mn_3CaO_4 cube by a mono-oxo bridge. In conclusion, a much higher resolution structure of the WO active site is required to determine unambiguously the geometry of the Mn_4Ca cluster responsible for catalysis.

2.3. X-ray Absorption Studies

In the absence of single-crystal X-ray diffraction data at the desired level of resolution, determination of the structure and electronic properties of the metal center(s) in PSII using X-ray absorption spectroscopy (XAS) has greatly aided researchers to establish structure−function paradigms.[25,26] From XAS studies, an estimate of formal oxidation state(s) of the metal center(s) is made using X-ray absorption near edge spectroscopy (XANES) while the local structure around the metal center(s) is determined using extended X-ray absorption fine structure spectroscopy (EXAFS). XAS is element-specific and does not require single crystals of the species studied. Thus, one can study a specific metal center in the presence of other elements using noncrystalline or frozen solution samples. Employing the specificity of XAS, several groups have been studying the manganese cluster of PSII for over two decades to elucidate the oxidation states and structural parameters for the various S states and to understand the mechanism of water oxidation. In combination with XANES, other spectroscopic techniques, such as X-ray emission spectroscopy (XES) and electron paramagnetic resonance (EPR), have been employed to determine oxidation states, coordination numbers, and ligand environment of the manganese cluster in PSII. Analysis and support for interpretation of the XANES and EXAFS data collected for the manganese cluster in PSII are deduced by comparisons to benchmarks provided by synthetic model compounds. Details of these studies have appeared in several excellent reviews, and readers are encouraged to look at the original references therein for further information.[11,14,18,27−29] This section will give a brief overview of XAS studies of the manganese cluster in PSII with special emphasis on major conclusions made therefrom (Table 1 summarizes XAS and EPR spectral information for the WO Mn_4 cluster).

2.3.1. XANES and XES

In the Mn K-edge XANES spectra, a positive shift in energy by 1.0−2.0 eV per one-electron oxidation of the Mn cluster is observed, provided no major structural changes occur. The Mn K-edge XANES spectra of single-flash saturable PSII samples for the S_0, S_1, S_2, and S_3 states have been recorded (Figures 4a and b).[30−33,35] Increases in the Mn K-edge energy for both S_0 to S_1 (2.1 eV) and S_1 to S_2 transitions (1.1

Table 1. Properties of the PSII Mn_4 Cluster

S state	EPR signals	Mn···Mn separations from XAS studies[14,46,51]	Mn oxidation states[12,14,30,82]
S_0	24−26 multiline signals, $g \approx 2$[95−97]	two 2.69 Å, 2.87 Å, one 3.3 Å	(a) II, III, III, III or (b) II, III, IV, IV or (c) III, III, III, IV
S_1	∥mode: broad signal, $g \approx 4.8$,[86] and 18+ multiline signals, $g \approx 12$[89]	two or three 2.7 Å, one >3.3 Å	(a) III, III, III, III or (b) III, IV, III, IV
S_2	19−21 multiline signals, $g \approx 2$, and broad signal, $g \approx 4.1$[66−68,72]	two or three 2.7 Å, one >3.3 Å	(a) III, III, III, IV or (b) III, IV, IV, IV
S_3	⊥mode, broad signal, $g \approx 6.7$, and broad signals, $g \approx 12$ and $g \approx 8$[88,89]	one or two 2.8 Å, 2.95 Å, one 3.3−3.5 Å	(a) III, III, IV, IV or (b) IV, IV, IV, IV

eV) have been reported, which is consistent with oxidation of the manganese center. In addition to the shift in edge position, characteristic changes in the shape of the edge are observed for these transitions. On the other hand, for the S_2 to S_3 transition two different values of the edge shift have been reported: 0.3 eV by Roelofs et al.[30] and 1.0 eV by Ono et al.[31] and Iuzzolino et al.[32] These observations have created divided opinions as to whether a manganese center is oxidized or a ligand is oxidized during the S_2 to S_3 transition; the EPR features of the S_2 state (with an $S = {}^1/_2$ spin state) disappear in the S_3 state with an integer spin. Furthermore, XANES spectra of Ca^{2+}-depleted PSII show that the Mn K-edge energy increases by 0.6−1.0 eV in each S state (S_1, S_2, and S_3).[36] An alternate explanation for a smaller shift for the S_2 to S_3 transition would be that a structural rearrangement occurs after oxidation of the manganese cluster.[29] Experimental evidence for ligand-centered oxidation for the S_2 to S_3 transition has come from a Mn Kβ XES study for the S_0, S_1, S_2, and S_3 states by Messinger et al.[37] Contrary to the positive edge shifts in the XANES, Kβ peaks shift to lower energy with higher oxidation states. These workers found that the 1st-moment shift in the XES spectrum for the S_1 to S_2 advancement is 0.06 eV, whereas the 1st-moment shift for the S_2 to S_3 transition is 0.02 eV, with a maximum possible deconvolution error of ±0.0025 eV. Further manipulation of the data generating derivative-shaped S_1-S_0 and S_2-S_1 difference spectra indicates that the K$\beta_{1,3}$ peak shifts to lower energy during both the S_0 to S_1 and S_1 to S_2 transitions, whereas the derivative-shaped feature is noticeably absent in the S_3-S_2 difference spectrum. This conclusion was further supported by the XANES and Kβ studies of two sets of structurally homologous Mn compounds in different oxidation states.[38] On the basis of X-ray spectroscopic evidence, the proposed oxidation states for the Mn_4 cluster in PSII are as follows: S_0, (II,III,IV,IV) or (III,III,III,IV); S_1, (III,III,IV,IV); S_2, (III,IV,IV,IV); S_3, (III,IV,IV,-IV).[30] Electronic spectroscopy and kinetic analyses support Mn-centered oxidation processes for every S state change.[39−44] While these studies agreed with the XAS results for the S_0 to S_1 and S_1 to S_2 transitions for Mn-centered oxidations, the same was not confirmed for the S_2 to S_3 transition.

2.3.2. EXAFS

Simulations of Mn K-edge EXAFS spectra based on well-established mathematical expressions provide reliable information about the numbers, types, and distances of the backscattering atoms from the absorbing Mn atoms. While the majority of the EXAFS studies have been performed on the dark-stable S_1 state and the S_2 state,[34] those for native S_0 and S_3 states and the chemically induced S_0 state (designated S_0*) have also been conducted.[45−59] EXAFS spectra of all S states of the manganese cluster in PSII show three prominent maxima, labeled peaks I, II, and III (Figure 4c and d), due to interactions between the absorber Mn atom and the backscattering atoms around it. Assignment of the peaks has been based on the relevant distances observed for synthetic model compounds. Peak I corresponds to first-shell Mn−ligand interactions (Mn−O or Mn−N distances), peak II arises from shorter Mn···Mn interactions, and peak III has been assigned to longer Mn···Mn interactions as well as the Mn···Ca interaction (see below). Fourier transforms of k^3 weighted EXAFS data for S_1 and S_2 states are similar with subtle differences in relative amplitudes.[47−50] This indicates that the overall structure of the Mn cluster is invariant and consistent with small changes in the bond distances for the S_1 to S_2 transition due to one electron oxidation of the S_1 state, which is found to be a Mn_4(III,III,IV,IV) cluster on the basis of EPR data (see section 2.4). For the S_1 and S_2 states, peak I has been assigned to two Mn−O/N interactions at a distance of ∼1.8 Å and approximately two to four Mn−O/N interactions at distances between 1.95 and 2.15 Å; peak II is fitted with two or three Mn···Mn interactions at a distance of ∼2.7 Å (similar to distances observed in [Mn(μ-O)$_2$Mn] cores in synthetic complexes; see Section 4.4.1); and peak III has been assigned to Mn···Mn (similar to distances reported for [Mn(μ-O)(μ-carboxylato)Mn] cores; see section 4.4.1) and Mn···Ca interactions at ∼3.3−3.4 Å. However, assignment of the Mn···Ca interactions based on Mn K-edge EXAFS data alone is not conclusive (see below).

On the other hand, in the EXAFS spectra of the S_0 state, peaks I and II show significant differences relative to those observed for the S_1 state (Figure 4c).[46] Changes in distance and amplitude for peak I are more pronounced than those for peak II. It appears that Mn−O/N distances corresponding to peak I are longer in the S_0 state than those in the S_1 state. More importantly, the amplitude of peak II in S_0 is 30% lower than that in the S_1 state. In fact, peak II in S_0 has provided a very good two-shell fit with a 2:1 ratio of Mn···Mn distances, which shows heterogeneity in the shorter Mn···Mn interactions. The authors concluded that there are likely two 2.7 Å interactions and one 2.85 Å interaction present in the S_0 state and therefore likely three 2.7 Å distances in

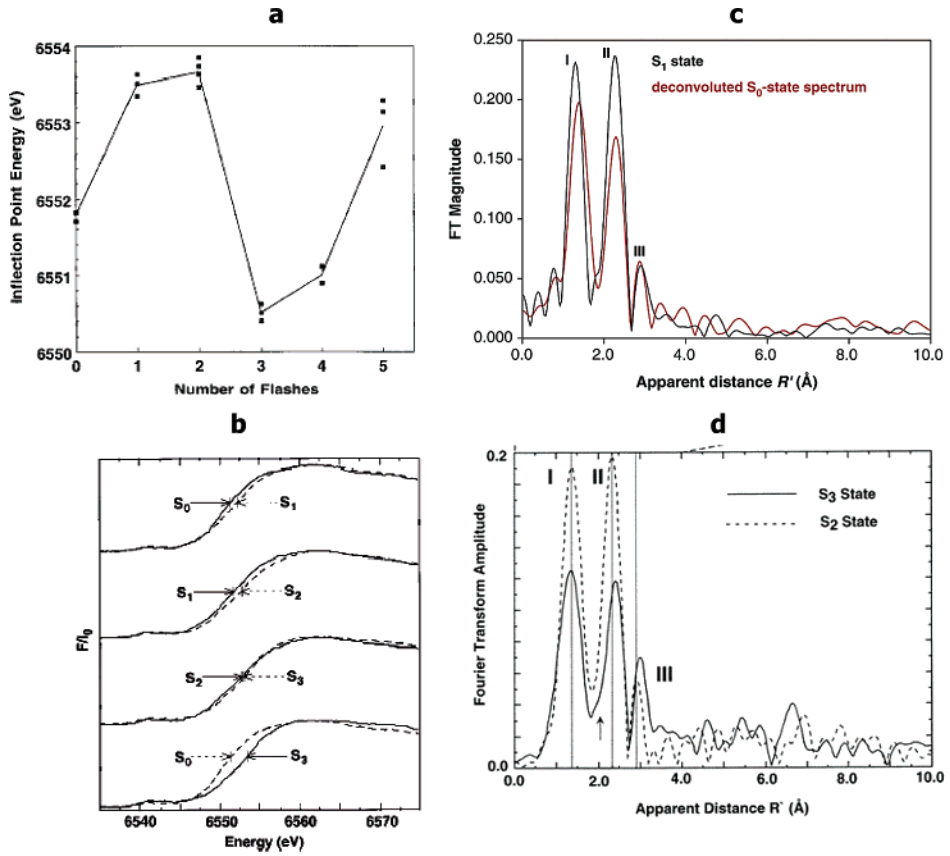

Figure 4. (a) Inflection-point energy (IPE, in eV) of the Mn K-edge of PSII membranes as a function of the number of applied flashes. Shown are the IPEs of three to four individual samples per flash number and their averages (Reprinted with permission from ref 14. Copyright 1996 American Chemical Society). (b) Normalized Mn K-edge spectra for the pure S states of the Mn cluster of PSII, as calculated from the flash-induced edge spectra of samples given zero, one, two, or three flashes. These are the averages of the S state spectra extracted from three different groups of samples; each group contains two to four sets of samples given zero to three flashes. A linear scatter background was subtracted, and the spectra were normalized at the energy of maximal absorption. To emphasize the changes during the various S state transitions, the spectra of successive S states are overlaid (Reprinted with permission from ref 14. Copyright 1996 American Chemical Society). (c) Fourier transforms of the average Mn K-edge EXAFS spectra of S_0 and S_1 states. The Fourier transform corresponding to the S_1 state is shown in black, and the Fourier transform corresponding to the pure S_0 state is shown in red (Reprinted with permission from ref 46. Copyright 2002 American Chemical Society). (d) Fourier transform power spectra of the S_2 (dashed line) and S_3 (solid line) states of PSII. The major Fourier peaks are labeled I, II, and III. The spectra are clearly different between the S_2 (dashed line) and S_3 states (solid line). The arrow points to a shoulder between peaks I and II at an apparent distance of 2.0 Å. There is a reduction in amplitude in all three peaks in the S_3 state compared to the S_2 state. Peaks II and III are at a greater apparent distance for the S_3 state compared to the S_2 state, as shown (Reprinted with permission from ref 51. Copyright 2000 American Chemical Society).

the S_1 state. Interestingly, there is no change in peak III for the S_0 to S_1 transition.

As can be seen in Figure 4d, EXAFS spectral features for the S_2 and S_3 states are quite different.[51] In this case, a decrease in amplitude is observed for peaks I and II and an increase in amplitude is observed for peak III upon the S_2 to S_3 advancement. For the S_3 state, peak II has been fit with two different Mn···Mn distances at 2.8 and 3.0 Å; peak III also lengthens and is fit with two distances at 3.4 Å (Mn···Mn interaction) and 3.6 Å (Mn···Ca interaction). The increase in Mn···Mn distances for peak II for the S_2 to S_3 transition was interpreted in terms of the formation of a bridging or terminal oxyl radical, suggesting oxidation of the oxo group rather than the Mn center. This interpretation is consistent with the XANES and XES data (see above); however, no analogous species has been reported in synthetic manganese chemistry. In contrast, Dau and coworkers suggested a structural rearrangement during the S_2 to S_3 state advancement involving oxidation of a coordinatively unsaturated Mn(III) center to a coordinatively saturated Mn(IV) center with the formation of an additional oxo bridge.[29]

Mn K-edge EXAFS studies have also been performed with the Ca^{2+}-depleted Mn cluster in PSII.[36] As expected, a decrease in amplitude of peak III was observed for all S states. Removal of Ca^{2+} does not cause large structural changes in the Mn cluster, but an increase in both Mn−O/N and Mn···Mn distances corresponding to peaks I and II, respectively, is observed. This change is more significant in the modified S_1' state compared to the S_2' and S_3' states (S_n' denotes Ca^{2+} depleted S states). In addition to the decrease in amplitude, all Fourier peaks were broader compared to the corresponding peaks in native samples.

As mentioned above, backscattering from the Ca atom contributes to the third Fourier peak at 3.3 Å in the Mn K-edge EXAFS spectrum. However, the location of the Ca^{2+} relative to the Mn cluster based on Mn K-edge EXAFS of PSII samples in which Ca^{2+}

is replaced with Sr^{2+} has been debated. This controversy has been addressed by examining Sr K-edge EXAFS data and more recently collected Ca K-edge EXAFS data of PSII samples.[60] These data indicate the possibility of Ca^{2+} being located within 3.3−3.4 Å from the Mn cluster of PSII. In addition, Penner-Hahn and co-workers[61,62] have reported two features at ∼3.3 and 4.2 Å attributed to Mn···Mn or Mn···Ca interactions, indicating that the latter feature, being weak in nature, cannot be unambiguously interpreted without further data. Unfortunately, no additional data have been published since then. Given the relatively close proximity of the Ca^{2+} to the Mn cluster, it is unfortunate that the Ca^{2+} could not be located in two of the recent X-ray diffraction studies, as the Ca^{2+} should contribute to the observed electron density (see section 2.2).

Finally, XAS studies with ammonia or fluoride inhibited forms of PSII[63,64] were conducted to look for structural and functional consequences that would shed light into the mechanism of water oxidation. The Mn K-edge spectra for PSII samples with or without ammonia treatment were very similar. On the other hand, EXAFS spectra of the S_2 state of ammonia treated PSII samples were different from those for the untreated ones. It appeared that one of the two Mn···Mn vectors in the manganese cluster elongated to 2.85 Å due to ammonia treatment. In fluoride treated PSII samples, the absolute energies and the resolution of the XANES spectra were perturbed compared to those of the native samples containing chloride, indicating some structural differences. EXAFS spectra of the fluoride treated PSII samples showed subtle differences in the amplitudes of the Fourier peaks in the S_1 state and more so in the S_2 state, where disorder of peak II was fit with two Mn- - -Mn vectors at 2.7 and 2.8 Å. These observations were correlated with the EPR studies of the corresponding samples (see section 2.4). A recent study by Pizarro et al. on the Mn−Cl binding has shed some light regarding the participation of chloride ions in the oxidation of water to dioxygen.[65]

2.4. EPR and Related Spectroscopic Studies

Continuous wave electron paramagnetic resonance (CW-EPR) spectroscopy and pulsed electron nuclear double resonance (ENDOR) and electron spin−echo envelope modulation (ESEEM) studies have proven to be invaluable techniques in obtaining electronic and structural information for the tetramanganese cluster and for monitoring the electron-transfer processes in PSII WO. CW and pulsed EPR data on the Mn cluster have been very useful in conjecturing the oxidation states and the interactions among the metal centers in different S states and for providing information about the immediate ligand environment.

EPR data of all stable S states (except short-lived S_4) are now available (summarized in Figure 5). The signals from the S_2 state have been studied most extensively.[12,66−72] The S_2 state EPR signal appears either as a hyperfine structured multiline signal centered at $g = 2$, believed to arise from an $S = {}^1/_2$ low-energy excited state, or as a broad signal at $g =$

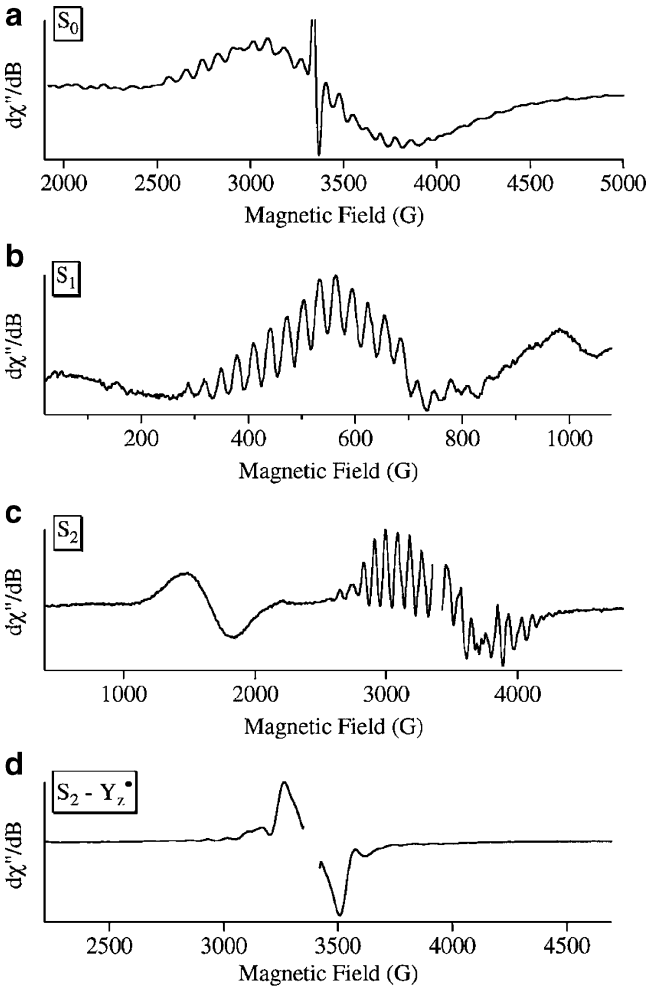

Figure 5. Comparison of the ^{55}Mn hyperfine resolved EPR signal associated with the S_0, S_1, and S_2 states of the water oxidase: (a) S_0 state of 5% MeOH spinach PSII centers; (b) S_1 state of *Synechocystis* PSII centers; (c) S_2 state of 3% MeOH spinach PSII centers; (d) S_2 state of ammonia-bound spinach PSII centers (Reprinted with permission from ref 81. Copyright 2000 American Chemical Society).

4.1, attributed to an $S = {}^3/_2$ or $S = {}^5/_2$ spin state.[71,73] These two signals are interconvertible. Upon annealing at 200 K in the dark, the $g = 4.1$ signal was found to convert into the multiline signal. Alternatively, the multiline signal converts reversibly to the broad signal via an intermediate $S = {}^5/_2$ state upon near-infrared illumination at 820 nm at ∼150 K.[71,74] The two signals are thought to originate from the same tetranuclear Mn cluster through a spin-conversion between $S = {}^1/_2$ excited state and a higher spin form, most likely $S = {}^3/_2$ or ${}^5/_2$.[75,76] Initially it was proposed that the $g = 4.1$ signal comes from an isolated Mn(IV) center.[77] However, the detection of ^{55}Mn hyperfine features in the $g = 4.1$ signal of an oriented NH_3 treated sample dispelled this notion.[78] The multiline S_2 signal has a strong resemblance to that of the dimanganese(III,IV) model complexes, although the latter have fewer hyperfine lines (∼16) and a narrower overall line width (see Figure 10). Mn_2(III,IV) model complexes as well as the PSII S_2 state have been studied with ^{55}Mn ENDOR spectroscopy.[79,80] The ENDOR data favor a tetranuclear model over a dinuclear one as the origin of the multiline signal. On the basis of the detailed spectral simulations of

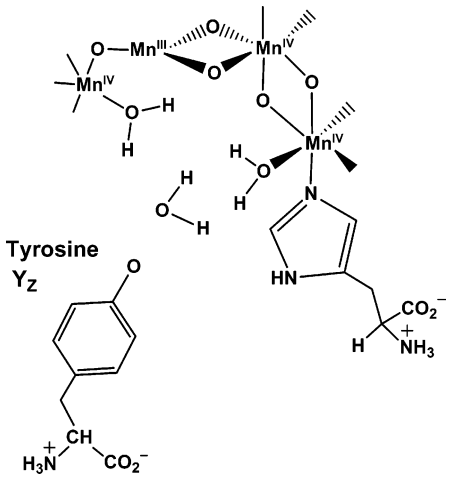

Figure 6. Suggested structure of the water oxidase of PSII in the S_2 state of MeOH treated PSII centers (Adapted from ref 81).

the hyperfine EPR signal, a "trimer-plus-monomer" topology, named the "dangler model" (Figure 6; a similar structure was also postulated on the basis of the EXAFS data[14]), has been suggested by Britt and co-workers.[12,81] On the basis of these studies, preferred Mn oxidation states for the S_2 state have been assigned to be $Mn^{III}Mn^{IV}_3$, although an alternate proposal involving $Mn^{III}_3Mn^{IV}$ has been offered.[82,83]

The S_1 and S_3 states yield integer spin (first excited state $S = 1$) EPR signals, best detected in the parallel polarization mode.[84−88] The S_1 state is described as a $g = 4.8$ broad signal, generated from weakly antiferromagnetically coupled Mn ions.[86,87] Later, a multiline signal at $g = 12$ was observed for *Synechocystis* and in spinach after the removal of the 23- and 17-kDa extrinsic proteins.[85]

Low-field EPR signals in both parallel and perpendicular modes were found for the S_3 state at $g = 6.7-12$, attributed to the $S = 1$ spin state.[88] It is still unclear whether this spin state results from manganese cluster oxidation during the S_2 to S_3 transition or from a strong exchange interaction between S_2 ($S = {}^3/_2$ spin) and an oxidized ligand of manganese in the form of a radical, such as histidine or oxyl.[88,89]

Another $g = 2$ signal with a width of ~240 G, designated as the "S_3' state signal", has been generated upon illumination of the Ca^{2+}-depleted or acetate-inhibited S_2 state. It is proposed to originate from the interaction between $Y_Z^{\bullet}$ and Mn_4, and it is commonly referred to as the $S_2Y_Z^{\bullet}$ or "split" signal.[90−94]

The most recent addition to the PSII EPR spectral family is the multiline signal of the S_0 state centered at $g = 2$, originating from an $S = {}^1/_2$ ground spin state. This signal was discovered independently by three different groups either by using chemical reduction or after illumination of the S_1 state with three flashes.[95−97] The S_0 state signal is found to be ~20% wider than the S_2 state signal (2200 vs 1850 G). Also, the S_0 signal has relatively weak intensity at the center of the spectrum. The line spacing of the multiline S_0 signal is smaller compared to that of the S_2 signal (82 vs 89 G). A Mn(II,III) mixed-valent pair is hypothesized to be responsible for the larger width of the signal.[96,98]

Methanol treatment is required to observe hyperfine splitting of the S_0 multiline signal. The S_2 hyperfine signal was observed in the absence of methanol; however, its intensity was increased by the addition of methanol. As the presence of methanol does not affect water oxidation, most probably it does not bind at the substrate-binding site.[98] It has been speculated that methanol binding modifies the energy gap between the ground state and the first excited spin state to produce stronger signals. It has also been proposed that in the absence of methanol the S_0 state has a high-spin ground state and binding of methanol stabilizes the $S = {}^1/_2$ state as the ground state.[98] ESEEM studies showed that the Mn and MeOH have bonding interactions.[99] However, *S. elongatus* was shown to have the S_0 hyperfine signal without MeOH or EtOH added (the signal was observed in the presence of DMSO).[100]

All of these signals originate reproducibly from the dark-adapted S_1 state with the expected number of flashes, and then they oscillate with every fourth flash.[98]

ESEEM studies have been very useful in obtaining specific information about the amino acid ligation of the Mn_4 cluster. Early pulsed EPR data on ^{14}N- and ^{15}N-grown *Synechococcus* indicated that at least one or two His residues serve as N ligands for the Mn centers.[101,102] Recent studies show that His ligation is not provided by the extrinsic protein subunits but instead by the D1 polypeptide chain.[21] This ligand has been identified as D1-His-332.[103,104] Pulsed EPR studies also implicated the D1-Glu-189 and D1-Asp-170 residues as potential ligands for the Mn_4 cluster.[105−107]

2.5. Chemical Modification Experiments

Site-directed mutagenesis and other chemical modification studies have been carried out to determine the amino acid residues that directly modulate the properties of Y_Z and also provide ligation to the Mn cluster and/or Ca^{2+} ion. It is believed that the Mn_4 cluster and Ca^{2+} ions are primarily ligated by D1 polypeptide residues. The Ca^{2+} ion is located in close vicinity to the Mn cluster and may be connected by a carboxylate bridge, as discerned by the EXAFS data and kinetic studies (see section 2.3).[18,36,61,108,109] Pulsed EPR experiments demonstrated at least one histidine ligated to the Mn cluster.[101,104] FTIR data support His ligation and also suggest a carboxylate bridge between Mn and Ca^{2+} ion (see section 2.6).[110,111]

Site-directed mutagenesis studies show that most mutants constructed at Asp-59, Asp-61, Glu-65, His-92, Asp-170, Glu-189, His-190, His-332, Glu-333, His-337, and Asp-42 of the D1 polypeptide were detrimental to O_2 evolution and have been investigated further.[112,113] These studies identify Asp-59 and Asp-61 as the possible ligands for Ca^{2+}, and Asp-170, His-190, His-332, Glu-333, His-337, Asp-342, and the C-terminus of Ala-344 as possible ligands for the manganese centers (see Figure 7). Mutation experiments also proved that Y_Z and D1-His-190 are functionally coupled.[114] It is less likely that the D2 polypeptide or CP43 and CP47 subunits provide ligation to the manganese cluster.[112,113]

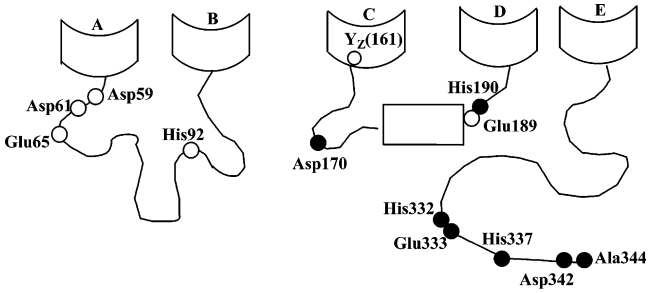

Figure 7. Schematic folding pattern and the amino acid residues that modulate the properties of Y_Z (shown by the open circles) and the Mn_4 cluster (shown by the filled circles) of the lumenal domains of the D1 protein (Adapted from ref 112).

The reduced states of the WO active site were attained by using different reducing agents, such as hydrazine, hydroxylamine, or nitric oxide. Hydrazine and hydroxylamine were shown to reduce the S_1 state of the Mn_4 cluster to S_0, S_{-1}, S_{-2}, and S_{-3} states.[115−120] Hydrazine can act as a two-electron donor to reduce S_1 directly to the S_{-1} state, while hydroxylamine is a one-electron donor.[116] A further reduced state, S_{-3}, can be obtained by hydrazine with a rate constant about 50 times slower.[120] Incubation of the PSII Mn_4 cluster with NO at −30 °C generates the S_{-2} state, which exhibits a multiline signal proposed to emanate from a dimanganese(II,III) motif.[121,122] The reduction has been shown to be reversible.[123] These data support the assignment of high oxidation states for the PSII Kok S states in the water oxidation cycle.

2.6. Vibrational Spectroscopic Studies

Vibrational spectroscopy (Raman,[124] resonance Raman,[125,126] and infrared, especially FTIR[127]) has developed over the years as a powerful tool for understanding the structural features as well as providing insights into the mechanism of various biomolecules including PSII.[128] FTIR in particular has been used extensively in both the mid-IR (1000−2000 cm^{-1}) and low-frequency (<1000 cm^{-1}) regions to garner information concerning the Mn cluster and its catalytically relevant cofactors.[129] Only a selected few of these studies pertaining to the enzyme and synthetic complexes will be discussed in this section. An excellent review by Chu et al. describes these and other studies in detail.[129]

NIR excitation Raman techniques have been demonstrated by Cua et al. to be a useful tool for probing selectively the WO site in PSII and also for characterizing the coordination environment of the Mn_4 cluster.[130] This methodology reduces the unwanted background contributions from the chlorophyll and peptide backbone and selectively examines the low-energy vibrational transitions derived from the Mn cluster. The Mn ligand vibrational features have been reported to be observed in the 200-620 cm^{-1} range. The S_1 state spectrum obtained with 820 nm excitation displays seven Raman bands, four of which (309, 348, 438, and 476 cm^{-1}) shift with D_2O/H_2O exchange. This indicates coordination of at least two H_2O or OH^- groups in the S_1 state, as $Mn-OH_2$ vibrational bands are expected to appear in this region. In contrast, for the S_2 state, the Raman spectra were much weaker. This effect is thought to be due to damping and/or an ultrafast dephasing processes. Furthermore, the weak S_2 state signal could be due to a change in the λ_{max} of the chromophore such that the 820 nm excitation no longer gives resonance enhancement.

Vibrations of the water molecule, the substrate for WO, have also been investigated by FTIR spectroscopy in the S_1 and S_2 states.[131] Bands at 3618 (S_2) and 3585 (S_1) cm^{-1} are observed, which shift downward by 12 cm^{-1} on ^{16}O to ^{18}O substitution. The H_2O to D_2O substitution causes the bands to be shifted to 2681 and 2652 cm^{-1}, respectively. These data suggest water binding and the appearance of O−H stretching vibrations being coupled in both the S_1 and S_2 states. They also indicate the presence of a weak hydrogen bond for the O−H group that becomes weaker on progressing to the S_2 state. Decoupling studies using H_2O/D_2O (1:1) mixtures showed downfield shifts of 4 cm^{-1} (in S_2) and 12 cm^{-1} (in S_1), indicating asymmetry in the hydrogen bond in comparison to the O−H bond in vapor (52 cm^{-1}). Furthermore, the S_2 state has a greater degree of asymmetry that signifies a lowering of the energy barrier for the proton release in the next step. A low-frequency (650−350 cm^{-1}) study on the S_2/S_1 FTIR difference spectrum has been reported recently.[132] Upon performing ^{15}N and ^{13}C isotope labeling experiments, an intense band at 577 cm^{-1} was found to be unaffected, indicating it arises from a mode involving neither carbon nor nitrogen atoms. It has been conjectured to result from a vibration within the Mn cluster or from a Mn ligand stretching mode. Importantly, upon isotopic replacement, most of the bands in this region altered their positions, indicating that couplings between the Mn cluster and the nitrogen and/or carbon atoms dominate the low-frequency region of the spectrum either directly or via hydrogen-bonding interactions. Also, a double difference S_2/S_1 FTIR spectrum has enabled the observation of a 606 cm^{-1} band in the S_2 state and a corresponding 625 cm^{-1} band in S_1.[133] These studies, along with those on model compounds (see below), have led to the assignment of these two bands as arising from a Mn−O−Mn cluster vibration. Isotope studies show that the bridged oxygen is exchangeable with solvent water. Sr^{2+} substitution causes small changes in the bond strengths of the Mn−O−Mn cluster, indicating that Ca^{2+} communicates with the Mn cluster core.[133]

Flash-induced S state transitions have also been studied by Sugiura and Noguchi to explore the vibrational changes accompanying S state advancement.[134] The oscillation features observed can be well explained by assuming the S state model, and a closer inspection of the symmetric (sym) (1300−1450 cm^{-1}) and asymmetric (asym) (1500−1600 cm^{-1}) carboxylate stretches and the amide I (1600−1700 cm^{-1}) region reveals dramatic coordination differences from S_1 to S_2 and S_2 to S_3 states that are reversed from S_3 to S_0 and S_0 to S_1 state changes. The frequency differences ($\Delta\nu$) between the sym and asym vibrational modes have prompted a tentative assignment of the carboxylate binding nature, based on a variety of metal ligand complexes.[135,136] This proposal has

been questioned by Vincent and co-workers, who have studied a family of Mn complexes possessing carboxylates bound in bidentate, bridging modes.[137] In another study by Kimura and co-workers, Ca^{2+} depletion followed by the addition of a variety of ions with ionic radii greater than that of Ca^{2+} has been reported to result in variations of the vibrational features in the double difference S_2/S_1 spectrum.[138] The affected regions include the ν_{sym} (1365 and 1404 cm^{-1}) and ν_{asym} (1587 and 1566 cm^{-1}) modes of the bridging carboxylate ligands and the amide I and II bands emanating from the polypeptide chains. These observations signify the presence of an elaborate H bonded network operational in the WO active site with Ca^{2+} being an integral part of it. Additionally, an FTIR study has allowed the detection of a carboxylate bridge between Mn and Ca^{2+} ion in the PSII active site.[111]

In PSII, Y_Z serves as an electron conduit between the primary Chl donor and the tetranuclear Mn cluster, and consequently, it has been extensively studied.[139,140] Upon oxidation, Y_Z forms neutral radicals $Y_Z^{\bullet}$, and the difference spectra of $Y_Z/Y_Z^{\bullet}$ and its symmetry related partner $Y_D/Y_D^{\bullet}$ have been reported by Berthomieu and co-workers.[141,142] Infrared vibrations are observed at 1279 and 1255 cm^{-1} for $Y_Z^{\bullet}/Y_Z$ and at 1275 and 1250 cm^{-1} for $Y_D^{\bullet}/Y_D$, arising from the stretching of the phenolic CO bonds. These data indicate that both the residues are H bonded, with $Y_Z^{\bullet}$ forming more and/or stronger H bonds with the acceptor, most probably D1-His190.[114] The band has been shown by Barry and co-workers to come from the $Y_Z^{\bullet}$. It displays ^{13}C isotopic shifts in labeling experiments[143−146] and decays with kinetics compatible with those of the decay observed in the EPR signal.[146] FTIR also provides explanations for the band shifts that are observed in chlorophyll on Y_Z oxidation, and these have been studied by various groups, including Babcock and co-workers.[147,148]

The above discussion has dealt with the impact of vibrational spectroscopy on the WO site: how it has provided invaluable information regarding the structural and functional aspects of PSII. Though a full picture has not yet been drawn, the unique perspective provided by vibrational techniques in conjunction with other biophysical methods may be crucial toward an understanding of the entire process of water oxidation. All of this spectral interpretation cannot be achieved unless a comparison of spectral data is made with relevant model complexes. The first IR signature characteristic of the $[Mn^{IV}_2(\mu\text{-}O)_2]$ core supported by Schiff base ligands was reported by Miller and Oliver in 1972 and by Boucher and Coe in 1975 in the spectral range 600−700 cm^{-1}.[149,150] Cooper and Calvin observed a similar band at 688 cm^{-1} that shifts on ^{16}O to ^{18}O substitution.[151] Dave and Czernuszewicz have reported characteristic Raman bands using dinuclear model complexes. Characteristic ^{18}O sensitive features for a $[Mn_2O(O_2CR)_2]^{2+}$ core are observed at ∼560 cm^{-1}, and those for $[Mn_2O_2]^{3+}$ and $[Mn_2O_2(O_2CR)]^{2+}$ cores, at ∼700 cm^{-1}.[152] This group has also reported a Mn(IV)-μ-oxo stretching mode at ∼695 cm^{-1} by performing Raman spectra on model complexes.[153] Sheats et al. have reported symmetric and asymmetric stretching vibrations at 558 and 717 cm^{-1}, respectively, for the Mn−O−Mn bridge in the $[Mn_2O(O_2CR)_2(HB(pz)_3)_2]$ (R = Me (**77**), Et or H) family of complexes.[154] ^{18}O incorporation caused the peaks to shift to 541 and 680 cm^{-1}, respectively.[154] A family of complexes with the formulations $[Mn_2O(OAc)_2(bpy)_2(L)_2]$ and $[Mn_2O_2(OAc)(bpy)_2(L)_2]$ (L = H_2O/Cl^-) have been studied by low-frequency resonance Raman by Cua et al.[155] Additionally, normal coordinate analysis using the **GF** matrix method was performed. These studies have assisted in the assignment of some resonances in the 200−600 cm^{-1} range attributable to metal−ligand bonds. In particular, a band at 310 cm^{-1}, which is sensitive to H_2O/D_2O and Cl^- substitution, has been proposed to possess Mn−OH_2 vibration character.

IR spectra and normal-mode analysis have also been performed on the adamantane-like complexes $[Mn_4O_6(bpea)_4]^{n+}$ (n = 3 (**162**) and 4 (**160**)) by Visser et al.[156] By using a method of subtraction that eliminates background contributions from solvent molecules and surrounding ligands and using ^{16}O to ^{18}O substitution, Mn−O vibrational modes have been identified. Two strong IR bands at 745 and 707 cm^{-1} and a weaker band at 510 cm^{-1} have been observed for the $[Mn^{IV}_4]$ complex, which upon reduction to the $[Mn^{IV}_3Mn^{III}]$ species displays two strong IR bands at 745 and 680 cm^{-1} and several weaker bands between 510 and 425 cm^{-1}. Though the shifts look significant, the vibrations may not emanate from the same modes, and thus, a one to one correspondence in the bands represents an overly simplistic approach in this case.

High-valent Mn=O (manganyl) complexes have also been the subject of intense interest due to their possible relevance in the mechanistic pathway of water oxidation. Collins and co-workers reported IR bands at 970 and 979 cm^{-1} corresponding to Mn^V=O stretching frequencies.[157,158] Hill and co-workers reported Mn^{IV}=O porphyrin complexes that displayed vibrations from this moiety around 712 and 755 cm^{-1}.[159−161] The Cl^- ion is an essential cofactor for the WO enzyme, and Mn−Cl vibrations have been reported in the range 150−350 cm^{-1}.[162] Little IR vibrational data is available regarding the Mn-histidine/imidazol stretching frequencies, nor is there a clear Ca−OH_2 or Ca−OH FTIR study.[163] If performed, they will be helpful in analyzing PSII structural properties and the mechanistic proposals involving Ca^{2+} involvement. Overall, vibrational data for synthetic analogue complexes are limited, and there is a need for analyzing crucial vibrational characteristics of dinuclear, trinuclear, and tetranuclear clusters. Undoubtedly, measurement and subsequent analysis of the FTIR bands reflecting the core characteristics of these higher nuclearity clusters will be a challenge but could be extremely rewarding in terms of obtaining a better understanding of the PSII Mn_4 and how it changes with the S state advances.

3. Mechanistic Proposals Regarding Water Oxidation

The complex and facile multielectron oxidation of water at ambient temperatures using solar energy

necessitates a special mechanism that can harness the driving force generated with each photon absorption at the photosynthetic reaction center. A large number of inroads toward elucidating the mechanism of water oxidation have been made over the years, and these have been well documented. Early proposed mechanisms (1975−1985) of water oxidation were limited by the lack of pertinent biophysical data and relevant structural information regarding the WO active site geometry, viz. appropriate nuclearity and oxidation state assignments, cofactor and inhibitor effects, and other properties. A handful of proposals were nonetheless put forward with the Joliot and Kok storage state cycle being the underlying basis.[33,164−169] All the mechanistic strategies involved water molecule binding at two neighboring Mn sites and then subsequent deprotonation steps followed by O−O bond formation.[170] Some of the steps in these mechanisms invoke the active involvement of a redox-active bridging ligand, a coligand, or a counterion. For these earlier ideas, considerable emphasis was placed on redistributing the charge developed during the process away from the metal cluster sites in the cycle toward surrounding ligands. All of these theories utilized only two metal centers, except the one by Govindjee et al., which proposed a catalytic cycle invoking four Mn centers divided into two groups on the basis of their environments: one located on a hydrophobic cavity on the intrinsic 34-kDa protein and the other located on the 33-kDa hydrophilic surface subunits.[168] Water oxidation was proposed to occur at the Mn_2 site located in the former cavity with the protons being transferred to the latter Mn ion pairs along a hydrogen bond created by the water molecules between them. Additionally, each of the Mn ions was conjectured to bind to a redox-active ligand (RAL), such as quinone or an aromatic amino acid residue.

The aforementioned proposals have undergone a gradual metamorphosis as the wealth of information from biophysical studies as well as the X-ray data has been made available. All the relevant modern mechanisms share a common unifying theme: (i) involvement of Ca^{2+}, an essential cofactor for the process, (ii) a concerted proton coupled electron transfer (PCET) from S_2 to S_3 and S_3 to S_4[171−173] (which, according to recent studies on water oxidation performed with Ru dimers, helps in avoiding buildup of excess charge),[174] or a hydrogen abstraction mechanism for other S state transitions,[175] (iii) a structural basis of the various intermediates (S_0 to S_4) derived from inorganic model chemistry, oftentimes involving the presence of a putative Mn^{V}═O intermediate, (iv) the O−O bond formation occurring after the S_3 state (based on H_2O^{18} labeling studies),[176] and (v) the importance of electroneutrality with every S state advancement, as the process occurs in a medium with low dielectric constant.

Bioinorganic chemists have prepared speculative structural analogues over the last two to three decades to gain insight into the PSII mechanism (see section 4.4 for detailed discussion). In one of the earliest proposed mechanisms involving well-defined structural types, the S_3 and S_4 structures were proposed to be $[Mn_4O_6]$ adamantane-like clusters.[177] The S_4 state ultimately released O_2 and rearranges to a $[Mn_4O_4]$ cubane-like structure. A quite different molecular "double-pivot" mechanism was suggested with the S_1 state $[Mn_4O_2]$ butterfly-like cluster transforming to a cubane-like $[Mn_4O_4]$ core followed by O−O bond formation between the oxygen atoms from opposite apexes of a cube.[178] Though the above mechanisms are inconsistent with current XAS and other spectroscopic data, they provided a useful foundation for subsequent mechanistic proposals.

The proposals which have emerged more recently can be divided into two categories involving (a) hydrogen abstraction[175,179−181] and (b) concerted proton-coupled electron transfer.[182−186] These models lead to two extreme cases of proton release: an electrostatic deprotonation into the lumen against a hydrogen bonded network from D1-His-190, though a simultaneous hydrogen bonded process resulting in electrostatic transmission of protons cannot be ruled out.[187] It should be clarified that the hydrogen abstraction model is not a true H-abstracting process but rather a special case of proton-coupled electron transfer where reduction of Y_Z by the Mn_4 cluster occurs with the proton emanating from solvent water. These two theories will now be described briefly.

A hydrogen atom abstraction process by the Y_Z residue in conjunction with a dimer-of-dimers structural template has led to an interesting hypothesis wherein an O atom is proposed as a terminal ligand to Mn (see Figure 8 (top)).[175,188] The Cl^- ion is proposed to migrate in S_1 to S_2 and S_2 to S_3 state transitions while $Y_Z^{\bullet}$ serves as the H atom abstractor and Ca^{2+} ion binds to Cl^- in the lower S states. In another proposal two dinuclear Mn complexes perform diverse functions: one oxidizes H_2O to peroxide while the other converts peroxide to water.[16,189−191] The final O−O bond forming step in the S_4 state is predicted to result from attack of the hydroxo group bound to Ca^{2+} to a strongly electrophilic Mn^{V}═O species. In a similar hypothesis, a Cl^- bridging between a Mn and a Ca^{2+} is responsible for modulating the nucleophilic attack of the hydroxide ion.[181,192] This was first predicted from mass spectrometric studies.[176] The product of this step has been argued to be similar to the ferric hydroperoxide in oxyhemerythrin. Oxygen release is envisioned in a manner similar to that of oxyhemerythrin concomitant with reduction of Mn and protonation of μ-oxo bridges.[192] On the basis of XAS and EPR data, another mechanism incorporating a "C-shaped" cluster has also been suggested recently involving one redox-active Mn per $[Mn_2(\mu\text{-}O)_2]$ dimeric moiety (see Figure 8 (bottom)).[17,193,194] Here, the O−O bond is formed between an oxyl radical and a μ-oxo atom. A hybrid density functional theory has been utilized to put forward a triangular Mn moiety closely coupled by μ-oxo groups as a potential model for the WO site. The previously suggested oxyl radical mechanism[14] has been reexamined in this work with an oxyl radical placed in a bridging fashion between two Mn atoms. Consistent with earlier studies, only one Mn is redox active in this model and the Ca^{2+} ion has been shown as playing the role of a bridging metal

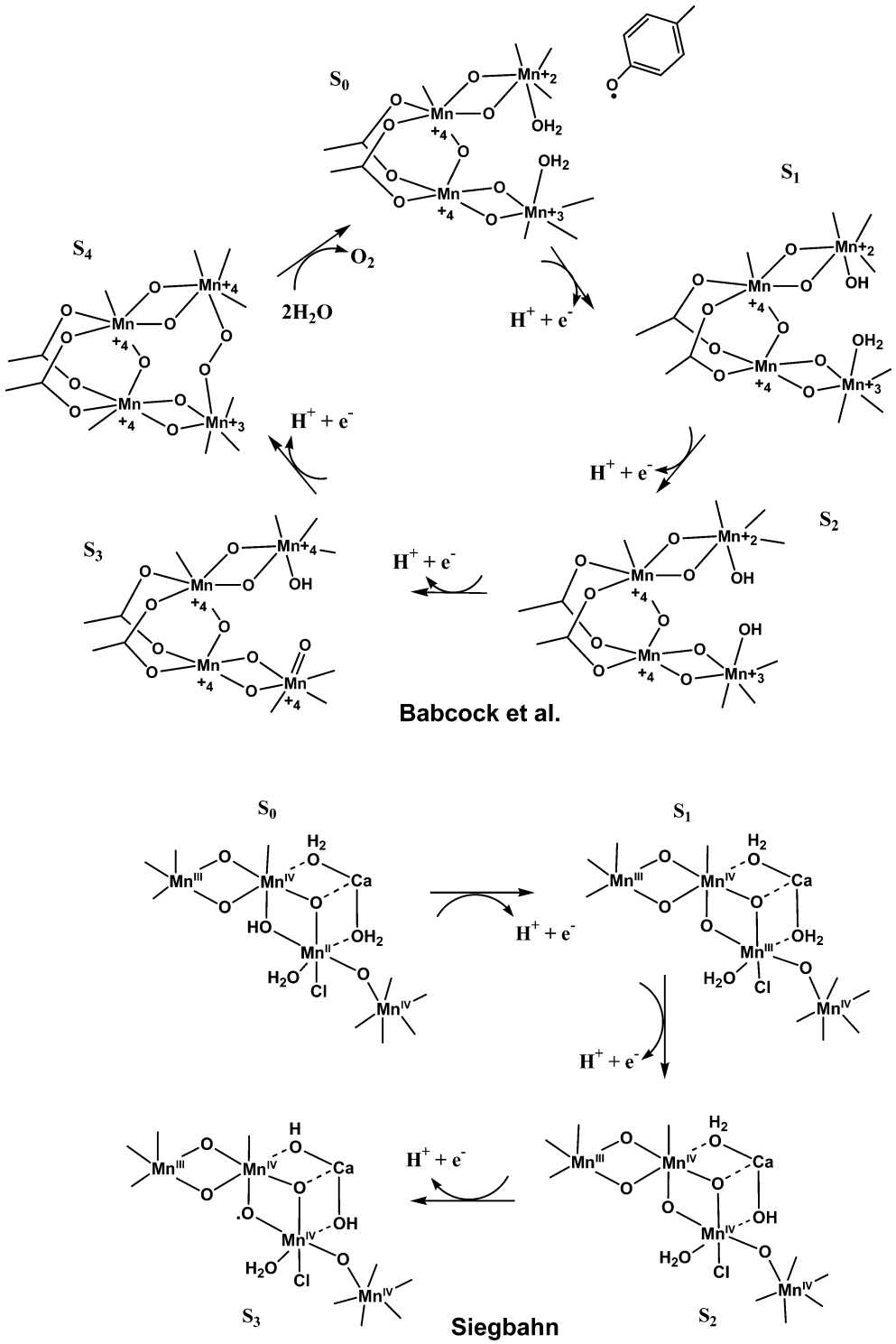

Figure 8. Proposed mechanistic cycles of photosynthetic water oxidation by Hoganson and Babcock (top) (adapted from ref 175) and by Siegbahn (bottom) (adapted from ref 17).

ion, which assists the formation of the radical. The presence of trans effects has been widely invoked, resulting in elongation of both short Mn···Mn distances in S_2 to S_3 state conversion, as suggested by EXAFS. Consecutive deprotonation steps from the corners of an incomplete cube are proposed as the system progresses through the S states. The final O−O bond-forming process involves the oxyl radical and the oxygen atom derived from a water molecule that comes in to occupy the missing corner of the cube.

The energetic requirements for the water oxidation process are also one of the key questions that have been addressed by many research groups. Among them is the ability of the WO to store the necessary oxidizing equivalents without liberating them prematurely and, furthermore, the manner by which WO builds up the required 1.26 V (vs NHE) though Y_Z is able to contribute only 1.1 V per oxidation step.[23] The hydrogen abstraction mechanism described above can explain these characteristics. Though energetically Y_Z might not be suitably favored to abstract hydrogen

from a water molecule, it can do so from a protonated oxo group and probably a water molecule coordinated to a Mn center.[195,196] If H atom abstraction is in fact occurring in WO, this also suggests that the redox potential of water bound to Mn in the cluster is affected such that the cluster is stabilized from premature loss of oxidizing equivalents and the potentials are tuned to make it accessible to Y_Z.[16]

The other critical participants in the catalytic cycle are the redox-active tyrosine residues, Y_Z (that serves as electron donor to P_{680}^+) and Y_D.[197,198] Y_Z and Y_D have been clearly characterized to be Tyr-161 and Tyr-160 belonging to D_1 and D_2 polypeptide chains, respectively.[199] Although Y_D is not directly involved in the electron-transfer processes, experiments by using mutated Tyr-160-Phe have shown it to affect the rate of oxygen evolution.[200] It has been proposed that during photoactivation the phenolic proton of Y_D is retained within the reaction center and raises the P_{680}^+/P_{680} reduction potential, which enhances the driving force for the photooxidation of the Mn_4Ca cluster.

In summary, the functional and structural data do not allow any conclusive decisions to be reached regarding the mechanisms proposed in the above section. The role of the protein matrix is not only as a "cofactor holder" but also for fine-tuning the various hydrogen-bonding networks for substrate coordination and ultimately resulting in O−O bond formation.[201] New and/or modified ideas will be undoubtedly suggested in the future, stimulating new experiments and novel approaches to better understand the mechanistic details regarding this critical transformation.

4. Biomimetic Approach

4.1. Introduction

This section will discuss the synthetic methodologies and physicochemical properties of manganese complexes that have served invaluable roles in gaining structural and mechanistic insights of the WO active site. The complexes are divided into three subsections on the basis of their nuclearity. This section will also give a brief synopsis of the chelating ligands that were designed and used in the formation of these compounds. We will also give an overview of the functional modeling and theoretical studies on the relevant species.

4.2. Assembly of Manganese-oxo Clusters

High-valent Mn-oxo species are believed to be actively involved in the WO catalytic cycle. This has been determined by extensive EPR and EXAFS studies, as discussed above. Consequently, much effort has been devoted to isolate Mn-oxo complexes with different nuclearities, aided by various chelating (N and/or O donors) ligands. The complexes synthesized have been invaluable in interpreting data obtained for PSII. From the synthetic studies it has been realized that the manganese ions in the +3 (d^4) and +4 (d^3) oxidation states in polynuclear manganese complexes are primarily stabilized with bridging oxide (O^{2-}) groups. The presence of suitable chelating ligands plays a very important role in the formation of clusters of different nuclearity, a process that is often determined by the thermodynamic stability of the final products.[170] However, it should be pointed out that in many cases the true thermodynamic end point would result in the formation of insoluble extended oxides. Additionally, carboxylate ligands in various bridging modes and halide ions have been employed to provide coordination to the metal centers because of their biological relevance. The spontaneous self-assembly approach has long been utilized in the formation of high-valent manganese-oxo complexes. Readily available Mn(II) starting materials can be oxidized in the presence of suitable reagents, such as bromine water, iodine, Ce(IV), iodosobenzene, peroxides, $HClO_4$, bromate, and also NaOH, to form high-valent Mn species.[202−206] Aerial oxidation of Mn(II) precursors has also been reported for the same purpose.[207−209] Many syntheses have also employed Mn(III) starting materials to prepare high-valent clusters.[204,210−214] Permanganate salts, which contain the Mn^{VII} ion, have been used extensively in delivering oxidizing equivalents and oxo ligands. The presence of permanganate in these reactions serves a dual purpose, as an oxidant as well as providing another source of Mn ions. A very common reaction pathway to high-valent manganese clusters involves the comproportionation reaction between Mn^{II} and Mn^{VII} ion sources. Potassium or sodium salts of permanganate are used for the reactions done in aqueous medium, whereas tetraalkylammonium salts are used for reactions conducted in organic solvents.[215−218] Several Mn-oxo species have also been synthesized via bulk-electrolysis, ligand substitution, and hydrolytic pathways.[217,219−223]

4.3. Ligand Design

As mentioned above, the ancillary N-donor and O-donor ligands perform a critical role in the formation and stabilization of oxomanganese clusters. Limitation of aggregation is a key attribute to consider when selecting a ligand. A large number of ligands ranging from bidentate to tridentate to template polydentates that include aliphatic, cyclic, polypyridyl, and Schiff bases have been employed for this purpose. Upon coordination to the metal centers, these ligands usually form stable five-membered and also six-membered chelate rings that in part determine the stability of the complexes. Scheme 2 displays the ligands used in the synthesis of biologically relevant Mn complexes that will be discussed in the next section.

4.4. Manganese-oxo Clusters: Synthesis and Properties

4.4.1. Dinuclear Manganese Complexes

Over the past two to three decades, growth in the chemistry of dinuclear manganese-oxo complexes is highly correlated with attempts at bioinorganic modeling of several manganese proteins and enzymes that contain dinuclear and polynuclear active sites. Since this review is intended to cover the synthetic efforts toward mimicking the manganese cluster in PSII, complexes with at least one bridging oxo (O^{2-})

Scheme 2. Oxygen and Nitrogen Donor Ligands

MONODENTATE

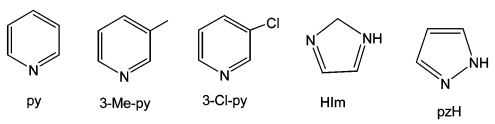

BIDENTATE

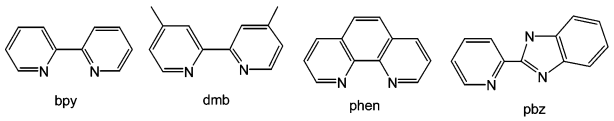

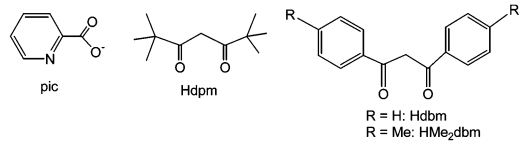

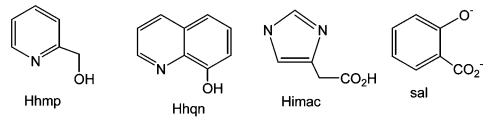

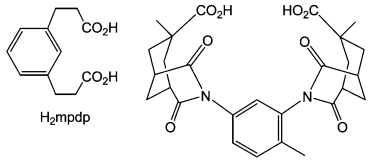

TRIDENTATE

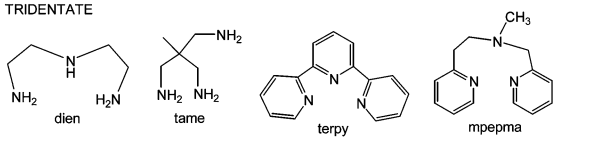

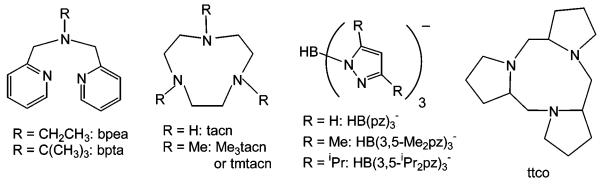

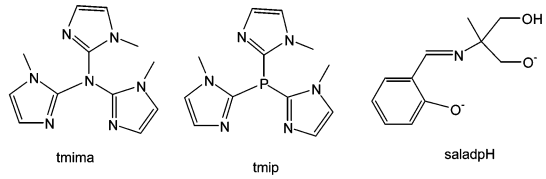

TETRADENTATE

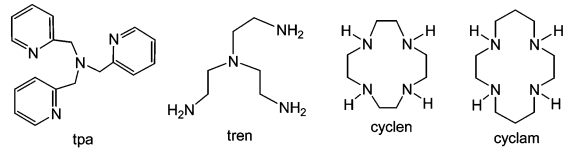

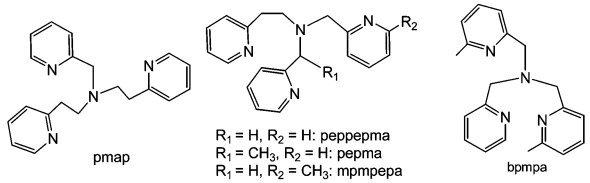

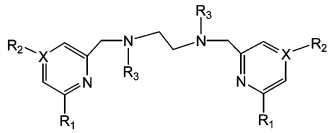

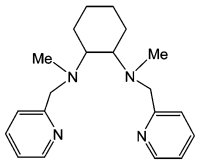

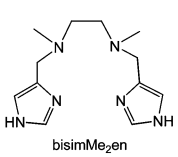

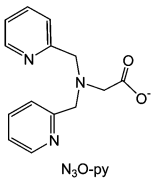

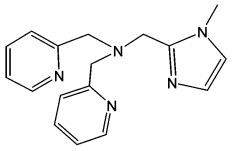

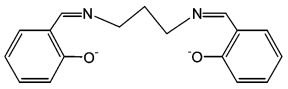

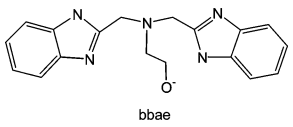

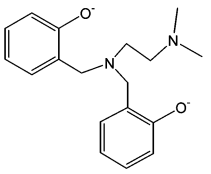

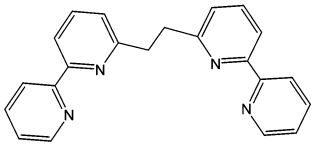

PENTADENTATE

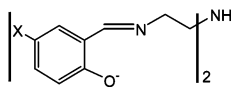

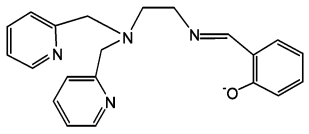

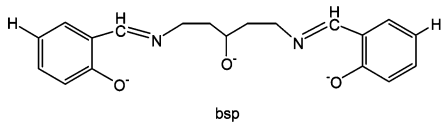

HEXADENTATE

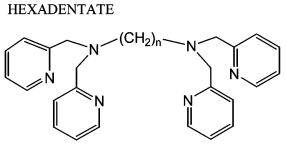

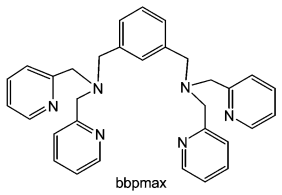

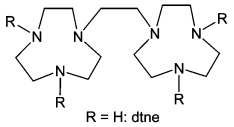

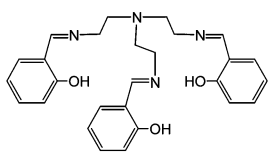

HEPTADENTATE

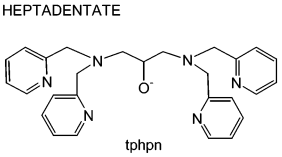

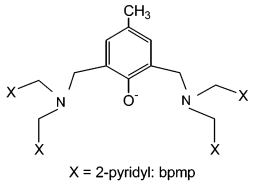

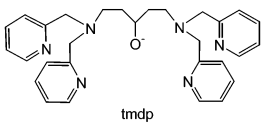

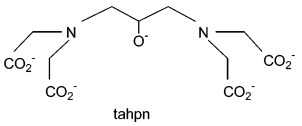

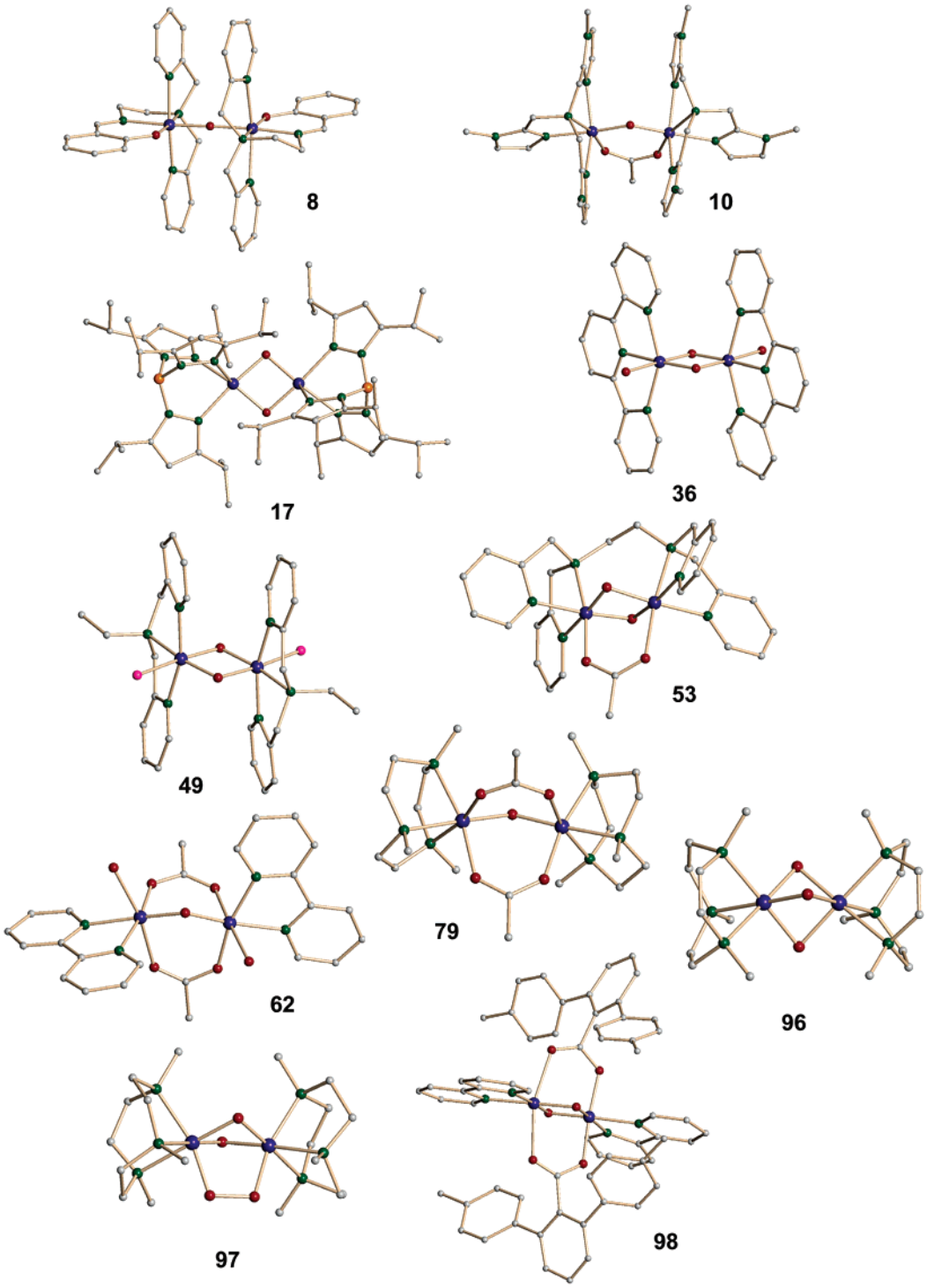

Figure 9. Crystal structures of selected dinuclear manganese complexes portraying various cores types. The Mn atoms are shown in blue, O atoms in red, N atoms in green, B atoms in orange, Cl atoms in pink, and C atoms in gray.

group between metals are considered here. Interestingly, complexes with all possible geometrically allowed numbers of bridges (mono-, di-, tri-, and tetra-) between the two manganese centers have been reported. In this section these complexes are grouped in eight different categories on the basis of the core types, as shown in Scheme 3. These are further subcategorized on the basis of their oxidation states (III,III; III,IV; and IV,IV). Crystal structures of selected dinuclear complexes possessing different core types are shown in Figure 9. Although these complexes are neither structural nor functional models for intact PSII, they are results of important discoveries in developing versatile and rich manganese-oxo chemistry. These act as good synthons for a number of higher nuclearity clusters (see sections 4.4.2 and 4.4.3 for trinuclear and tetranuclear complexes, respectively) that have shown some characteristic structural and spectroscopic features similar to those of the manganese cluster in PSII. Dinuclear complexes have been used extensively for comparative spectroscopic and theoretical studies in order to

Table 2. Structural and Magnetic Properties of Dinuclear Manganese Complexes[a]

no.	compound	Mn···Mn (Å)	Mn−O_b−Mn (deg)	J (cm^{-1})	ref
		(i) (μ-Oxo)			
		(a) Mn^{III}−Mn^{III}			
1	[{Mn(pc)py}$_2$O]·2py	3.42	178		226, 227
2	$K_7[Mn_2O(CN)_{10}](CN)$	3.446	180.0		228
3	[Mn_2O(5-NO_2-saldien)$_2$]	3.490(2)	168.4(2)	−120.0	229
4	[Mn_2O(bpmsed)$_2$](ClO_4)$_2$	3.516(2)	180	−108.0	230
5a	*cis*-[Mn_2O(terpy)$_2$(CF_3CO_2)$_4$]·H_2O·2CH_2Cl_2	3.493	176.7(4)		231
5b	*trans*-[Mn_2O(terpy)$_2$(CF_3CO_2)$_4$]·1.5CH_2Cl_2	3.504	178.0(2)		231
6	[Mn_2O(bpia)$_2Cl_2$](ClO_4)$_3$·2CH_3CN	3.5326(9)	180		232
7	[Mn_2O(HB(3,5-^{i}Pr$_2$-pz)$_2$·(3-^{i}PrO-5-^{i}Pr-pz))$_2$]	3.530(4)	174.9(7)		233
		(b) Mn^{III}−Mn^{IV}			
8	[Mn_2O(bpmsed)$_2$](ClO_4)$_{2.37}$(PF_6)$_{0.63}$	3.524	178.7(2)	−176.5	230
		(c) Mn^{IV}−Mn^{IV}			
9	[{(N_3)Mn(TPP)}$_2$O]	3.537	180		234
		(ii) (μ-Oxo)(μ-carboxylato)			
		(a) Mn^{III}−Mn^{III}			
10	[Mn_2O(OAc)(tmima)$_2$](ClO_4)$_2$·2CH_3CN	3.2503(8)	130.9(2)	+1.33	235
11	[Mn_2O(OAc)(bispicen)$_2$](ClO_4)$_3$	3.276(3)	130.8(4)	+19.5	236
12	[Mn_2O(OAc)(bispicMe_2en)$_2$](ClO_4)$_3$	3.29(1)			236
13	[Mn_2O(OAc)(bpia)$_2$](ClO_4)$_3$·CH_3CN	3.2544(8)	131.0(1)		232
		(iii) Bis(μ-oxo)			
		(a) Mn^{III}−Mn^{III}			
14	[Mn_2O_2(bpen)$_2$](ClO_4)$_2$·H_2O	2.676(3)	94.5(4), 92.1(4)	−86.4	237, 238
15	[Mn_2O_2(bpmpa)$_2$](NO_3)$_2$·6H_2O	2.674(4)	93.9(3)		238
16	[Mn_2O_2(bped)$_2$](ClO_4)$_2$·7H_2O	2.686(1)	93.3(2) 93.9(2)		238
17	[Mn_2O_2(HB(3,5-^{i}Pr$_2$pz)$_3$)$_2$]	2.696(2)	96.5(3) 97.0(3)		239
18	[Mn_2O_2(bispicMe_2en)$_2$](ClO_4)$_2$·5H_2O	2.699(2)	93.8(2)	−100.5	240
		(b) Mn^{III}−Mn^{IV}			
19	[Mn_2O_2(bpy)$_4$](ClO_4)$_3$·3H_2O	2.716(2)	96.6(2) 96.3(1)	−147.0	243, 244
20a	[Mn_2O_2(phen)$_4$](PF_6)$_3$·CH_3CN (100 K)	2.700(1)	96.0(1)	−148	244
20b	[Mn_2O_2(phen)$_4$](PF_6)$_3$·CH_3CN (200 K)	2.695(9)	96.0(1)		244
21	[Mn_2O_2(pbz)$_4$](ClO_4)$_3$·H_2O	2.729(3)	99.9(5) 97.2(5)		153
22	[Mn_2O_2(bispicen)$_2$](ClO_4)$_3$·3H_2O	2.659(2)	94.3(2)	−140.0	245
23	[Mn_2O_2(bispicMe_2en)$_2$](ClO_4)$_3$·H_2O	2.679(2)	94.7(2) 94.5(2)	−160.0	240
24	[Mn_2O_2(bispicMe_2(−)chxn)$_2$](ClO_4)$_3$	2.693(2)	95.1(3) 94.9(3)	−146.5	240
25	[Mn_2O_2(tren)$_2$](CF_3SO_3)$_3$	2.679(1)	95.4(2) 95.3(2)	−146	208
26	[Mn_2O_2(tpa)$_2$](S_2O_6)$_{1.5}$·7H_2O	2.643(1)	93.9(2) 94.1(1)	−159.0	247
27	[Mn_2O_2(cyclam)$_2$]Br_3·4H_2O	2.731(2)	97.2(1)	−118.5	409
27	[Mn_2O_2(cyclam)$_2$](S_2O_6)$_{1.5}$	2.729(5) 2.738(5)	97.1(6) 97.1(5)		409
29	[Mn_2O_2(cyclam)$_2$](CF_3SO_3)$_3$·2H_2O	2.741(1)	97.7(1) 97.1(2)		248
30	[Mn_2O_2(N_3O-py)$_2$](ClO_4)·2.5H_2O	2.656(2)	94.0(3) 94.9(3)	−151.0	246
31	[Mn_2O_2(pepma)$_2$](ClO_4)$_3$·CH_3CN	2.691(3)	96.0(1) 95.7(1)		249
32	[Mn_2O_2(peppepma)$_2$](ClO_4)$_3$	2.682(9) 2.702(10)			249
33a	[Mn_2O_2(cyclen)$_2$]Cl_3·LiCl·5H_2O	2.694(1)	95.7(1)	−138	250
33a	[Mn_2O_2(cyclen)$_2$](ClO_4)$_3$·2H_2O			−156.5	250
34	(Bu_4N)(Ph_4P)[Mn_2O_2(pic)$_4$]$_2$	2.721(1) 2.726(1)	96.78(1) 97.26(1) 97.23(1) 96.84(1)		410
35	[Mn_2O_2(dmb)$_4$](OTf)$_3$·7(H_2O)	2.701(1)	96.4(2) 96.0(2)	−148	203
36	[Mn_2O_2(terpy)$_2$(H_2O)$_2$](NO_3)$_3$·6H_2O	2.723(3) 2.7315(12) 2.7327(12)	97.5(3) 97.6(1) 97.8(1)		254
37	[Mn_2O_2(terpy)$_2$(CF_3CO_2)$_2$](ClO_4)·CH_3CN	2.7265(5)	97.5(1) 97.7(1)		253
38	[Mn_2O_2(pmap)$_2$](ClO_4)$_3$·CH_3CN	2.7393(13) 2.7379(13)	97.9(1) 97.9(1)		252

Table 2 (Continued)

no.	compound	Mn···Mn (Å)	Mn−O_b−Mn (deg)	J (cm^{-1})	ref
39	$[Mn_2O_2(bisimMe_2en)_2](ClO_4)_3 \cdot H_2O$	2.677(2)	94.6(3)	−139	251
40	$[Mn_2O_2(bpia)_2](ClO_4)_2(PF_6)$	2.624(2)	92.7(1)		232
	(c) Mn^{IV}−Mn^{IV}				
41	$[Mn_2O_2(phen)_4](ClO_4)_4 \cdot CH_3CN$	2.748(2)	99.5(2)	−144	244
42	$[Mn_2O_2(pbz)_4](ClO_4)_4 \cdot H_2O$	2.724(2)	98.5(2)		153
43	$[Mn_2O_2(pic)_4] \cdot MeCN$	2.747(2)	98.1(2)	−86.5	256
44	$[Mn_2O_2(bispicen)_2](ClO_4)_4 \cdot 2MeCN$	2.672(1)	95.2(2)	−125.6	245
			95.0(2)		
45	$[Mn_2O_2(mpmpepa)_2](ClO_4)_4$	2.747(18)	101.5(1)	−131.0	249
46	$[Mn_2O_2(tacn)_2(OH)_2][Mn_3(ox)_4(H_2O)_2] \cdot 6H_2O$	2.625(2)	91.9(2)		255
47	$[Mn(salpn)O]_2 \cdot 2DMF$	2.728(1)	97.2(1)	−82.0	257
		2.731(2)	97.7(3)		258
48	$[Mn_2O_2F_2(bpea)_2](ClO_4)_2$	2.746(2)	99.0(2)		216
49	$[Mn_2O_2Cl_2(bpea)_2](ClO_4)_2$	2.757(3)	99.2(2)	−147	216
50	$[Mn_2O_2(dmb)_4](ClO_4)_4 \cdot 7H_2O$	2.736(1)	99.2(1)		203
			98.2(1)		
	(iv-A) Bis(μ-oxo)(μ-carboxylato)				
	(a) Mn^{III}−Mn^{IV}				
51	$[Mn_2O_2(OAc)(tacn)_2](BPh_4)_2 \cdot MeCN$	2.588(2)	91.1(1)	−220.0	260
52	$[Mn_2O_2(OAc)(bpy)_2Cl_2]$	2.667(2)	94.5(0)	−114	265
			94.4(1)		
53	$[Mn_2O_2(OAc)(tpen)](ClO_4)_2 \cdot 2CH_3CN$	2.5906(6)	91.7(1)	−125	262
54	$[Mn_2O_2(OAc)(Me_3tacn)(OAc)_2]$	2.665(1)	93.1(2)	−90	261
			94.4(2)		
55	$[Mn_2O_2(OAc)(Me_3tacn)(bpy)(MeOH)](ClO_4)_2 \cdot MeOH$	2.630(2)	92.9(2)	−117	261
			92.9(2)		
56	$[Mn_2O_2(OAc)(dtne)](BPh_4)_2$	2.553(1)	90.0(1)	−110	264
			89.9(1)		
57	$[Mn_2O_2(OAc)(Me_4dtne)](BPh_4)_2$	2.574(2)	90.6(2)	−112	264
			90.7(2)		
58	$[Mn_2O_2(O_2CPhNIT)(Me_4dtne)](ClO_4)_2$	2.580(2)	90.4(1)	−127	206
			91.1(1)		
59	$[Mn_2O_2(OAc)(bpea)_2](ClO_4)_2 \cdot CH_2Cl_2$	2.6333(7)	92.4(1)	−164	211
			93.4(1)		
60	$[Mn_2O_2(OAc)(mpepma)_2](BF_4)_2 \cdot 2CH_3CN$	2.622(4)	93.5(4)	−144	263
			93.9(4)		
	(b) Mn^{IV}−Mn^{IV}				
61	$[Mn_2O_2(OAc)(bpea)_2](ClO_4)_3 \cdot CH_3CN \cdot 0.5CHCl_3$	2.580(1)	91.5(2)	−124	211
			91.7(2)		
62a	$[Mn_2O_2(OAc)(H_2O)_2(bpy)_2](ClO_4)_3 \cdot HClO_4 \cdot H_2O$	2.642(?)	95.0(2)	−67	205
62b	$[Mn_2O_2(OAc)(H_2O)_2(bpy)_2](ClO_4)_3 \cdot H_2O$	2.640(1)	94.6(2)	−43.7	266
			94.79(5)		
			94.24(5)		
63	$[Mn_2O_2(OAc)(tpen)](ClO_4)_3 \cdot CH_3CN$	2.591(1)	92.4(1)		222
			92.1(1)		
			92.1(1)		
			92.3(1)		
64	$[Mn_2O_2(OAc)(mpepma)_2](ClO_4)_3 \cdot H_2O$			−122	263
65	$[Mn_2O_2(OAc)(Me_4dtne)](ClO_4)_3$	2.599(4)	92.6(2)	−100	264
66	$[Mn_2O_2(OAc)(bpy)_2(Cl_2)]_2(MnCl_4) \cdot 2CH_2Cl_2$	2.672(2)	95.4(2)	−45.0	202
			95.30(3)		
67a	$[Mn_2O_2(OAc)Cl(bpy)_2(H_2O)](NO_3)_2 \cdot (H_2O)$	2.670(1)	94.2(2)	−36.6	202
			95.4(1)		
67b	$[Mn_2O_2(OAc)Cl(bpy)_2(H_2O)](ClO_4)_2 \cdot CH_3CN$	2.652(1)	95.1(1)	−39.3	202
			94.7(1)		
	(iv-B) Bis(μ-oxo)(μ-hydrophosphato)				
	(a) Mn^{IV}−Mn^{IV}				
68a	$[Mn_2O_2(HPO_4)(H_2PO_4)_2(bpy)_2] \cdot H_2O$	2.702(2)			267
68b	$[Mn_2O_2(HPO_4)(H_2PO_4)_2(bpy)_2] \cdot 3H_2O$	2.703(2)	96.4(2)		267
			97.1(2)		
	(v-A) (μ-Oxo)bis(μ-carboxylato)				
	(a) Mn^{III}−Mn^{III}				
69	$[Mn_2O(OAc)_2(bpy)_2(H_2O)(S_2O_8)] \cdot H_2O$	3.145(5)	125.1(6)		275
70	$[Mn_2O(OAc)_2(H_2O)_2(bpy)_2](PF_6)_2 \cdot 1.75H_2O$	3.132(?)	122.9(?)	−3.4	269
71	$[Mn_2O(OAc)_2(H_2O)_2(bpy)_2](ClO_4)_2$	3.152(2)	122.7(2)		277
72	$[Mn_2O(OAc)_2(H_2O)_2(phen)_2](BF_4)_2 \cdot 3H_2O$	3.153(2)	123.3(4)		286
73	$[Mn_2O(OAc)_2(H_2O)(OAc)(phen)_2](BF_4) \cdot CH_3OH$	3.147(10)	121.5(2)		286
74	$[Mn_2O(O_2CC_6H_5)_2(N_3)_2(bpy)_2] \cdot MeCN \cdot 4H_2O$	3.153(4)	122.0(5)	+8.8	271, 277
75	$[Mn_2O(OAc)_2Cl_2(bpy)_2] \cdot CH_3COOH \cdot H_2O$	3.154(4)	124.3(7)	−4.1	277
76	$[Mn_2O(OAc)_2(HB(pz)_3)_2] \cdot 4CH_3CN$	3.159(1)	125.1(1)	−0.2	154
77	$[Mn_2O(OAc)_2(HB(pz)_3)_2] \cdot CH_3CN$	3.175(1)	125.0(3)	−0.7	154
78	$[Mn_2O(OAc)_2(tacn)_2](ClO_4)_2$	3.084(3)	117.9(2)	+9.0	268

Table 2 (Continued)

no.	compound	Mn···Mn (Å)	Mn−O_b−Mn (deg)	J (cm^{-1})	ref
	(v-A) (μ-Oxo)bis(μ-carboxylato) (a) Mn^{III}−Mn^{III} (Continued)				
79	$[Mn_2O(OAc)_2(Me_3tacn)_2](ClO_4)_2 \cdot H_2O$	3.150	120.9(1)	+9.0	268
80	$[Mn_2O(OAc)_2(Me_3tacn)_2](I_3)I \cdot H_2O$	3.096(2)	119.9(3)		272
81	$[Mn_2O(OAc)_2(tacn)(Me_3tacn)](ClO_4)_2$	3.121(2)	122.6(3)		153
82	$[Mn_2O(OAc)_2(bpea)_2](ClO_4)_2$	3.121(6)	124.1(8)		280
		3.106(6)	122.1(8)		
83	$[Mn_2O(OAc)_2(tmip)_2](ClO_4)_2 \cdot CH_3CN \cdot 0.5(CH_3)_2O$	3.164(5)	124.4(6)	−0.2	274
84	$[(Mn_2O(OAc)_2)_2(bbpmax)_2](ClO_4)_4 \cdot 3CH_3NO_2$	3.261	118.5(3)		279
85	$[Mn_2O(xdk)(4,4'\text{-}Me_2bpy)_2(NO_3)_2] \cdot 2.5CH_3OH$	3.170(2)	124.6(4)		281
86	$[Mn_2O(mpdp)(bpy)_2(MeCN)(H_2O)](ClO_4)_2 \cdot CH_3CN$	3.139	122.9		287
87	$[Mn_2O(phth)_2(bpy)_2(H_2O)_2](NO_3)_2$	3.148(3)	125.2(6)		287
88	$[Mn_2O(phth)_2(bpy)_2(H_2O)(NO_3)](NO_3)$	3.155(3)	121.8(5)		287
89	$[Mn_2O(OAc)_2(ttco)_2](PF_6)_2$	3.155(2)	122.2(3)	+4.6	285
90	$[Mn_2O(OAc)_2(bbae)_2](ClO_4)_2$			−1.72	270
91	$[Mn_2O(OAc)_2(mpepma)_2](PF_6)_2 \cdot H_2O$			+1.0	278
92	$[Mn_2O(OAc)_2(tmip)_2](ClO_4)_2$			−0.2	274
93	$[Mn_2O(OAc)_2(tppn)]_2(ClO_4)_4 \cdot CH_3CN$			+11	273
	(b) Mn^{III}−Mn^{IV}				
94	$[Mn_2O(OAc)_2(Me_3tacn)_2](ClO_4)_3$	3.230(3)	125.1(3)	−40	290
	(v-B) (μ-Oxo)bis(μ-phenylboronic acid) (a) Mn^{IV}−Mn^{IV}				
95	$[Mn_2O(O_2BPh)_2(Me_3tacn)_2](PF_6)_2$	3.180(3)		+10	291
	(vi) Tris(μ-oxo) (a) Mn^{IV}−Mn^{IV}				
96	$[Mn_2O_3(Me_3tacn)_2](PF_6)_2 \cdot H_2O$	2.296(2)	84.0(3)	−390	255
	(vii) Bis(μ-oxo)(μ-peroxo) (a) Mn^{IV}−Mn^{IV}				
97	$[Mn_2O_2(\mu\text{-}O_2)(Me_3tacn)_2](ClO_4)_2$	2.531(7)	83.1(7)		293
			83.5(7)		
	(viii) Bis(μ-oxo)bis(μ-carboxylato) (a) Mn^{III}−Mn^{IV}				
98	$[Mn_2O_2(Ar^{Tol}CO_2)_2(bpy)_2](ClO_4)$	2.505(1)	88.5(1)		221
			88.1(1)		

[a] Employing the $H = -2JS_1 \cdot S_2$ convention.

Scheme 3. Observed Core Types for the Dinuclear Manganese Complexes

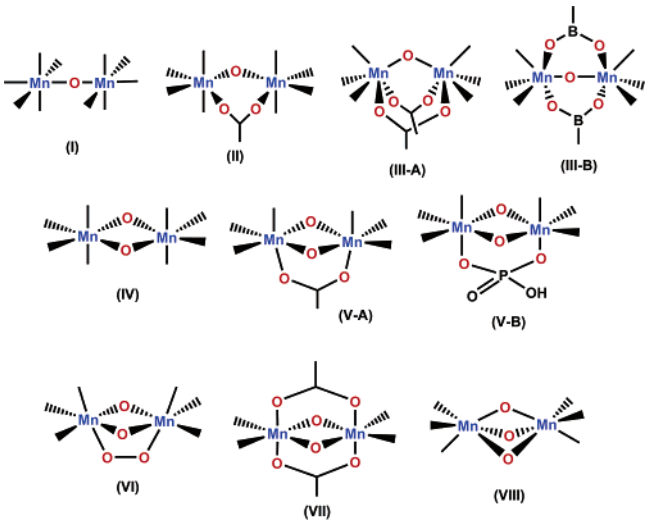

elucidate the structure and function of the manganese cluster in PSII. Although we are not discussing the dimanganese(II,III) complexes in this review, it should be mentioned that a hydroxo bridged $Mn^{II,III}_2$ complex, $[Mn_2(\mu\text{-}OH)(\mu\text{-}O_2CC(CH_3)_3)_2]^{2+}$, was reported by Wieghardt and co-workers.[224,225] This complex exhibits a 21-line hyperfine EPR signal at 7.2 K, which has similarity with the reduced S_{-2} state.[121−123] A similar structural motif is also postulated to be present in the PSII S_0 state.[96,98]

In general, the manganese centers in dinuclear manganese-oxo complexes are six-coordinate. Thus, the number of coligands that can be attached to the manganese centers in a particular core type depends on the denticity of the ligands. On the other hand, in some cases the formation of a particular core type has been achieved through the use of steric effects of the ligands. It should be noted that the stabilization of high oxidation states (III and IV in Scheme 3) in these complexes can be influenced by the choice and design of the coligands to some extent, as only two core types (I and IV) exist in all three combinations of oxidation states. Out of these three combinations, one set (III, IV) gives the inequivalency of the manganese centers. This inequivalency can easily be identified in the dinuclear complexes with localized oxidation states due to the fact that only the Mn(III) center with a d^4 electronic configuration undergoes a Jahn−Teller distortion. Selected structural and magnetic properties of these complexes are presented in Table 2.

4.4.1.1. (μ-Oxo). Complexes with core type I have either strong field ligands, such as CN^-, Pc, (phthalocyanate), and TPP (tetraphenyl porphyrin), or Schiff base ligands and have been prepared and structurally characterized for (III,III), (III,IV), and (IV,IV) oxidation states. Regardless of the oxidation

states, the Mn−O−Mn unit in the dinuclear complexes is linear in most cases.

4.4.1.1.1. Mn^{III}−Mn^{III}. The first such complex, $[\{Mn(pc)py\}_2O]\cdot 2py$ (**1**), was reported by Vogt et al. in 1966.[226,227] $K_7[Mn_2O(CN)_{10}](CN)$ (**2**), an organometallic complex, was synthesized from the reaction of $KMnO_4$ and KCN.[228] The Mn···Mn separations in **1** (3.42 Å) and **2** (3.446 Å) and the Mn−O−Mn angles in **1** (178°) and **2** (180°) are very similar.

Complexes with pentadentate Schiff base ligands, $[Mn_2O(5\text{-}NO_2\text{-saldien})_2]$ (**3**) and $[Mn_2O(bpmsed)_2](ClO_4)_2$ (**4**), show differences in structural properties.[229,230] The Mn···Mn separations in **3** (3.490(2) Å) and **4** (3.516(2) Å) are similar, while the Mn−O−Mn angles in **3** and **4** are 168.4(2)° and 180°, respectively. The deviation from collinearity of the Mn−O−Mn angle in **3** has been attributed to steric constraints imposed by the Schiff base ligand.[229] Complex **3** is the only example for core type I with an Mn−O−Mn angle that deviates markedly from linearity. Both complexes show strong antiferromagnetic interaction between the metal centers with the extent of the interaction ($J = -120$ cm^{-1} for **3** and -108 cm^{-1} for **4**, where the expression $\hat{H} = -2J\hat{S}_1\hat{S}_2$ has been employed here and for all other magnetic exchange interactions discussed in this review) perhaps being related to the Mn−O−Mn angles.

Tridentate and tetradentate ligands, terpy and bpia, also stabilize such a core: $[Mn_2O(terpy)_2(CF_3CO_2)_4]$ (**5**)[231] and $[Mn_2O(bpia)_2Cl_2](ClO_4)_2$ (**6**).[232] Complex **5** is stable only in the solid state, as its dissolution in CH_3CN results in formation of the corresponding di-oxo bridged mixed-valent species, $[Mn_2O_2(terpy)_2(CF_3CO_2)_2](ClO_4)$ (**37**), and a mononuclear Mn^{II} complex. Interestingly, compound **5** was obtained during an attempt to recrystallize the mixed-valent species, **37**. X-ray crystallographic studies of **5** show two forms having cis and trans configurations with respect to the orientation of the monodentate $CF_3CO_2^-$ ligands. Complex **6** was prepared by allowing a DMF solution of $[Mn_2O(OAc)(bpia)_2](ClO_4)_3$ (**13**) to react with 0.12 M HCl in acetonitrile. The bridging oxygen atom lies on a crystallographic inversion center, generating a linear Mn−O−Mn unit, with an Mn···Mn distance of 3.5326(9) Å. The cyclic voltammogram of **6** exhibits two quasireversible oxidation waves ($E_{1/2}$ values of 1.09 and 1.54 V vs SCE) and one quasireversible reduction wave ($E_{1/2}$ value of 0.63 V vs SCE). The complex $[Mn_2O(HB(3,5\text{-}^iPr_2\text{-}pz)_2(3\text{-}^iPrO\text{-}5\text{-}^iPr\text{-}pz))_2]$ (**7**) is the other example, which resulted from the oxidation of one of the isopropyl groups of the ligand as a coproduct during the synthesis of **17** under aerobic conditions from the corresponding bis(μ-hydroxo)-dimanganese(II,II) species.[233]

4.4.1.1.2. Mn^{III}−Mn^{IV}. $[Mn_2O(bpmsed)_2](ClO_4)_{2.37}(PF_6)_{0.63}$ (**8**), reported by Girerd and co-workers, is the only example of an Mn(III,IV) complex in this class.[230] It was prepared by bulk-electrolysis of **4** in CH_3CN. The authors noted that the source of PF_6^- in **8** was from a contaminated electrode. With an Mn−O−Mn angle of 178.7(2)°, complex **8** shows strong antiferromagnetic interaction between the manganese centers ($J = -176.5$ cm^{-1}), resulting in an $S = {}^1/_2$ ground state. As expected, the Mn(IV)−O_{oxo} distance (1.727(2) Å) is shorter than the Mn(III)−O_{oxo} distance (1.797(2) Å). At liquid nitrogen temperature it displays a 16-line EPR signal centered at $g \approx 2$ with rhombic symmetry of ligands around the Mn(III) center.

4.4.1.1.3. Mn^{IV}−Mn^{IV}. Using a porphyrin ligand, the only complex with core type I at the $Mn^{IV}Mn^{IV}$ oxidation state, $[\{(N_3)Mn(TPP)\}_2O]$ (**9**), has been isolated.[234] Interestingly, the Mn···Mn separation (3.537 Å) in **9** is the longest for all dinuclear complexes reported here. The Mn−O−Mn angle in **9** is 180°.

4.4.1.2. (μ-Oxo)(μ-carboxylato). *4.4.1.2.1. Mn^{III}−Mn^{III}.* Complexes with core type II have been obtained only with tetradentate ligands such as tmima, bispicen, bispicMe_2en, and bpia (**10**−**13**).[232,235,236] These complexes are prepared by a reaction between the corresponding ligand and either $Mn(OAc)_3\cdot 2H_2O$ in methanol/ethanol followed by the addition of $NaClO_4$ or a mixture of $Mn(ClO_4)_2\cdot 6H_2O$ and $NaOAc\cdot 3H_2O$ in water followed by the addition of $HClO_4$ to adjust the pH to 5. The Mn···Mn separations and the Mn−O−Mn angles in these complexes (**10**−**13**) range from 3.25 to 3.29 Å and from 130.8° to 131.0°, respectively. These complexes show weak to moderate ferromagnetic interaction between the metal centers ($J = +1.33$ for **10**; $+19.5$ cm^{-1} for **11**). The solution electronic spectra of these complexes display ligand to metal charge transfer and d−d transitions.

4.4.1.3. Bis(μ-oxo). This is one of the two core types that exists in (III,III), (III,IV), and (IV,IV) oxidation states. Interestingly, examples for the mixed-valent complexes are much more prevalent than those for the other two.

4.4.1.3.1. Mn^{III}−Mn^{III}. There are only a few examples of the dimanganese(III,III) species with tetradentate N-donor ligands, such as bpen, bpmpa, bped, and bispicMe_2en, and the tridentate $HB(pz)_3^-$ ligand (**14**−**18**) (see Table 2).[237−240] In these complexes, the Mn···Mn separations and the Mn−O−Mn angles vary from 2.674 to 2.699 Å and from 92.1° to 97.0°, respectively. The manganese(III) centers in these complexes are strongly antiferromagnetically coupled ($J = -86.5$ to -100.5 cm^{-1}). While complexes with tetradentate ligands have octahedral geometry at the manganese centers, steric crowding of the tridentate ligand, $HB(3,5\text{-}^iPr_2pz)_3^-$, results in five coordinate manganese centers.[239] The solution electronic spectra of these complexes are characteristic of the $[Mn_2(\mu\text{-}O)_2]^{2+}$ core.

4.4.1.3.2. Mn^{III}−Mn^{IV}. Compared to the few examples of bis(μ-oxo) dimanganese(III,III) complexes mentioned above, there are a multitude of examples for the corresponding (III,IV) cores, representing the second largest group after those with the core type III-A (see below). More than four decades ago, Nyholm and Turco[241] reported the first complex of this type, $[Mn_2O_2(bpy)_4](ClO_4)_3$ (**19**), the detailed spectroscopic and magnetic properties of which were studied by Cooper et al.[242] Compound **19** was structurally characterized in 1972 by Plaksin et al.[243] The corresponding phen derivative (**20**) was also synthesized and structurally characterized.[244] A number of bi-

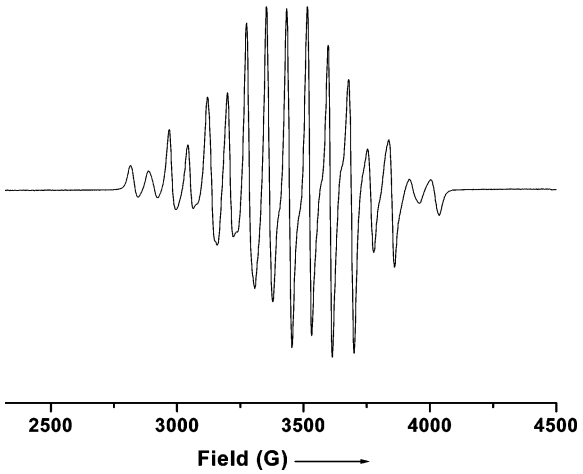

Figure 10. Typical X-band 16-line EPR signal for the dinuclear $Mn^{III}Mn^{IV}$ complex in the perpendicular mode at ≤77 K.[221]

dentate and tetradentate ligands have been used to make many such complexes (**21**−**35** and **38**−**40**).[153,208,232,238,240,245−252] Obviously, complexes with two bidentate ligands or one tetradentate ligand on each manganese center do not have an open site for the binding of a labile group, such as halide, water, or carboxylic acids. The most common method used to synthesize these complexes is a comproportionation reaction between Mn^{II} and Mn^{VII} starting materials in a 7:3 ratio in the presence of the various ligands. A complex with the tridentate ligand terpy, $[Mn_2O_2(terpy)_2(H_2O)_2](NO_3)_3$ (**36**), has been reported recently, independently by Collomb et al. and Limburg et al.[253,254] In this complex one water molecule is terminally coordinated to each metal center. It was prepared by oxidizing a Mn^{II} salt with an equivalent amount of oxone ($2KHSO_5{\cdot}KHSO_4{\cdot}K_2SO_4$) or $KMnO_4$ in water followed by appropriate workup. A similar complex, $[Mn_2O_2(terpy)_2(CF_3CO_2)_2](ClO_4)$ (**37**), was prepared following the synthesis of the diaquo species except that solid CF_3CO_2Na was added to the resulting reaction mixture.[231] In both complexes, the terminal triflate ligands are anti to each other and lie in the plane of the Mn_2O_2 moiety.

The Mn···Mn separations in this class of complexes (**19**−**40**) range between 2.624(2) and 2.741(1) Å. These compounds possess Jahn−Teller distortion at the Mn(III) center. The metal ions in these complexes are intramolecularly coupled through strong antiferromagnetic interactions ($J = -118.5$ to -221 cm^{-1}). Below 77 K in frozen solutions, all of them display the typical 16−19-line EPR signal centered at $g \approx 2$ (as shown in Figure 10).

4.4.1.3.3. Mn^{IV}−Mn^{IV}. A number of complexes (**41**−**50**) with bidentate, tridentate, and tetradentate ligands has been reported.[153,216,244,245,249,255−258] While the complexes with bidentate and tetradentate ligands have all sites occupied on each manganese center, complexes with tridentate ligands, such as tacn or bpea, have one vacant site on each manganese center for an additional ligand, such as OH^-, F^-, or Cl^- (**46**, **48**, **49**). These donors are anti to each other with respect to the Mn_2O_2 unit. These complexes also have strongly antiferromagnetically coupled dimanganese centers ($J = -82$ to -147 cm^{-1}). The value of this exchange coupling greatly depends on the Mn−O−Mn angle. A recent magnetostructural correlation has been established between the J and Mn−O−Mn angle, where J values range over 110 cm^{-1} with an Mn−O−Mn range of only 3.9°.[259]

4.4.1.4A. Bis(*μ*-oxo)(*μ*-carboxylato). *4.4.1.4A.1. Mn^{III}−Mn^{IV}.* Most of the symmetric complexes with core type V-A have been synthesized with tridentate or spanning hexadentate ligands (**51**−**60**).[206,211,260−264] Following the discovery of $[Mn_2O_2(OAc)(tpen)](ClO_4)_2$ (**53**) by Pal and Armstrong,[262] two other complexes with aliphatic hexadentate ligands (dtne and Me_4-dtne) were reported: $[Mn_2O_2(OAc)(dtne)](BPh_4)_2$ (**56**) and $[Mn_2O_2(OAc)(Me_4dtne)](BPh_4)_2$ (**57**).[264] $[Mn_2O_2(OAc)(bpy)_2Cl_2]$ (**51**) is the only example with a bidentate terminal ligand.[265] Two complexes, $[Mn_2O_2(OAc)(Me_3tacn)(OAc)_2]$ (**54**) and $[Mn_2O_2(OAc)(Me_3tacn)(bpy)(MeOH)](ClO_4)_2$ (**55**), isolated and structurally characterized by Wieghardt and co-workers,[261] possess different structural features at the Mn(III) centers. In the first complex, the Mn(III) center is six-coordinate with bpy and methanol as terminal ligands while, in the latter complex, the Mn(III) center is bound only to two monodentate acetate groups and is thus five-coordinate. The Mn(IV) center in both cases is coordinated to the Me_3tacn ligand. Similar to the complexes with core type IV, these complexes with a third bridging group have short Mn···Mn distances (2.553(1) to 2.667(2) Å) with metal centers strongly antiferromagnetically coupled ($J = -90$ to -220 cm^{-1}). Below 77 K they also display 16-line EPR signals centered at $g \approx 2$.

Recently, Marlin, Wieghardt, and co-workers reported synthesis and spectroscopic properties of a dinuclear system, $[Mn_2O_2(O_2CPhNIT)(Me_4dtne)](ClO_4)_2$ (**58**) (where $HO_2CPhNIT$ = 2-(4-carboxyphenyl)-4,4,5,5-tetramethyl-3-oxyimidazolidin-1-oxide), where the antiferromagnetically coupled $Mn^{III}Mn^{IV}$ dinuclear unit ($J = -127$ cm^{-1}) interacts with a radical from the nitronyl nitroxide (NIT) moiety of the bridging carboxylate (with $J = -1$ (± 1) cm^{-1}) to give rise to a triplet spin ground state.[206] As a result, the EPR spectra of the complex are altered dramatically. A broad signal at $g \approx 2$ with less overall splitting was detected at 20 K in the perpendicular mode, which is quite distinct from the typical "16-line" spectrum. In addition, a well-resolved multiline signal that resembles somewhat the "16-line" pattern of other $Mn^{III}Mn^{IV}$ dinuclear species was observed with a lower intensity at $g \approx 4$. The intensity of this signal was greatly improved with parallel mode detection as a result of the allowed transition. The authors emphasize that interaction between the radical and the dimanganese unit observed in **58** is relevant to the "so-called" "$S_2Y_Z^{\bullet}$ EPR signal" or "split" signal (see section 2.4). More precise studies are currently underway to recognize a relationship between the $g \approx 4$ signal and the S_2-state EPR signal.

4.4.1.4A.2. Mn^{IV}−Mn^{IV}. Complexes with an $[Mn_2O_2(OAc)]^{3+}$ core have been reported with bidentate, tridentate, and hexadentate ligands (**61**−**67**).[202,205,211,222,263,264,266] For the bidentate bpy ligand, the complex $[Mn_2O_2(OAc)(H_2O)_2(bpy)_2](ClO_4)_3$ (**62**) has one site on each manganese center bound to a

water molecule. The Mn···Mn distances in these complexes vary between 2.580 and 2.642 Å). However, the intermolecular interaction between the metal ions in the diaqua complex (two measurements: $J = -43.7$ or -67 cm^{-1}) is weaker than those ($J = -100$ to -124 cm^{-1}) for the complexes with tridentate and hexadentate ligands. Recently, several bis(μ-oxo)(μ-carboxylato) complexes with terminally bound chloride and water were synthesized with bpy as the chelating ligand, where Ce^{4+} served as the oxidant.[202] The complexes, $[Mn_2O_2(OAc)(Cl)_2(bpy)_2]^+$ (**66**) and $[Mn_2O_2(OAc)(H_2O)Cl(bpy)_2]^{2+}$ (**67**), were structurally characterized. The coupling interactions between Mn centers in these complexes were found to be weaker as well ($J = -36$ to -45 cm^{-1}; see Table 2).

4.4.1.4B. Bis(μ-oxo)(μ-hydrophosphato). *4.4.1.4B.1. $Mn^{IV}-Mn^{IV}$.* Reaction of $[Mn_2O_2(bpy)_4](ClO_4)_3$ (**19**) with H_3PO_4 in acetonitrile at room temperature generates the hydrophosphato-bridged complex, $[Mn_2O_2(HPO_4)(H_2PO_4)_2(bpy)_2]$ (**68**) by ligand exchange.[267] The core is shown as type V-B in Scheme 3. It is similar to the tribridged complexes with a type V-A core except that the bridging carboxylate group is replaced with the hydrophosphato group. It has an Mn···Mn distance of 2.703(2) Å. The terminal dihydrogen phosphate groups are configured anti to one another.

4.4.1.5A. (μ-Oxo)bis(μ-carboxylato). As can be seen below, this core with oxidation state III is very common. Complexes with this core type have been used to synthesize other dinuclear or higher nuclearity complexes.

4.4.1.5A.1. $Mn^{III}-Mn^{III}$. Complexes containing the core type III-A with various bidentate and tridentate ligands as well as spanning hexadentate polypyridyl coligands represent the largest group of dinuclear complexes described in this section (**69**−**93**).[152,154,210,224,268−288] For these triply bridged complexes, a tridentate ligand or half of a spanning hexadentate ligand completes the coordination site of each hexacoordinated manganese center, while the bidentate ligands leave one coordination site on each manganese(III) center to be filled by an easily exchangeable ligand, such as water,[269,275,277,286] nitrate ion,[287] chloride,[277] or azide.[271,277] Use of the spanning hexadenate ligands, such as tppn and bbpmax, results in tetranuclear complexes containing two $[Mn_2(\mu\text{-O})(\mu\text{-OAc})_2]^{2+}$ cores (**93** and **84**, respectively). Most of these complexes contain monofunctional carboxylates such as acetate, benzoate, and so forth as bridging ligands, but dicarboxylates such as mpdp or XDK have also been employed. There are two common synthetic routes used in making these complexes: (i) oxidation of a Mn(II) salt, such as MnX_2 (X = OAc^-, Cl^-, or ClO_4^-), with $HClO_4$, $(NH_4)_2S_2O_8$, Cl_2, $NaIO_4$, or $KMnO_4$ in the presence of the ligand; and (ii) reaction of $Mn(OAc)_3$ with the ligand.

A recent example of such a complex, $[Mn_2O(OAc)_2(ttco)_2](PF_6)_2$ (**89**), reported by Bolm et al., contains the chiral ttco ligand and thus has been found to be catalytic in enantioselective epoxidations.[285] In the cation of $[(Mn_2O(OAc)_2)_2(bbpmax)_2](ClO_4)_4$ (**84**), the two dinuclear units are related to each other by a mirror plane. Tanase and Lippard used a sterically crowded dicarboxylate ligand XDK in anticipation of synthesizing a complex with terminal ligands cis to each other.[281] However, the complex $[Mn_2O(xdk)(dmb)_2(NO_3)_2]$ (**85**) contains instead nitrate ligands anti to each other.

The Mn···Mn separations in these complexes range from 3.08 to 3.26 Å, while the Mn−O−Mn angles vary between 117.9 and 125.1°. Variable temperature magnetic measurements for these complexes indicate both weakly ferromagnetic and antiferromagnetic interactions between manganese(III) centers (see Table 2). Solution electronic absorption spectra observed for these complexes show a characteristic pattern that can be associated with this core type.[289]

4.4.1.5A.2. $Mn^{III}-Mn^{IV}$. Mixed-valent (III,IV) complexes with core type III-A are unusual, as evidenced by the fact that there is only one such complex, $[Mn_2O(OAc)_2(Me_3tacn)_2](ClO_4)_3$ (**94**), that has been reported to date.[290] It was prepared by the oxidation of the corresponding (III,III) complex with $S_2O_8^{2-}$. The Mn···Mn distance (3.230(3) Å) in this complex is longer than that of the corresponding (III,III) complex but with a similar Mn−O−Mn angle (125.1(3)°). Furthermore, the interaction between manganese centers is stronger in this complex with a J value of -40 cm^{-1}.

4.4.1.5B. (μ-Oxo)bis(μ-phenylboronic Acid). *4.4.1.5B.1. $Mn^{IV}-Mn^{IV}$.* As seen in the section above, stabilization of a tribridged (μ-oxo)bis(μ-carboxylato) core at the +4 oxidation state has not been achieved. However, using a dianionic congener of a caboxylate group, $PhBO_2^{2-}$, as a bridging ligand, Wieghardt and co-workers were able to synthesize and structurally characterize the first and only complex with core type III-B: $[Mn_2O(O_2BPh)_2(Me_3tacn)_2](PF_6)_2$ (**95**).[224,291] The Mn···Mn separation (3.180(3) Å) in this complex is very similar to those with core type III-A. Variable temperature magnetic measurements show that the metal centers are ferromagnetically coupled by an exchange interaction ($J = +10$ cm^{-1}) that gives rise to an unusual ground state of S = 3. For both frozen acetonitrile solution and solid state, it exhibits integer-spin EPR signals at Q-band and X-band frequencies at 12 K.

4.4.1.6. Tris(μ-oxo). *4.4.1.6.1. $Mn^{IV}-Mn^{IV}$.* Wieghardt et al. reported the first and only example of a tris(μ-oxo) complex, $[Mn_2O_3(Me_3tacn)_2](PF_6)_2$ (**96**), which has the shortest Mn···Mn distance (2.296(2) Å).[255,292] It was prepared from the reaction of $[Mn_2O(OAc)_2(Me_3tacn)_2](ClO_4)_2$ (**79**) with NEt_3 in a water/ethanol solvent mixture. On the basis of variable temperature magnetic measurements, it shows the strongest antiferromagnetic interaction between the metal centers ($J = -390$ cm^{-1}). The authors concluded that a direct Mn···Mn exchange pathway does not contribute to this strong coupling interaction.

4.4.1.7. Bis(μ-oxo)(μ-peroxo). *4.4.1.7.1. $Mn^{IV}-Mn^{IV}$.* The only example of a dinuclear peroxo-bridged complex, $[Mn_2O_2(\mu\text{-}O_2)(Me_3tacn)_2](ClO_4)_2$ (**97**), was reported by Wieghardt and co-workers.[293] Brown crystals of it were obtained by keeping a reaction mixture of $Mn(ClO_4)_2 \cdot 6H_2O$, Me_3tacn, and NaOMe in methanol for 3 days in the presence of air at −5 °C.

Table 3. Trinuclear Manganese Complexes

no.	compound	characterization	core type	ref
99	$[Mn_3O(O_2CMe)_2(O-O)(dien)_3]^{3+}$	X-ray, EPR, Raman	i	296
100	$[Mn_3(saladpH)_2(OAc)_4(CH_3OH)_2]$	X-ray, conductivity, EPR, IR, magnetism, UV−vis	ii	294
101	$[Mn_3(saladpH)_2(sal)_4]$	X-ray, EPR, FAB-MS, magnetism, NMR, IR, UV−vis	ii	300
102	$[Mn_3(\mu\text{-}OH)_2(\mu\text{-}OAc)_4(HB(3,5\text{-}^iPr_2\text{-}pz)_3)_2]$	X-ray, IR, magnetism	ii	303
103	$[Mn_3(bhdmen)_2(2,6\text{-}dcba)_2(OH)_2]$	X-ray, IR, magnetism	ii	304
104	$[MnL'_2Mn(H_2O)]^{3+}$	X-ray, CD, EPR, magnetism, UV−vis	iii	305
105	$[Mn_3(mcoe)_6]^+$	X-ray, IR, magnetism, powder XRD	iii	307
106	$[Mn_3(L'')(\mu\text{-}OMe)]^{3+}$	X-ray, CV, EPR, magnetism, UV−vis (NIR), XPS	iii	309
107	$[Mn_3(pko)_4(CH_3O)_2(SCN)_2]$	X-ray, EPR, magnetism, XAS	iv	310
108	$[Mn_3O_4(OAc)_4(bpy)_2]$	X-ray, magnetism	v	312
109	$[Mn_3(\mu\text{-}O)_3(tacn)_3(\mu_3\text{-}PO_4)]^{3+}$	X-ray, magnetism, IR, UV−vis	vi	292
112	$[Mn_3(\mu\text{-}O)_4(bpy)_4Cl_2]^{2+}$	X-ray, EPR, magnetism	vii-A	313
113	$[Mn_3(\mu\text{-}O)_4(bpy)_4(H_2O)_2]^{4+}$	X-ray, CV, EPR, UV−vis	vii-A	314
114	$[Mn_3(\mu\text{-}O)_4(bpea)_3(OH)]^{3+}$	X-ray, CV, EPR, IR, magnetism, UV−vis	vii-B	211
115	$[Mn_3(\mu\text{-}O)_4(phen)_4(H_2O)_2]^{4+}$	X-ray, EPR, magnetism, UV−vis	vii-A	315
116	$[\{Mn_3(\mu\text{-}O)_4(OH)\}_2(tpen)_3]^{6+}$	X-ray, CV, EPR, IR, UV−vis	vii-B	222

The Mn···Mn distance (2.531(7) Å) and the average Mn−O−Mn angle (83.3°) are the shortest distance and smallest angle for a triply bridged bis(μ-oxo) core. It is stable in organic solvents but releases O_2 (100%) in an aqueous chloride solution and generates Mn(III) species. The O_2 release step can be considered as a model of O_2 release in PSII.

4.4.1.8. Bis(μ-oxo)bis(μ-carboxylato). *4.4.1.8.1. $Mn^{III}-Mn^{IV}$.* Utilizing steric effects of a bulky carboxylate ligand, 2,6-di(*p*-tolyl)benzoate ($Ar^{tol}CO_2^-$), Mukhopadhyay and Armstrong recently synthesized and structurally characterized a species possessing an unprecedented core (type VII in Scheme 3): $[Mn_2O_2(Ar^{tol}CO_2)_2(bpy)_2](ClO_4)$ (**98**).[221] This mixed-valent complex is obtained in high yield (~87%) from the substitution reaction of $[Mn_2O_2(bpy)_4](ClO_4)_3$ (**19**) with $Ar^{tol}CO_2Na$ (in a 1:2 ratio) in CH_3CN. Interestingly, a heaxanuclear complex, $[Mn_6O_8(dmb)_6(Ar^{tol}CO_2)_2]^{4+}$ results if the corresponding 4,4′-dimethyl-2,2′-bpy (dmb) derivative (**35**) was used as the starting material.[218] The tetrabridged solid-state valence-trapped complex, **98**, shows a characteristic Jahn−Teller elongation at the Mn^{III} center, antiferromagnetic interaction between the manganese centers, and a 16-line EPR signal centered at $g \approx 2$ at 4 K. However, it has several unique features: (a) the shortest Mn···Mn distance (2.505(1) Å) for any bis(μ-oxo)dimanganese species, (b) distinct UV−vis and NMR spectra, (c) inertness toward oxidation or reduction, and (d) bpy ligands that are coplanar with the Mn_2O_2 moiety while the bulky carboxylates reside on each side of the $[Mn_2O_2]$ plane.

4.4.2. Trinuclear Manganese Complexes

Synthesis of trinuclear manganese clusters (Mn_3) as a goal in modeling the active site of water oxidase originally stem from the idea that a trinuclear unit is in electron-transfer equilibrium with a mononuclear center in PSII.[294] Recent crystallographic data in addition to the EXAFS,[13] pulsed EPR,[81] and DFT calculations[17] support a topology where a fourth Mn center is predicted to be connected to a trinuclear unit. Several possibilities are shown in Scheme 1 (A−D, F, G, J, and K). Numerous high-valent trinuclear complexes containing varied core types have been synthesized and characterized. Some of these core structures are shown in Scheme 4. Table 3 lists the complexes that are discussed in this section.

Scheme 4. Observed Core Types for Trinuclear Manganese Complexes

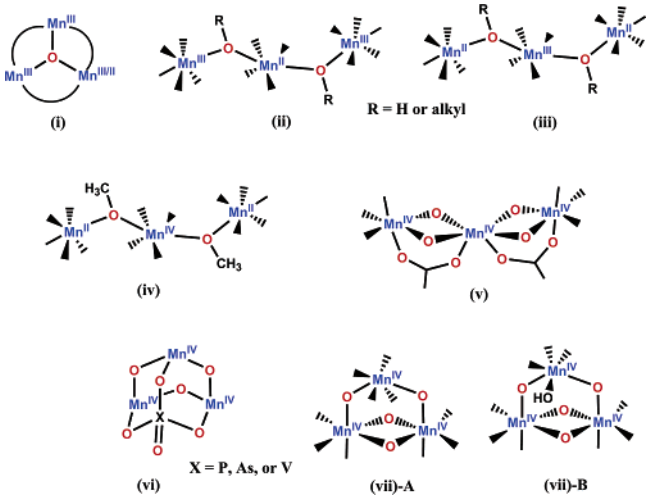

4.4.2.1. Basic Carboxylates with a $[Mn_3O]$ Core. Trinuclear complexes containing a $[Mn_3O(O_2CR)_6]^{+/0}$ core with Mn_3(III) or mixed-valent Mn_3(II,III,III) centers possess what is referred to as the "basic carboxylate" structure. These complexes have been thoroughly structurally and spectroscopically characterized[287,295] and used as starting materials for the synthesis of several higher-valent manganese clusters.[204,212,213] Another noteworthy complex with the same triangular geometry, $[Mn^{III}_3O(OAc)_2(O-O)(dien)_3]^{3+}$ (**99**), was reported by Weatherburn and coworkers. In this structure a peroxo group instead of a carboxylate was shown to bridge two of the three Mn(III) centers.[296] This complex was formed when either $Mn(OAc)_2$ or $Mn(OAc)_3$ was allowed to react with dien in refluxing methanol solution. An intense band at 814 cm^{-1} in the Raman spectrum was assigned as the peroxo O−O stretching frequency. A 16-line EPR signal centered at $g = 2$ at −160 °C was reported for this species, the origin of which is unclear. This complex was the first crystallographic evidence of dioxygen bound to a manganese cluster. The poor quality of the crystal structure leaves room for other interpretations. A possible mechanism for

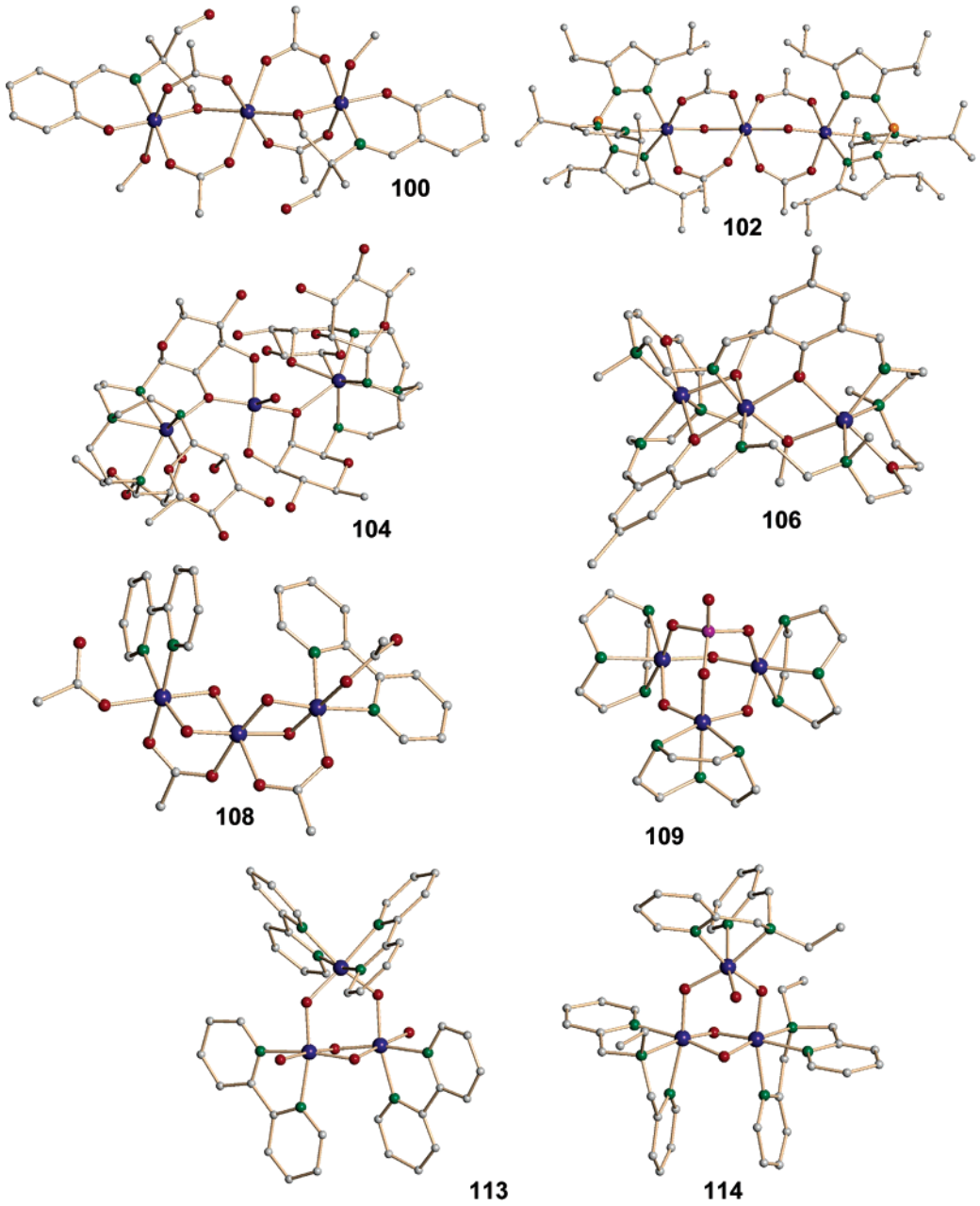

Figure 11. Crystal structures of selected trinuclear manganese complexes portraying various core types. The Mn atoms are shown in blue, O atoms in red, N atoms in green, B atoms in orange, P atom in purple, and C atoms in gray.

the release of O_2 observed in acidic medium can be considered for this complex, which is relevant to the PSII active site. Recent DFT calculations on this complex by Delfs and Stranger suggested that although the O−O bond is somewhat longer (calculated 1.35 Å vs observed 1.6 Å) in this complex compared to the calculated value, it does not cleave to form two Mn^{IV}═O bonds in the Mn_3 complex, as the calculated bond length for the latter would be 1.94 Å, 0.35 Å longer than the observed value. This theoretical study predicts that the $[Mn^{III}_3(\mu\text{-O}-\text{O})]^{3+}$ structure is stabilized by only 0.2 eV over the $[Mn^{III}Mn^{IV}_2(O)_2]^{3+}$ structure.[297] For a detailed discussion see section 4.5.

4.4.2.2. Open-Structure Mixed-Valent Trinuclear $Mn^{III}Mn^{II}Mn^{III}$ Complexes. The first open-structure mixed-valent trinuclear $Mn^{III}Mn^{II}Mn^{III}$ complex supported by a tridentate Schiff base ligand, saladpH$_3$, $[Mn_3(saladpH)_2(OAc)_4(CH_3OH)_2]$ (**100**), was reported by Pecoraro and co-workers.[294] This was followed by a series of trinuclear complexes with the general formula $Mn^{III}_2Mn^{II}L_2(OAc)_4X_2$ (where L = Schiff base ligands and X = solvents).[298,299] These complexes have linear (α-isomer) or bent (β-isomer) geometry with Mn···Mn separations of ∼3.5 Å. A representative structure of the α-isomer is shown in Figure 11. Most of these mixed-valent compounds show very weak antiferromagnetic coupling among the manganese centers with J ranging from −3 to −7 cm^{-1}, giving rise to a $S = {}^3/_2$ ground state. These complexes exhibit a broad low-field EPR signal at $g \approx 4$, supporting an $S = {}^3/_2$ spin ground-state assignment.[295,299]

Kessissoglou and co-workers recently reported an EPR- and ^{1}H NMR-active mixed-valent $Mn^{III}Mn^{II}$-Mn^{III} complex, $[Mn_3(saladpH)_2(sal)_4]$ (**101**), with a Mn···Mn separation of 3.495 Å and a Mn−Mn−Mn

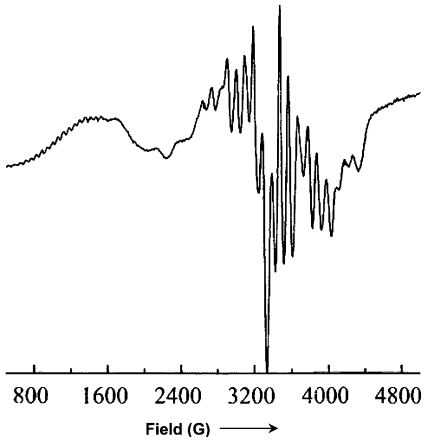

Figure 12. X-band EPR spectra of **101** in $CHCl_3$ glassy solution at ~4 K in the range 400−4800 G (Reproduced with permission from ref 300. Copyright 2000 American Chemical Society).

angle of 180°.[300] The terminal Mn(III) centers possess distorted square-pyramidal geometry, having an open coordination site indicating the possibility of potential substrate/water binding, as could be the case for the Mn_4 cluster in the PSII active site. This compound exhibits a broad EPR signal around $g \approx 3.6$ and $g \approx 4$ arising from an $S = {}^3/_2$ state and a ~19-line hyperfine signal centered at $g \approx 2$ at 4 K (Figure 12), which is relevant to the S_2 multiline signal. Several other phenolato-, alkoxo-, or carboxylato-bridged $Mn^{III}Mn^{II}Mn^{III}$ complexes have been reported.[301,302]

A mixed-valent $Mn^{III}Mn^{II}Mn^{III}$ complex comprising a [Mn(μ-OH)(μ-OAc)$_2$Mn(μ-OH)(μ-OAc)$_2$Mn] core, supported by tridentate HB(3,5-^{i}Pr$_2$-pz)$_3^-$, [Mn_3(μ-OH)$_2$(μ-OAc)$_4$(HB(3,5-^{i}Pr$_2$-pz)$_3$)$_2$] (**102**), was reported by Kitajima and co-workers.[303] The Mn centers are weakly antiferromagnetically coupled with an average Mn···Mn separation and Mn−Mn−Mn angle of ~3.4 Å and ~177°, respectively. The crystal structure is shown in Figure 11. Another μ-hydroxo, μ-carboxylato linear $Mn^{III}Mn^{II}Mn^{III}$ complex, [Mn_3(bhdmen)$_2$(2,6-dcba)$_2$(OH)$_2$] (**103**), was synthesized recently with a tripodal tetradentate ligand, bhdmen (where 2,6-dcba = 2,6-dichlorobenzoic acid).[304] The Mn···Mn separation was found to be 3.124(1) Å. The Mn−O(H)−Mn and Mn−O(R)−Mn angles are 102.1(2)° and 97.8(1)°, respectively. Very weak antiferromagnetic interactions ($J = -1.26$ cm^{-1}) were detected between the adjacent manganese centers by using magnetic susceptibility measurements.

4.4.2.3. Open-Structure Mixed-Valent Trinuclear $Mn^{II}Mn^{III}Mn^{II}$ Complexes. The first linear trinuclear $Mn^{II}Mn^{III}Mn^{II}$ complex (Mn−Mn−Mn angle of ~177°), [MnL′$_2$Mn(H$_2$O)]$^{3+}$ (**104**), was synthesized with a heptadentate *N*-glycoside carbohydrate ligand, L′ (where L′ = tris[(*N*-aldosyl)aminoethyl]amine), by Tanase and co-workers.[305] The crystal structure is shown in Figure 11. This carbohydrate-supported family of trinuclear complexes shows a 6-line EPR signal at 77 K arising either from the terminal Mn(II) center or from a partially dissociated Mn(II) species. The antiferromagnetic interaction in these complexes (Mn···Mn ≈ 3.845 Å) is markedly weaker (−1.3 vs −7 cm^{-1}) than that in the $Mn^{III}Mn^{II}Mn^{III}$ complexes (Mn···Mn ≈ 3.42−3.55 Å).[306]

Another example of a linear $Mn^{II}Mn^{III}Mn^{II}$ complex, [Mn_3(mcoe)$_6$]$^+$ (**105**), was synthesized recently by Murray and co-workers with the use of a bridging oximate ligand, methyl(2-cyano-2-hydroxyimino)ethanimidate (mcoe$^-$).[307] Two terminal Mn(II) ions are bridged to the central Mn(III) ions by the oxime groups of the mcoe$^-$ ligand, providing an entirely oxygen coordination sphere at the distorted octahedral Mn(III) ions. The Mn(II) ions are, on the other hand, seven coordinate with an approximately pentagonal−bipyrimidal arrangement, where two water molecules occupy the axial sites. The Mn^{III}−Mn^{II} centers are very weakly ferromagnetically coupled ($J \sim +1$ cm^{-1}), owing to the long Mn^{III}−O−N(R)−Mn^{II} superexchange pathway.

The mixed-valent class-1 type[308] $Mn^{II}Mn^{III}Mn^{II}$ complex, [Mn_3(L″)(μ-OMe)$_2$]$^{3+}$ (**106**), supported by a macrocyclic Schiff base ligand, L″ (where L″ = 1,11-diamino-3,9-dimethyl-3,9-diazo-6-oxaundecane), was reported by Asato and co-workers.[309] The manganese ions are encapsulated in the macrocycle in a bent-chain geometry with an Mn−Mn−Mn angle of 129.45(6)°, as depicted by the crystal structure (Figure 11). Variable temperature magnetic susceptibility studies show that adjacent Mn^{II}−Mn^{III} centers are overall weakly ferromagnetically coupled with a J value of +1.83(5) cm^{-1}, while the terminal Mn^{II}−Mn^{II} interaction is negligible.

4.4.2.4. Open-Structure Mixed-Valent Trinuclear $Mn^{II}Mn^{IV}Mn^{II}$ Complex. The first example of a trinuclear complex containing an $Mn^{II}Mn^{IV}Mn^{II}$ core, [Mn_3(pko)$_4$(CH$_3$O)$_2$(SCN)$_2$] (**107**) (where Hpko = 2,2′-dipyridyl ketonoxime), was reported by Pecoraro and co-workers.[310] Two other manganese complexes, both tetranuclear, are known to contain adjacent Mn^{II} and Mn^{IV} ions (**166** and **171**).[207,311] On the basis of the crystal structure of this trinuclear complex, a central Mn ion, coordinated to six oximato oxygen atoms, has been assigned as a +4 ion possessing a regular octahedral geometry. The Mn−O bond distances are comparable to those of Mn(IV) mononuclear complexes. The Mn···Mn separation is slightly shorter than that of the $Mn^{III}Mn^{II}Mn^{III}$ complexes (3.37 vs 3.42−3.55 Å), which also possess an Mn_3^{8+} core. The Mn^{IV} and Mn^{II} centers are ferromagnetically coupled with $J = +6.13$ cm^{-1}, whereas the terminal Mn^{II}−Mn^{II} interaction is insignificant, as was also observed for a valence-trapped trinuclear $Mn^{II}Mn^{III}Mn^{II}$ complex (**106**). XANES studies were also very helpful in making the Mn oxidation state assignment for this complex. The manganese oxidation states in this complex are relevant to those of the S_0 state of PSII water oxidase, which has been proposed to be $Mn^{II}Mn^{III}Mn^{IV}_2$. This study again supports the reliability of XAS studies in assigning oxidation states of the Mn centers in various S states.

4.4.2.5. Open-Structure Trinuclear Mn^{IV}_3 Complex. Recently an oxo-bridged trinuclear manganese complex, [Mn_3O_4(OAc)$_4$(bpy)$_2$] (**108**), consisting of a bent [Mn(μ-O)$_2$(μ-OAc)Mn(μ-O)$_2$(μ-OAc)Mn] core, was reported by Christou and co-workers.[312] This complex has a nonlinear [Mn_3O_4] moiety that is found in a number of proposed PSII active site structures, as depicted in Scheme 1 and Figure 6.[13,81] The crystal

structure is shown in Figure 11. The Mn−Mn−Mn bent angle is ∼136.5°. The average Mn−O−Mn angle and short Mn···Mn distances are ∼94° and 2.58−2.64 Å, respectively, which are typical for any $[Mn^{IV}_2(\mu\text{-}O)_2(\mu\text{-}O_2CR)]^{3+}$ complex (see section 4.4.1). The central Mn ion has only oxygen atoms coordinated to it whereas a chelating bpy binds to each terminal Mn center along with an acetate bound in monodentate fashion. Magnetic susceptibility studies reveal that the complex possesses a $^3/_2$ spin ground state with two adjacent Mn ions being antiferromagnetically coupled with $J = -24.6$ cm^{-1} and terminal Mn centers being ferromagnetically coupled with $J = +8.2$ cm^{-1}. Recently, several mechanisms of water oxidation involving similar trinuclear $[Mn_3O_4]$ moieties have been proposed (see section 3).[17,29,193]

4.4.2.6. Adamantane-Shaped Mn^{IV}_3 Complex. A series of oxo-bridged trinuclear Mn(IV) complexes of composition $[Mn_3(\mu\text{-}O)_3(tacn)_3(\mu_3\text{-}XO_4)]^{3+}$ (X = P, As, or V (**109**−**111**)) were reported by Wieghardt and co-workers.[292] The crystal structure of the phosphorus analogue was determined (shown in Figure 11). This complex possesses an adamantane skeleton similar to those of tetranuclear clusters containing a $[Mn_4O_6]$ core (section 4.4.3), except that in this case a P atom replaces one of the Mn ions. These complexes were synthesized by treating the dinuclear complex, $[Mn_2(\mu\text{-}O)(OAc)_2(tacn)_2]^{3+}$ (**78**), with Na_2HPO_4 or Na_2HAsO_4 (pH = 8−9) or $(NH_4)VO_4$ (pH = 8−9) under ambient condition. The crystal structure of **109** reveals that the Mn···Mn and Mn···P separations are about 3.23 and 3.02 Å, respectively. The Mn−O−Mn angles are ∼129.3°, whereas the Mn−O−P angles are ∼123.5°. The short Mn−O bond length is 1.785 Å, which is typical for any bent Mn^{IV}−O−Mn^{IV} moiety. The Mn−O bond for the Mn−O−P unit is ∼1.883 Å. On the basis of the magnetic data, an $S = {}^1/_2$ spin ground state, which results from the antiferromagnetic exchange interactions, has been determined for the Mn_3 complex. In contrast, weak ferromagnetic coupling was observed for $[Mn_4O_6(tacn)]^{4+}$ (see section 4.4.3).

4.4.2.7. Triangular Mn^{IV}_3 Complexes. Several oxo-bridged manganese clusters containing a triangular $[Mn_3O_4]$ core were synthesized and characterized in the early 1990s. The first compound, $[Mn_3(\mu\text{-}O)_4(bpy)_4Cl_2]^{2+}$ (**112**), was reported by Auger and Girerd[313] followed by the synthesis of the isostructural complex $[Mn_3(\mu\text{-}O)_4(bpy)_4(H_2O)_2]^{4+}$ (**113**) by Sarneski et al.[314] Synthesis of $[Mn_3(\mu\text{-}O)_4(bpy)_4Cl_2][MCl_4]$ (**112**) (where M = Mn or Cd) was carried out in DMF by treating $MnCl_2$ and NEt_4MnO_4 in the presence of bpy and TsOH followed by the addition of the $(NEt_4)_2MCl_4$ salt. The crystal structure, depicted in Figure 11, shows that Mn centers occupy the corners of an isosceles triangle. The long Mn··· Mn separations, where the manganese centers are bridged by a single oxo group, are about 3.24 Å, whereas the Mn···Mn distance for the dinuclear "basal" unit, where the manganese centers are bridged by two oxides, is ∼2.68 Å. Magnetic susceptibility measurements suggest that the manganese centers are strongly antiferromagnetically coupled to generate an $S = {}^1/_2$ ground state, with coupling constants of −85 cm^{-1} for the Mn- - -Mn interaction in the $[Mn(\mu\text{-}O)_2Mn]$ unit and −54 cm^{-1} for the $[Mn(\mu\text{-}O)Mn]$ interactions. A hyperfine structured multiline EPR signal consisting of 35 lines with axial symmetry centered at $g = 2$ was observed at 7.7 K. However, this EPR signal is very different from that exhibited by PSII at the S_0 or S_2 oxidation state.

The second complex, **113**, was obtained when the dinuclear Mn(III,IV) species, $[Mn_2(\mu\text{-}O)_2(bpy)_4]^{3+}$ (**19**), was mixed with HNO_3 (pH = 1.9).[314] The mechanism for this conversion was proposed to be a proton-coupled electron transfer where the starting Mn(III,IV) complex first undergoes disproportionation to generate Mn^{III}_2 and Mn^{IV}_2 species prior to the formation of the trinuclear $[Mn^{IV}_3O_4]^{3+}$ and a mononuclear Mn^{II} species, as illustrated in eqs 1 and 2.

$$2[Mn^{III,IV}_2O_2(bpy)_4]^{3+} + 4H^+ \rightarrow [Mn^{IV}_3O_4(bpy)_4(OH_2)_2]^{4+} + Mn^{2+} + 4bpyH^+ \quad (1)$$

$$2[Mn^{III,IV}_2O_2(bpy)_4]^{3+} + H^+ \rightarrow [Mn^{III}_2O(OH)(bpy)_4]^{3+} + [Mn^{IV}_2O_2(bpy)_4]^{4+} \quad (2)$$

Compound **113** showed similar structural and spectroscopic properties as **112**. Cyclic voltammetric studies further support the proton-coupled electron-transfer mechanism showing that at pH ∼ 4.5 or greater the trinuclear species undergoes reduction to form the Mn(III,IV) dimer, whereas it has an irreversible reduction at ∼0.6 V vs Ag/AgCl below pH 2.5. Solution studies suggested that the trinuclear complex is stable in aqueous medium at acidic pH but is in equilibrium with the dinuclear complex at pH 4.5. It was proposed, on the basis of the EPR studies, that a species other than manganese, possibly the bpy ligand, gets oxidized to bipyridine *N*-oxide, to provide the reducing equivalents needed for the $[Mn^{IV}_3O_4]$ to $[Mn^{III,IV}_2]$ conversion.

The third complex of the triangular $[Mn_3O_4]^{4+}$ family, $[Mn_3(\mu\text{-}O)_4(bpea)_3(OH)]^{3+}$ (**114**), was synthesized by Armstrong and co-workers by employing a tridentate N-donor ligand, bpea.[170,211] The perchlorate salt was prepared by stirring a 1:5 acetonitrile/H_2O mixture of $[Mn^{IV}_2(\mu\text{-}O)_2(OAc)(bpea)_2]^{3+}$ (**61**) for 1.5 h followed by the addition of an aqueous solution of $NaClO_4$. The crystal structure, shown in Figure 11, portrays a structural distortion for **114** relative to **112** and **113**. The apical Mn center has a terminally coordinated hydroxide group, which provides an intramolecular hydrogen-bonding interaction with the syn bridging oxo group from the basal $[Mn_2(\mu\text{-}O)_2]$ moiety, making the Mn-oxo bond slightly longer. The most striking feature of this compound was revealed by EPR and magnetic studies. Instead of a multiline signal, this complex shows a characteristic signal of a nearly axial $S = {}^3/_2$ ground spin state with a baseline crossing point for the low-field resonance of $g = 3.6$ and a minimum at higher field of $g = 1.9$. Magnetic susceptibility studies are consistent with an $S = {}^3/_2$ ground state, which suggests that the basal magnetic interaction is antiferromagnetic and the apical interactions are also antiferromagnetic but much weaker. The data are well fit with J ($Mn^{IV}(\mu$-

Table 4. Tetranuclear Manganese Complexes

no.	compound	characterization	core type	ref
117	$[Mn_4(\mu_3\text{-}O)_2(OAc)_6(bpy)_2]$	X-ray, EPR, IR, magnetism, NMR, UV−vis	i-A	213
118	$[Mn_4(\mu_3\text{-}O)_2(\mu\text{-}O_2CPh)_7(bpy)_2]$	X-ray, CV, EPR, IR, magnetism, NMR, UV−vis	i-B	213
119	$[Mn_4(\mu_3\text{-}O)_2(\mu\text{-}O_2CMe)_7(bpy)_2]^+$	X-ray, EPR, IR, magnetism, NMR, UV−vis,	i-B	213
120	$[Mn_4(\mu_3\text{-}O)_2(\mu\text{-}O_2CEt)_7(bpy)_2]^+$	X-ray, CV, IR, magnetism, NMR, UV−vis	i-B	213
121	$[Mn_4(\mu_3\text{-}O)_2(\mu\text{-}O_2CPh)_7(bpy)_2]^+$	X-ray, EPR, IR, magnetism, NMR, UV−vis	i-B	213
122	$[Mn_4(\mu_3\text{-}O)_2(\mu\text{-}O_2CPh)_7(hmp)_2]^+$	X-ray, conductivity, CV, IR, magnetism, NMR	i-B	326
123	$[Mn_4(\mu_3\text{-}O)_2(\mu\text{-}O_2CMe)_7(hqn)_2]^+$	X-ray, conductivity, CV, IR, magnetism, NMR	i-B	326
124	$[Mn_4(\mu_3\text{-}O)_2(\mu\text{-}O_2CMe)_7(imac)_2]^+$	X-ray, CV, IR, magnetism, NMR	i-B	327
125	$[Mn_4(\mu_3\text{-}O)_2(\mu\text{-}O_2CMe)_7(pic)_2]^+$	X-ray, CV, IR, magnetism, NMR	i-B	320
126	$[Mn_4(\mu_3\text{-}O)_2(\mu\text{-}O_2CMe)_6(dbm)_2]$	X-ray, CV, IR, magnetism, NMR	i-A	220
127	$[Mn_4(\mu_3\text{-}O)_2(\mu\text{-}O_2CMe)_7(dpm)_2]^+$	CV, IR, magnetism, NMR	i-B	325
128	$[Mn_4(\mu_3\text{-}O)_2(O_2CCPh_3)_6(OEt_2)_2]$	X-ray, EPR, IR	i-A	329
129	$[Mn_4O_2(OAc)_2(bsp)_2]$	X-ray, CV, conductivity, IR, magnetism, UV−vis	i-A	330, 331
130	$[Mn_4O_2(saltren)_2]^{2+}$	X-ray, EPR, CV, magnetism	i	332
131	$[Mn_4(\mu_3\text{-}O)_2(O_2CMe)_4(bbpe)_4]^{2+}$	X-ray, IR, NMR	i	333, 334
132	$[Mn_4(\mu_3\text{-}O)_2(O_2CEt)_4(bbpe)_4]^{2+}$	magnetism	i	334
136	$[Mn_4(\mu_3\text{-}O)_2(OMe)_3(O_2CR)_4(bbpe)_4(MeOH)]^{2+}$	X-ray, IR, magnetism	i	334
137	$(H_2Im)_2[Mn_4O_3Cl_6(HIm)(OAc)_3]$	X-ray, EPR, IR, magnetism, NMR	ii	336, 337
138	$[Mn_4O_3Cl_4(OAc)_3(HIm)_2]$	X-ray, EPR, IR, magnetism	ii	337
139	$[Mn_4O_3Cl_4(O_2CEt)_3(HIm)_2]$	X-ray, EPR, IR, magnetism	ii	337
140a	$[Mn_4O_3Cl_4(OAc)_3(py)_3]$	X-ray, CV, EPR, IR, magnetism, NMR, XAS	ii	337, 344
140b	$[Mn_4O_3Cl_7(O_2CMe)_3(Hpy)_3]$	X-ray, CV, EPR, IR, magnetism, NMR, XAS	ii	338, 344
141	$[Mn_4(\mu_3\text{-}O)_3Cl(OAc)_3(dbm)_3]$	X-ray, CV, EPR, IR, magnetism, NMR, XAS	ii	321, 344
144	$[Mn_4(\mu_3\text{-}O)_3(OAc)_4(dbm)_3]$	X-ray, CV, EPR, IR, magnetism, NMR, XAS	ii	220, 344
151	$[Mn_4(\mu_3\text{-}O)_3(O_2CPh)_4(dbm)_3]$	X-ray, CV, EPR, IR, magnetism, NMR, XAS	ii	220, 344
152	$[Mn_4O_4(O_2PPh_2)_6]$	X-ray, CV, EPR, IR, MS, NMR, UV−vis, XAS	iii	345
153	$[Mn_4O_4(O_2PPh_2)_6]^+$	X-ray, CV, EPR, MS, NMR, UV−vis	iii	346
154	$[Mn_4O_3(OH)(O_2PPh_2)_6]$	EPR, IR, MS, NMR, UV−vis	ii	348
155	$[Mn_4(\mu\text{-}O)_6(tacn)_4]^{4+}$	X-ray, CV,[217] IR, magnetism, UV−vis	iv-A	255, 352
156	$[Mn_4O_5(OH)(tame)_4]^{5+}$	X-ray, IR, magnetism, UV−vis	iv-B	209
157	$[Mn_4O_6(tame)_4]^{4+}$	UV−vis	iv-A	209
158	$[Mn_4O_5(OH)(tacn)_4]^{5+}$	X-ray, magnetism, UV−vis,	iv-B	209
159	$[Mn_4O_4(OH)_2(tacn)_4]^{6+}$	magnetism (soln), NMR, UV−vis	iv-C	353
160	$[Mn_4O_6(bpea)_4]^{4+}$	X-ray, CV, EPR, IR and normal-mode analysis, MS, magnetism, NMR, UV−vis	iv-A	156, 217
162	$[Mn_4O_6(bpea)_4]^{3+}$	X-ray, CV, EPR, IR and normal-mode analysis, MS, magnetism, NMR, UV−vis	iv-A	156, 217, 356
163	$[Mn_4(\mu\text{-}O)_6(bpy)_6]^{4+}$	X-ray, CV, EPR, magnetism, UV−vis	v	359, 360
164	$[Mn_4O_6(bpy)_6]^{3+}$	EPR	v	361
165	$[\{Mn_2(tphpn)_2(OAc)(H_2O)\}_2O]^{4+}$	X-ray, CV, EPR, magnetism, UV−vis	vi-A	362, 363
166	$[Mn_4O_2(tphpn)_2(OTf)_2(H_2O)_2]^{3+}$	X-ray, CV, EPR, magnetism, UV−vis	vi-B	207, 364
167	$[Mn_4O_4(tphpn)_2]^{4+}$	X-ray, EPR, magnetism	vii-A	365, 366
168	$[Mn_4O_4(tmdp)_2(H_2O)_2]^{4+}$	X-ray, CV, EPR, magnetism, UV−vis	vii-B	367, 368
169	$[Mn_4(\mu\text{-}O)(\mu\text{-}OH)(\mu\text{-}OAc)_2(tahpn)_2]^{4-}$	X-ray, MS	vii-C	369, 370
170	$[Mn_4(\mu\text{-}O)_5(dmb)_4(dmbO)_2]^{4+}$	X-ray, CV, EPR, IR, MS, UV−vis	viii	203
171	$[Mn_4(\mu_4\text{-}O)(pko)_4(dcpaa)_4]$	X-ray, magnetism	ix	311

$O)_2Mn^{IV}$ interaction) = −76 cm^{-1} and J' ($Mn^{IV}(\mu$-O)-Mn^{IV} interaction) = −11 cm^{-1}. The hydroxide group can be replaced by chloride, fluoride, isocyanide, or water.[211]

Several years later, the synthesis of the $[Mn_3(\mu\text{-}O)_4(phen)_4(H_2O)_2]^{4+}$ (**115**) complex was reported by Reddy et al.[315] Here the phen ligand was added to a solution of $Mn(OAc)_2$ in dilute HNO_3, followed by addition of an aqueous solution of $(NH_4)_2Ce(NO_3)_6$, forming a brown reaction mixture. This complex has very similar properties compared to its bpy analogue (**113**).

The hexadentate ligand tpen was employed to isolate a heaxanuclear species, $[\{Mn_3(\mu\text{-}O)_4(OH)\}_2(tpen)_3]^{6+}$ (**116**), that comprises two discrete $[Mn_3O_4]$ moieties.[222] This compound was formed when an aqueous solution of **53** was stirred in air for ∼0.5 h. The Mn···Mn distance in the basal unit, obtained from the crystal structure, is 2.625(2) Å, and that for the Mn atoms bridged by a single oxo group is 3.192(2) Å. The EPR signal, recorded at 6 K, suggested an $S = {}^3/_2$ ground spin state for **116**.

Even though the spectroscopic properties of these $[Mn_3O_4]^{4+}$ complexes and open-structured Mn_3 species are very different compared to that of the PSII active site, recent X-ray crystallographic data support a structure for the WO S_1 state where a manganese triangle is linked to a fourth manganese atom. These "3 + 1" structural motifs are also consistent with EXAFS and EPR studies. However, to date, none of the aforementioned Mn_3 complexes have been converted to a 3 + 1 model compound. Current efforts are being directed toward obtaining such a synthetic analogue.

4.4.3. Tetranuclear Manganese Complexes

There is no debate that an oxo-bridged tetranuclear manganese (Mn_4) cluster is responsible for the process of photosynthetic oxygen evolution. Despite recent progress in obtaining crystallographic data of fully functional PSII crystals, the precise structure of the Mn_4 cluster is unclear.[8−10] As stated above, the cofactors Ca^{2+} and Cl^-, which have electron density comparable to that of the Mn ions, have not been

Scheme 5. Observed Core Types for Tetranuclear Manganese Complexes

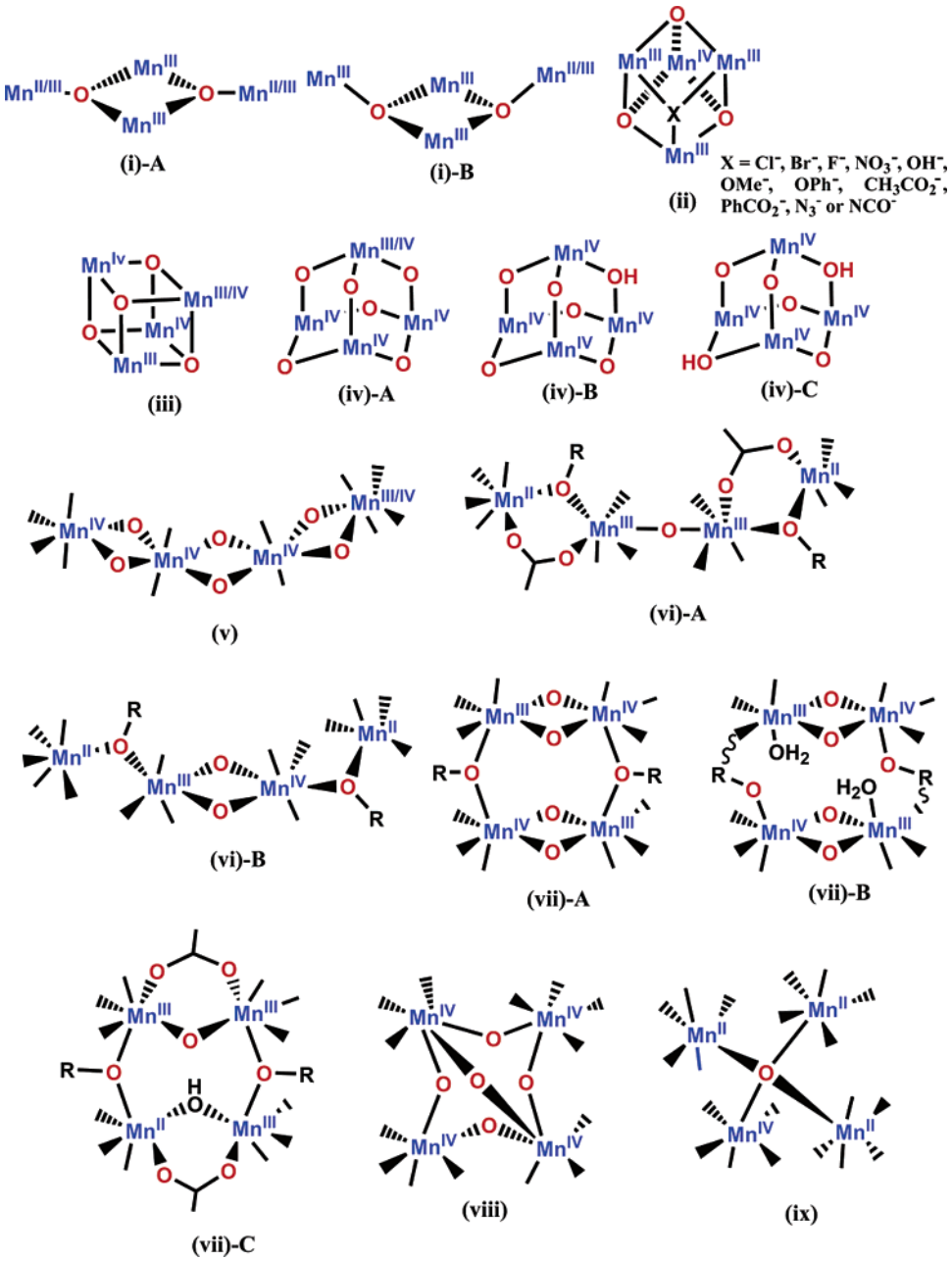

located in two of the crystal structures. The X-ray data indicate a "3 + 1" motif, presumably for the "dark-adapted" S_1 state. Possible damage to the PSII crystals, due to the X-ray radiation and thus structural changes to the Mn_4 cluster, cannot be ruled out completely. On the other hand, recent X-ray absorption studies point toward significant elongation in the Mn···Mn distances during the $S_2 \rightarrow S_3$ transition that may result from a considerable structural rearrangement.[37] Thus, the "3 + 1" motif may not be representative of the higher S states: S_3 or S_4. On the basis of EXAFS data, Klein and co-workers proposed an open "dimer-of-dimers" structure, a prevalent template in the literature for the PSII active site.[14,47] To date, several other PSII Mn_4 structures with varying geometries have been proposed, and the synthesis of some of these model complexes has been accomplished. These synthetic models have been investigated by X-ray absorption, EPR, and other physicochemical techniques in order to achieve structural information pertaining to the water oxidase (WO) Mn_4 cluster. Different tetranuclear cores that have been accessed synthetically are shown in Scheme 5. The tetranuclear model compounds along with their structural and spectroscopic properties and their relevance to PSII will be assessed in this section. These complexes are also listed in Table 4.

4.4.3.1. Complexes with a $[Mn_4O_2]$ Core. In one of the earlier proposals for the Kok catalytic cycle, a $[Mn_4(\mu_3\text{-}O)_2]$ species, commonly referred to as the "butterfly" core, was presented as a possible structural model for the lower S states.[178,316] According to the proposed mechanism, upon consumption of water, the butterfly complex was postulated to be transformed to an "active" cubane species with a $[Mn_4(\mu_3\text{-}O)_4]$ core, which would then release O_2 by reverting back to the butterfly complex, thus closing the cycle. The formation of such complexes containing a [M_4-

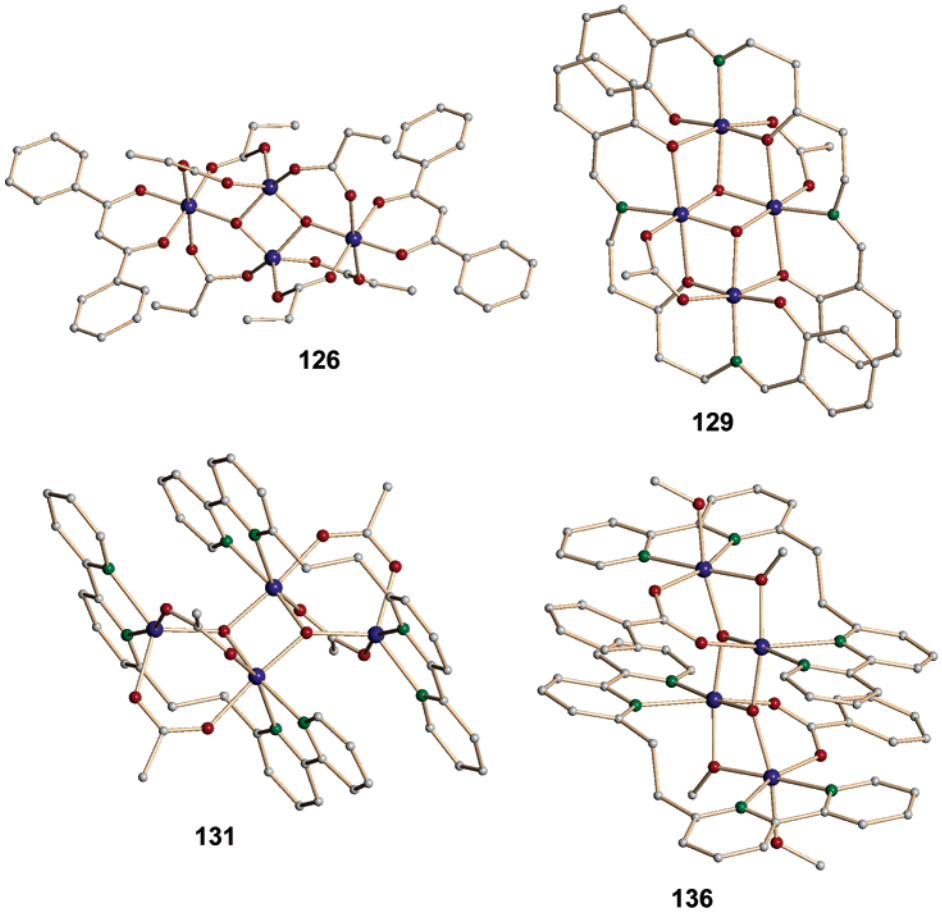

Figure 13. Crystal structures of selected tetranuclear manganese complexes portraying various $[Mn_4O_2]$ cores. The Mn atoms are shown in blue, O atoms in red, N atoms in green, and C atoms in gray.

$(\mu_3-O)_2]$ core, where M = transition metal, has also been observed in iron chemistry.[317−319] Henceforth, many complexes with $[Mn_4(\mu_3\text{-}O)_2]^{6+/7+/8+}$ cores have been synthesized possessing a variety of bridging carboxylates and terminal ligands. Christou and coworkers contributed significantly in synthesizing and characterizing this class of complexes. The "doubly reduced" complex, $[Mn^{II}_2Mn^{III}_2(\mu_3\text{-}O)_2(OAc)_6(bpy)_2]$ (**117**), was synthesized from the basic acetate starting material, $[Mn^{II}Mn^{III}_2O(OAc)_6(py)_3]$, by treatment with bpy.[213] The Mn_4 unit in this complex is planar, as depicted by the crystal structure, shown in Scheme 5, i-A. The Mn···Mn separations fall between ∼2.78 and 3.48 Å in this complex (see below). Magnetic susceptibility measurements reveal weak antiferromagnetic coupling interactions among the manganese centers, resulting in an $S = 2$ ground spin state ($J = -1.97$ and -3.12 cm^{-1}). However, the low average Mn oxidation state of +2.5 in this complex does not make it a good candidate for any of the natural PSII S states, although it may serve as a model for the reduced S_{-3} state.

The "singly reduced" species, $[Mn_4(\mu_3\text{-}O)_2(\mu\text{-}O_2CPh)_7(bpy)_2]$ (**118**), was synthesized similarly from the benzoate analogue of the neutral triangular complex, $[Mn^{II}Mn^{III}_2O(O_2CPh)_6(py)_2(H_2O)]$.[213] The Mn^{III}_4 complexes, with the general formula $[Mn_4(\mu_3\text{-}O)_2(\mu\text{-}O_2CR)_7(bpy)_2]^+$ (R = Me, Et, Ph) (**119-121**), were prepared from the charged trinuclear complex, $[Mn^{III}_3O(OAc)_6(py)_3]^+$, followed by ligand substitution reactions with the appropriate carboxylic acids.[213] Additionally, they can be prepared by direct comproportionation reactions involving Mn^{II} and Mn^{VII} sources. The Mn_4 unit is not planar in these complexes and, thus, is referred to as butterfly-like, where two of the Mn centers occupy the "hinge" sites and the other two Mn atoms reside at the "wingtip" sites. Presumably, the seventh bridging carboxylate is responsible for the non-coplanarity of this family of complexes. The Mn centers residing at the hinge sites are ∼2.85 Å apart, whereas it is ∼3.30 Å between the wingtip Mn centers. The Mn- - -Mn interactions, both between the two hinge site Mn centers and between a hinge site Mn center and a wingtip site Mn center, are weakly antiferromagnetic in nature: $J \approx -7.8$ and -23.5 cm^{-1}, respectively, to give rise to integer-spin ground states. This intermediate spin ground state has been ascribed to a spin-frustration effect.[320] A multitude of tetranuclear manganese(III) carboxylate complexes with planar $[Mn_4O_2(O_2CR)_6]^{2+}$ (R = Me, Et, or Ph) cores and the butterfly-like $[Mn_4O_2(O_2CR)_7]^+$ (R = Me, Et, CF_3, or Ph) cores have been synthesized by using bidentate chelating ligands, such as hmp^-, hqn^-, $imac^-$, pic^-, dbm^-, and dpm^- (**122**−**127**).[213,220,223,320−328] The crystal structure of one such complex, $[Mn_4O_2(O_2CEt)_6(dbm)_2]$ (**126**), is shown in Figure 13. These tetranuclear Mn(III) compounds show no EPR signal in the perpendicular mode, even at liquid He temperatures. The spectroscopic properties of these complexes rule them out as electronic models for the WO active site in its native oxidation states.

Another doubly reduced mixed-valent complex composed of all oxygen donor ligands, $[Mn_4(\mu_3\text{-}O)_2(O_2CCPh_3)_6(OEt_2)_2]$ (**128**), was reported by Brudvig, Crabtree, and co-workers.[329] Two of the four manganese(III) centers in **128** have unusual distorted square-pyramidal geometry. The compound shows a broad EPR signal at $g \approx 2$ in frozen dichloromethane solution, implying, the authors suggest, an integer-spin ground state. Although the Mn···Mn distances are comparable (~2.77 and 3.27 Å) with those of the PSII S_1 and S_2 states, the oxidation states of the Mn centers are too low for it to be a relevant structural model, though it has been said to represent a "super-reduced" form of the WO Mn_4 cluster.

Two $[Mn_4(\mu_3\text{-}O)_2]^{8+}$ complexes that possess a "fused cubane" geometry are known. Mikuriya and co-workers reported the synthesis of the first complex of this type, $[Mn_4O_2(OAc)_2(bsp)_2]$ (**129**) (bsp = 1,5-bis(salicylideneamino)-3-pentanol).[330] The Mn···Mn separations in this complex are between 2.87 and 3.12 Å. The crystal structure is shown in Figure 13. Variable temperature magnetic measurements demonstrate weak antiferromagnetic interactions ($J = -10.0$ cm^{-1} and $J' = -3.7$ cm^{-1}) among the manganese(III) centers. Cyclic voltammetry in methanol shows one quasi-reversible oxidation wave at 0.01 V and two quasi-reversible reduction waves at about −0.4 and −0.7 V vs SCE.[331] The second complex, $[Mn_4O_2(saltren)_2]^{2+}$ (**130**), was prepared by Chakravorty and Chandra, who used a polydentate ligand, saltren.[332] The Mn···Mn distances were found to be ~2.9−3.0 Å, as determined by crystal structure analysis. There is no carboxylate ligand present in **130**. This complex is antiferromagnetic in nature and shows no EPR signal. A cyclic voltammogram in acetonitrile reveals four quasi-reversible one-electron responses that correspond to the overall oxidation state change $Mn^{IV}_2Mn^{III}_2$ to $Mn^{III}_2Mn^{II}_2$, two of which have $E_{1/2}$ above the water oxidation potential.

Recently, another family of $[Mn_4(\mu_3\text{-}O)_2]^{6+}$ complexes with a general formula of $[Mn_4(\mu_3\text{-}O)_2(O_2CR)_4(bbpe)_4]^{2+}$ (**131**−**133**) (where R = Me, Et, and Ph) was synthesized by Christou and co-workers.[333,334] These complexes formed when $[Mn_3O(O_2CR)_6(py)_3]^+$ was treated with the tetradentate ligand 1,2-bis(2,2′-bipyridine-6-yl)ethane (bbpe) in acetonitrile. As evidenced by the crystal structure of the acetate analogue, shown in Figure 13, two $[Mn_2O(OAc)_2(bbpe)]^+$ fragments are held together through two triply bridging oxides, and therefore, the full complex is described as a dimer-of-dimers structure. The shortest and longest Mn···Mn distances in this complex are ~2.78 and 3.63 Å, respectively. These complexes display net antiferromagnetic coupling among the Mn centers to generate an $S = 0$ ground state. When the aforementioned reaction was carried out in MeOH instead of MeCN, complexes $[Mn_4(\mu_3\text{-}O)_2(OMe)_3(O_2CR)_4(bbpe)_4(MeOH)]^{2+}$ (**134**−**136**), with one Mn(II) center and three Mn(III) centers, resulted. The benzoate derivative (**136**) was structurally characterized and described as having a "ladderlike" $[Mn_4O_2(OMe)_2]$ core (shown in Figure 13). The Mn···Mn distances range from ~2.99 to 3.79 Å. Magnetic susceptibility data indicate an $S = {}^7/_2$ spin system for this complex. Zero field splitting ($D = -0.77$ cm^{-1}) and intermolecular interactions probably through the π−stacking of the bipyridine rings also were found to be present in this complex. Below 1.7 K this compound displays slow magnetization relaxation in the ac susceptibility measurements, making it a "single-molecule magnet" (SMM). However, the two sets of $[Mn_4(\mu_3\text{-}O)_2]$ complexes described above are structurally akin to the planar $[Mn_4(\mu_3\text{-}O)_2(OAc)_6(bpy)_2]$ (**117**) complex described earlier. The nature of the N-donor ligand as well as the bridging mode of the carboxylate or methoxy groups is responsible for the observed structural changes.

The spectroscopic properties, low oxidation states, and symmetric nature of the structures for these $[Mn_4(\mu_3\text{-}O)_2]$ compounds make them incompatible as synthetic analogues for the PSII active site.[48,55]

4.4.3.2. Cubane Structure with a $[Mn_4(\mu_3\text{-}O)_3X]^{6+}$ Core. A $[Mn_4(\mu_3\text{-}O)_4]$ cubane core was featured as the structure of several S states in early proposed mechanisms for the water-to-oxygen catalytic cycle.[177,316] A large family of complexes possessing a mixed-valent $[Mn^{III}_3Mn^{IV}(\mu_3\text{-}O)_3X]^{6+}$ core is now known. The complex $(H_2Im)_2[Mn_4O_3Cl_6(HIm)(OAc)_3]$ (**137**) (H_2Im^+ = imidazolium cation) was the first reported in this series of distorted cubane complexes (with X = Cl and Br) by Christou and co-workers.[335−337] The reaction of $Mn(OAc)_3{\cdot}2H_2O$ with Me_3SiCl followed by addition of imidazole resulted in the formation of **137**. Reaction of $[Mn_3O(O_2CR)_6(py)_3](ClO_4)$ (R = Me, Et) with Me_3SiCl leads to the formation of $[Mn_4O_3Cl_4(OAc)_3(HIm)_2]$ (**138**) and $[Mn_4O_3Cl_4(O_2CEt)_3(HIm)_2]$ (**139**). The terminal imidazole ligand has also been replaced by pyridine in an isostructural complex, $[Mn_4O_3Cl_4(OAc)_3(py)_3]$ (**140a**).[212,337] An analogous cubane complex, $[Mn_4O_3Cl_7(O_2CMe)_3]^{3-}$ (**140b**), resulted from the reaction between $[Mn_3O(O_2CMe)_6(py)_3]^+$ and Me_3SiCl followed by addition of H_2O and acetic acid.[338] Similar complexes of the type $[Mn^{III}_3Mn^{IV}(\mu_3\text{-}O)_3X(OAc)_3(dbm)_3]^{6+}$ with X = Cl^-, Br^-, F^-, ^-OAc, ^-OH, ^-OMe, ^-OPh, NO_3^-, N_3^-, and NCO^- (**141**−**150**) supported by the chelating ligand dibenzoylmethane (dbm^-) were also reported.[219,220,223,339−341] Cubane complexes of the type $[Mn_4O_3X(OAc)_3(dbm)_3]$ (**141**−**143**) (X = Cl^-, Br^-, F^-) containing both oxygen and halide atoms have been obtained by disproportionation reactions triggered by carboxylate abstraction from the $[Mn^{III}_4]$ butterfly clusters.[339,342] They can also be prepared by a ligand-exchange reaction using reagents Me_3SiX (X = Cl^-, Br^-) from $[Mn_4O_3(O_2CR)_4(dbm)_3]$ (R = Me, Ph) (**144**, **151**). Both of these reactions are initiated by treatment with Me_3SiX reagents that utilize the strength of Si−O bonds over Si−X bonds (X = Cl^-, Br^-). To prepare the F^- derivative requires a stronger fluoride donor, namely diethylammonium sulfur trifluoride (DAST).

The all-oxygen ligand containing $[Mn^{III}_3Mn^{IV}]$ cubanes have been prepared by alcoholysis, hydrolysis, and acidolysis. Also, controlled potential electrolysis has permitted the conversion of $[Mn_4O_2]^{8+}$ with a butterfly core to a distorted cubane-like complex with a $[Mn_4O_3(O_2CR)]^{7+}$ core.[220] This process was suggested to mimic one of the basic features of S state

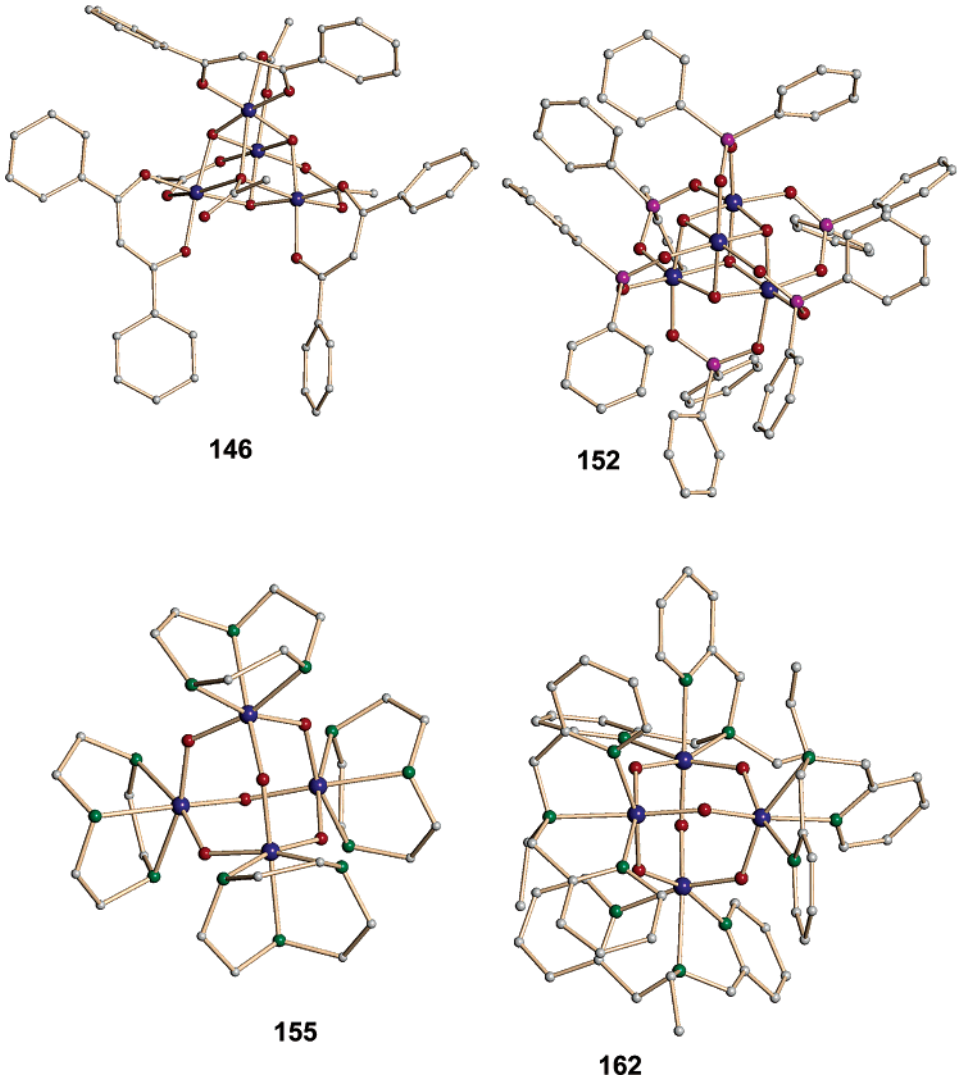

Figure 14. Crystal structures of selected tetranuclear manganese complexes portraying cubane- and adamantane-type cores. The Mn atoms are shown in blue, O atoms in red, N atoms in green, P atoms in purple, and C atoms in gray.

catalytic water oxidation cycle, that is, one electron oxidation of a tetranuclear Mn-oxo cluster. The identity of the bridging ligand X^- has minimal influence on the resultant structural, redox, spectroscopic, and magnetic properties. The Mn ions in all of these cubane complexes are trapped-valent in nature with a trigonal pyramidal geometry where all three Mn^{III} ions are at the base of a pyramid and the Mn^{IV} ion is at the apex. A representative structure, $[Mn^{III}_3Mn^{IV}O_3(OMe)]^{6+}$ (**146**), is shown in Figure 14. The Mn^{III} ions are distinguished by longer metal−ligand bonds (average distance ∼ 2.1 Å) compared to those surrounding the Mn^{IV} ion (average distance = 1.9 Å). The distances between Mn^{IV} and oxide ions are shorter (∼1.86 Å) than those to the carboxylate (∼1.94 Å). The $Mn^{III}\cdots Mn^{III}$ separations range from ∼3.1 to 3.2 Å while those between Mn^{III} and Mn^{IV} are from ∼2.7 to 2.8 Å. These distances closely resemble those found by EXAFS measurements of the S_0-S_2 state of the PSII active site, making it a potential structural model.[14,47] In these complexes, the Jahn−Teller effect causes elongation of the axial bonds at the Mn^{III} centers (average axial bond distance = 2.2 Å; average nonaxial bond distance = 1.9 Å) relative to the equatorial bonds.

All of the complexes possess effective C_3 symmetry in solution and display characteristic ^1H NMR spectra. These clusters manifest a distinct spin ground state $S = {}^9/_2$, which was initially described as the result of "spin-frustration", a phenomenon where an intermediate spin ground state results due to the competition between similar magnetic exchange interactions in complexes with certain topologies.[341] Later, the spin state was described by ferromagnetic coupling between the Mn^{III} ions (J = ∼4−14 cm^{-1}) and antiferromagnetic interaction between adjacent Mn^{III} and Mn^{IV} pairs (J = ∼ −20 to −35 cm^{-1}) instead of spin-frustration.[343] Furthermore, the near-parallel alignment of the three Jahn−Teller axes results in relatively high magnetic anisotropy (D ∼ −0.30 to −0.62 cm^{-1}) for these complexes. The relatively high spin, coupled with the high magnetoanisotropy, causes the distorted-cubane complexes to display SMM behavior at low temperatures (<0.9 K).[343] Recently, a comproportionation reaction involving Mn^{II} and Mn^{VII} (NBu_4MnO_4) sources has provided an easy route to the acetate bridged $[Mn_4O_3(OAc)_4(dbm)_3]$ (**144**) cluster.[223] In this complex, the acetate at the μ_3 site bridges in a $[\eta^1{:}\mu_3]$ manner while in **151** the benzoate binds $[\eta^2{:}\mu_3]$. These observations have

been rationalized as the result of steric interactions between the phenyl ring of the dbm ligand and the carboxylate. Consequently, the $[Mn_4O_3(O_2CPh)]^{6+}$ (**151**) core possesses effective C_s symmetry, the lowest symmetry cluster reported in this family.

Due to the fact that the abovementioned cubane complexes have predominantly oxygen donor ligands and Mn···Mn distances that closely relate to the PSII active site, several of them have been analyzed with Mn K-edge EXAFS and XANES and compared with those of the WO Mn_4 complex.[344] These studies show that the phases and the amplitude of the *k*-space Mn EXAFS and the Fourier transforms differ significantly from those of the enzyme. On the basis of these results, the cubane topology with C_3 symmetry has been excluded as a structural analogue for the PSII Mn_4 cluster. The cubane complex, $[Mn_4O_3(O_2CPh)]^{6+}$ (**151**), with C_s symmetry, however, shows a slight resemblance to the PSII Mn_4 cluster EXAFS properties, which suggests that an even more distorted cubane framework is needed to approach the observed PSII EXAFS data.

4.4.3.3. Cubane Structure with a $[Mn_4O_4]$ Core. A new family of cubane complexes with a $[Mn_4O_4]$ core, $[Mn_4O_4(O_2PPh_2)_6]^{0/1+}$, involved in some proposed mechanistic cycles, has been reported by Dismukes and co-workers.[345,346] The addition of diphenylphosphinate salts to a solution of $[Mn^{III,IV}{}_2O_2(bpy)_4](ClO_4)_3$ (**19**) results in the formation of $[Mn^{III}{}_2Mn^{IV}{}_2O_4(O_2PPh_2)_6]$ (**152**), where all the bpy ligands have been displaced. No appreciable Jahn−Teller distortions are observed in the Mn−O bond lengths, and this absence is thought to be not due to a superposition of nonequivalent Mn valences, owing to disorder. The absence of appreciable differences in the anisotropic displacement factors for different phosphinate O atoms suggests that this complex is a very rare example in multinuclear manganese-oxo chemistry of a class III (delocalized) mixed-valent $Mn^{III}Mn^{IV}$ compound.[308] Further support for delocalization derives from variable-temperature ^1H NMR spectra, which show that in solution only one set of three paramagnetically shifted resonances for all twelve phenyl rings is observed. The structure of this complex is shown in Figure 14. The Mn···Mn distances in the complex vary between 2.90 and 2.95 Å, markedly longer than that observed for the di-μ-oxo dinuclear complexes (2.6−2.7 Å). The Mn···Mn distances are similar to the those of the $Mn^{IV}{}_4$ cubane substructures embedded within the larger clusters $Mn_{12}O_{12}$ and $Mn_8Fe_4O_{12}$ (2.82−2.99 Å) and to those of the central pair in the Mn_4O_2 butterfly complexes (see above, 2.85 Å), all of which contain solely triply bridging-oxo atoms.[214] This compound exhibits no readily detectable EPR signal in dichloromethane between ~10 and 300 K, indicating antiferromagnetic coupling present in the tetranuclear core. However, no magnetic susceptibility data have been reported for this species. Cyclic voltammograms of **152** display a quasi-reversible oxidation wave corresponding to $Mn^{III}{}_2Mn^{IV}{}_2 \rightarrow Mn^{III}Mn^{IV}{}_3$ at $E_{1/2} = +680$ mV vs Fc^+/Fc. An irreversible reduction was also observed at −730 mV. This complex undergoes a reduction process whereby it takes up four or five H atoms (see below). The K-edge absorption of this complex is 0.25 eV higher than that for the PSII S_1 state, attributed by the authors to the highly symmetric nature of this cubane core.

Upon treatment of **152** with 2 equiv of triflic acid (HOTf), the one-electron-oxidized product $[Mn_4O_4(O_2PPh_2)_6]^+$ (**153**) was formed in high yield.[346] This oxidized species can also be obtained by the reaction of **152** with trimethylsilyltriflate in the presence of HOTf and oxygen. Electrochemical or chemical oxidation with $NO(BF_4)$ or Cl_2 is possible, although these processes generate Mn(II) side products, as evident from EPR spectra. The crystal structure of **153** demonstrates a significant trigonal distortion compared to the tetragonal symmetry present in the parent molecule, **152**. The resulting oxidized complex is described to contain a trigonal-pyramidal Mn_4 cubane core with shorter Mn(IV)−O and Mn(IV)···Mn(III) bonds compared to Mn(III)···Mn(III) and Mn(III)−O bonds. The short Mn···Mn distances are reduced by 0.08−0.14 Å compared to those of the parent complex and yet are ~0.1−0.2 Å longer than that of dinuclear $[Mn_2O_2]^{3+/4+}$ species. No noticeable axial tetragonal (JT) elongation was observed for the Mn(III) centers, unlike in the $[Mn_4O_3X]^{6+}$ complexes discussed above. This species has a paramagnetic ground spin state that exhibits an intense EPR signal (at $g \approx 2$) in frozen solution. The signal intensity obeys the Curie law between 7 and 29 K with zero-field splitting and no hyperfine structure, implying an odd-spin ground state ($S \geq {}^3/_2$). This complex can be reduced quantitatively to the parent cubane by triethlyamine (Et_3N) or in solvents such as MeOH, EtOH, DMF, and DMSO. NMR titration studies show that the reduction with Et_3N proceeds through an intermediate with lower symmetry, the identity of which is unknown but is proposed as $[Mn_4(\mu_3\text{-}O)_3(\mu_3\text{-}ONEt_3)]^{6+}$.[346] Such an intermediate could potentially be involved in the water oxidation cycle as well.

Reaction of **152** with a hydrogen atom donor, phenothiazine (phzH), has been shown to form the dehydrated cluster $[Mn_4O_2(O_2PPh_2)_6]$, which has lost two oxo bridges by conversion to water.[347] The formation of the latter was established by electrospray mass spectrometry (ESI-MS), whereas FTIR spectroscopy confirmed the release of water molecules into solution during reduction. UV−vis and EPR spectroscopies established that 4 equiv of phenothiazine are necessary for this process, yielding 4 equiv of the neutral phz$^\bullet$ radical. On the other hand, **152** undergoes irreversible decomposition to Mn(II) species if an aprotic reductant, such as cobaltocene, was used. The same fate was observed when the reduction was performed electrochemically. Solution NMR studies reveal that the resulting reduced species possesses a more symmetrical core. This complex, $[Mn_4O_2(O_2PPh_2)_6]$, exhibits a broad EPR signal with a width of ~400 G, centered at $g = 2$ in the low-temperature range. Chloride ion was shown to bind to this species, as evidenced by the alteration of the EPR spectrum. This suggests that the resulting complex has open coordination sites for water or anion binding. No Mn(II) decomposition products were detected even after addition of excess phenothi-

Scheme 6. Reactivity of 152 (Adapted from Refs 350 and 351)

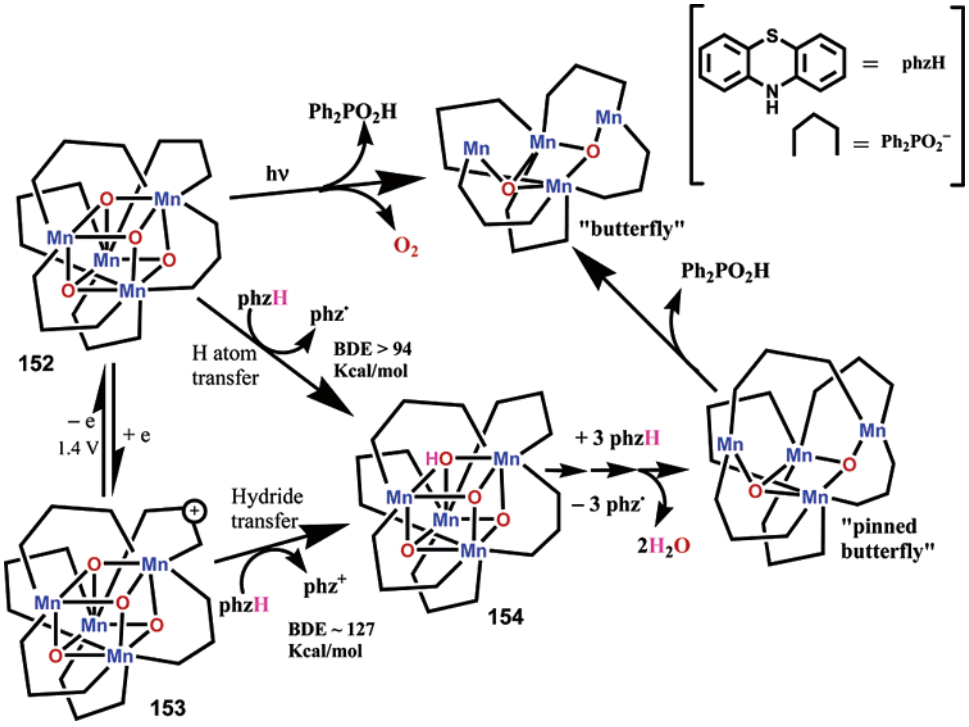

azine. EPR spectra coupled with titration studies suggest that the reduced species contains two Mn(II) and two Mn(III) ions. Mass spectral data show that the new species results by the loss of two oxygen atoms from the parent complex to give $[Mn_4O_2(O_2PPh_2)_6]$, the structure of which was proposed as a "pinned butterfly" (as shown in Scheme 6).[347] Structural analysis was not possible, as this complex is not stable in the solid state. On the basis of the above-stated observations, the $[Mn_4O_4]^{6+}$ cubane complex was proposed to undergo a coupled four-electron/four-proton reduction process with the release of two water molecules, a reaction analogous to the reverse sequence of photosynthetic water oxidation leading to O_2 evolution.

In contrast, the complex $[Mn_4O_4(O_2PPh_2)_6]^+$ (**153**) was found to react with excess phenothiazine via four sequential reduction steps that transfer a total of five electrons and four protons to it to produce water.[348] The final Mn product was proposed to be a "pinned butterfly" in this case as well. After the addition of 1 equiv of phenothiazine, $[Mn_4O_3(OH)(O_2PPh_2)_6]$ (**154**) was formed and isolated. One equivalent of the cation radical, $phzH^{\bullet+}$, was shown to transfer an H atom to the oxidized cubane complex to generate a phz^+ cation. A similar $[Mn_4O_3(OH)]^{6+}$ core exists in $[Mn_4O_3(OH)(OAc)_3(dbm)_3]$ (**145**).[340] The resulting species, $[Mn_4O_3(OH)(O_2PPh_2)_6]$ (**154**), was characterized by various spectroscopic techniques; however, X-ray quality single crystals were not obtained. Kinetic studies of the proton-coupled-electron-transfer reactions of both the cubane complexes, **152** and **153**, show that the rate constants differ by only 25% despite the large difference in the formal charges of the molecules.[349] These studies also support hydride transfer to the oxidized cubane in a two-electron proton-coupled-electron-transfer process that is hypothesized for the O−H bond cleavage step in photosynthetic water oxidation.

Bond enthalpy data predict that $[Mn_4O_4(O_2PPh_2)_6]$ is thermodynamically capable of generating dioxygen; however, it is kinetically prevented from doing so because of a large activation barrier. Thus, laser-desorption−ionization time-of-flight mass spectroscopy (LDI-TOF-MS) was conducted on the complex using a pulsed N_2 laser.[350] One of the two major peaks observed was the fragment $[Mn_4O_2(O_2PPh_2)_5]^+$, corresponding to the loss of one ligand and two oxide bridges. No fragment was found for either loss of one ligand only or loss of just two oxo groups. This experiment was also done on ^{18}O-labeled compound, and similar results were obtained. A quadrupole mass spectrometer interfaced to a Nd:YAG laser for excitation at 355 nm was applied to detect molecular oxygen. The authors propose that the loss of one ligand is necessary to bring two O atoms closer to form an O−O bond, as the O···O distance in this complex is much longer (2.53−2.60 Å) than that of O_2 or H_2O_2 (1.21 and 1.50 Å, respectively) molecules. On the basis of the LDI-TOF-MS studies and reduction studies mentioned above, mechanistic steps, shown in Scheme 6, were proposed to explain the photochemical O_2 generation and reductive dehydration.[350,351]

4.4.3.4. Adamantane-Shaped Complexes with a $[Mn_4(\mu\text{-}O)_6]$ Core. The first tetranuclear manganese complex, $[Mn_4(\mu\text{-}O)_6(tacn)_4]^{4+}$ (**155**), possessing an "adamantane" skeleton was reported by Wieghardt and co-workers.[352] Partially on the basis of this finding, Brudvig and Crabtree hypothesized an adamantane topology for the S_3 and S_4 states in a previously proposed mechanistic cycle.[177] The complex was isolated in crystalline form by treating the Mn(II) salt with the aqueous alkaline solution of the

ligand in the presence of dioxygen followed by the addition of sodium bromide. Interestingly, if the trimethyl-substituted form of the ligand (denoted as me_3tacn or tmtacn) is used instead, the corresponding Mn_4 species does not form. The tacn oxo-bridged Mn_4 complex has all Mn centers in their +4 oxidation state. The crystal structure reveals that the four Mn centers occupy the corners of a perfect tetrahedron (Figure 14) and that six bridging oxides are located above the center of each of the six edges. The average Mn···Mn distance in this complex is 3.21 Å. Characteristic electronic absorption bands at 336, 552, 770 (sh), and 1010 nm were observed for this complex in acetonitrile solution. Initial electrochemical studies showed neither oxidation nor reduction processes.[255] However, Armstrong and co-workers found later that there are two quasi-reversible redox processes for the perchlorate salt of this complex in dry acetonitrile at ~1.32 V (for $Mn^{V}Mn^{IV}_3 \rightarrow Mn^{IV}_4$) and at around −0.68 V (for $Mn^{IV}_4 \rightarrow Mn^{III}Mn^{IV}_3$) vs SCE.[217] Magnetic susceptibility data ranging between room temperature and 7.5 K show that there is an effective ferromagnetic exchange interaction present in this tetranuclear complex that gives rise to a $S = 6$ ground-spin state.[255]

An adamantane-shaped mixed oxo/hydroxo-bridged Mn^{IV}_4 complex, $[Mn_4O_5(OH)(tame)_4]^{5+}$ (**156**), was isolated and characterized by Armstrong and co-workers.[209] This complex was formed in 30% yield when $Mn(OTf)_2$ salt was allowed to react with the protonated ligand, tame·3HOTf, in the presence of Et_3N and atmospheric O_2 in acetonitrile for 36 h. This tetranuclear cluster can be deprotonated by using Et_3N in acetonitrile, generating the species $[Mn_4O_6(tame)_4]^{4+}$ (**157**), which has an electronic spectrum very similar to that of the tacn analogue (**155**) described above. The protonated form of the tacn-adamantane compound, $[Mn_4O_5(OH)(tacn)_4]^{5+}$ (**158**), was synthesized (by treating it with a 70% aqueous solution of $HClO_4$) and structurally characterized by the same research group.[209] The Mn_4 unit of the protonated tame-adamantane complex sits on an S_4 crystallographic axis, so that the OH group is disordered among four equivalent positions. The OH-proton was not detected in the crystal structure of $[Mn_4O_5(OH)(tacn)_4]^{5+}$ (**158**) either. However, the Mn-oxo distance for one of the oxygen atoms is much longer, indicating it is the OH group. The Mn···Mn distances fall within the range 3.22−3.45 Å. Additionally, protonation of the $[Mn_4(\mu\text{-}O)_6]^{4+}$ core not only results in lowering of the overall crystallographic symmetry in these complexes but also causes a dramatic change in the magnetic properties. The net Mn- - -Mn exchange interactions in these protonated adamantane complexes are antiferromagnetic in nature.

Successive double protonation of the $[Mn_4(\mu\text{-}O)_6(tacn)_4]^{4+}$ core was achieved by the addition of HOTf in acetonitrile under argon, as reported by Dubé et al.[353] Quantitative reversibility of the first and second protonation steps by the addition of Et_3N was demonstrated by spectrophotometric titration. The resulting magnetic and structural changes for double protonation of the $[Mn_4(\mu\text{-}O)_6]^{4+}$ core were investigated by ^1H NMR spectroscopy. Both the cis and trans isomers of doubly protonated $[Mn_4O_4(OH)_2(tacn)_4]^{6+}$ (**159**) species were found to be present in the solution in nearly equal amounts. Formation of the trans isomer is favored, since the *trans*-oxo group would be the most basic after single protonation and because of lesser columbic repulsion between the trans OH-protons. On the other hand, the statistical factor is higher for the four *cis*-oxo bridges over one *trans*-oxo bridge. The Mn- - -Mn exchange interaction changes from ferromagnetic in the parent complex to moderately antiferromagnetic in the singly protonated complex and to more strongly antiferromagnetic in the doubly protonated complex. NMR data support the fact that the *cis*-$[Mn_4O_4(OH)_2(tacn)_4]^{6+}$ isomer experiences much weaker coupling interactions compared to its trans counterpart. The core symmetry has been predicted to be D_{2d} for the trans isomer and C_s for the cis isomer. On the basis of this study, it has been postulated that the significant shift in the magnetic moment (by 9−17 μ_B^2) that was found for the PSII S_1 to S_2 transition[354,355] may involve changes in the protonation state of water-derived bridging ligands accompanying S state change.

Several other adamantane-shaped complexes containing the terminal "bpxa" series of the ligands have been synthesized and thoroughly characterized.[217] In contrast to tacn or tame, this series of ligands is capable of coordinating to the metal centers in both facial and meridional fashions. Furthermore, the basicity difference can appreciably alter redox and protonation behavior, as well as the reactivity of the resulting oxo-manganese complexes toward ligand dissociation and substitution. The all Mn(IV) bpxa-adamantane complexes have been prepared by comproportionation reactions of Mn^{II} and Mn^{VII} (MnO_4^-) starting materials. The bpea complex, $[Mn_4O_6(bpea)_4]^{4+}$ (**160**), has been structurally characterized. The Mn^{IV} centers are found to be at the apexes of a tetrahedron, and the bridging oxides are at the corners of an octahedron. Due to the low symmetry imposed by the facially coordinated bpea ligands, this complex possess only S_4 point symmetry. The Mn···Mn separations are ~3.24−3.25 Å. Cyclic voltammetric studies show that the complex undergoes a quasi-reversible first one-electron reduction at $E_{1/2} = 0.10$ V and an irreversible second one-electron reduction at −0.63 V vs SCE. The lower basicity of the ligand is accountable for the large positive shift in potential for the one-electron reduction compared to the tacn or tame analogues. The overall Mn- - -Mn exchange interaction is found to be ferromagnetic in nature, which is attributed to either intrinsic pairwise ferromagnetism or "spin-frustration" arising from the T_d symmetry of the $[Mn_4O_6]^{4+}$ core. One of the oxo groups can be protonated by HOTf to form $[Mn_4O_5(OH)(bpea)_4]^{5+}$ (**161**) in solution. The protonation process can be reversed by the addition of an equimolar amount of Et_3N, as illustrated by the spectrophotometric studies. ^1H NMR studies suggest similar structural and magnetic changes in this complex as were observed for the other adamantane complexes upon protonation (see above).

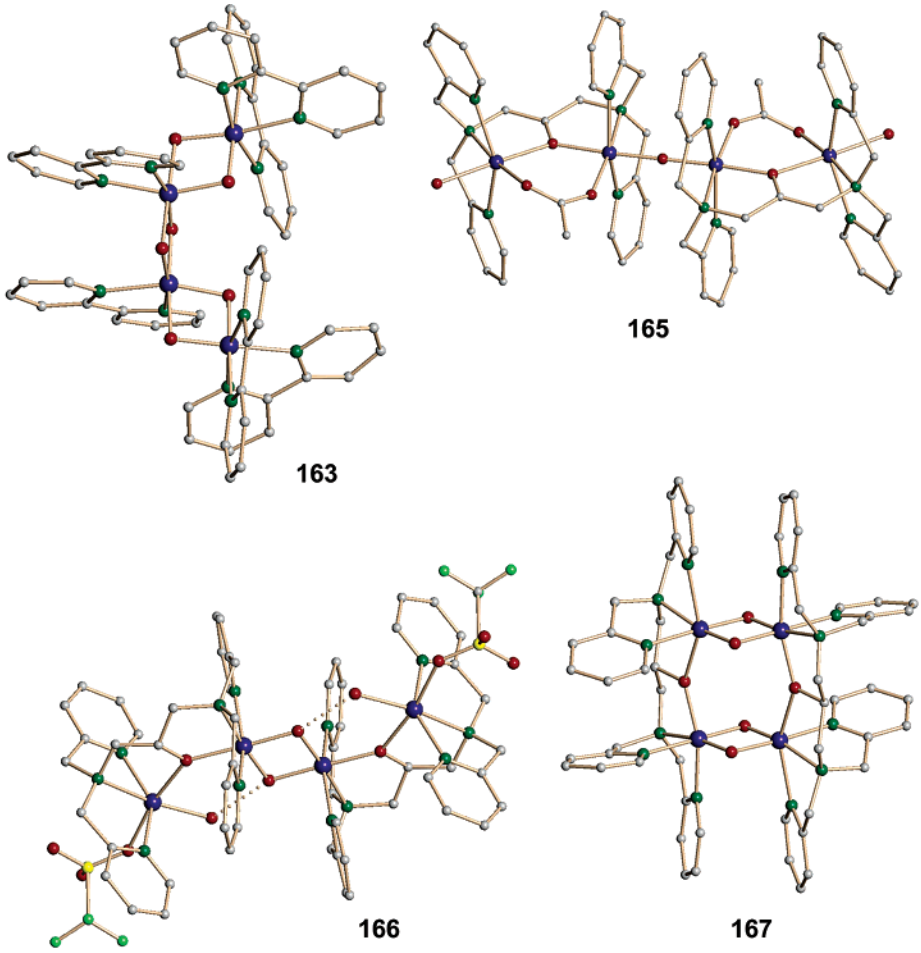

Figure 15. Crystal structures of selected tetranuclear manganese complexes portraying various core types. The Mn atoms are shown in blue, O atoms in red, N atoms in green, S atoms in yellow, Fl atoms in light green, and C atoms in gray.

One-electron reduction of **160** was accomplished by controlled potential electrolysis at −0.1 V.[217] The reduction can also be performed by using $Fe(Cp^*)_2$ or tertiary amines (such as Me_3tacn) as the reducing agents. The crystal structure showed that $[Mn_4O_6(bpea)_4]^{3+}$ (**162**) also has an adamantane skeleton, as shown in Figure 14. This reduced adamantane species contains a crystallographically distinguishable Mn^{III} center that has Jahn−Teller elongated Mn−N_{alkyl} and Mn−O bonds. The Mn···Mn distances range between 3.23 and 3.25 Å. Interestingly, the solution magnetic susceptibility of an acetonitrile solution of the mixed-valent adamantane complex prepared by bulk coulometry (μ_{eff}/Mn of 3.19 μ_B at 295 K) indicated that the reduction of $[Mn_4O_6]^{4+}$ to $[Mn_4O_6]^{3+}$ is accompanied by a change from net ferromagnetic coupling to overall moderately antiferromagnetic coupling within the manganese-oxo core. Magnetic susceptibility studies and EPR analysis show that this complex has an $S = {}^5/_2$ ground state and displays a broad signal centered at $g \approx 4$ analogous to one of the EPR signals of the PSII S_2 state.[356] Consequently, this complex was proposed as the first "spin-topological" model for the $g = 4.1$ S_2 state of the PSII water oxidase Mn_4 cluster.

Although the adamantane complexes mentioned above display a variety of reactivities that have mechanistic implications for the water oxidation process and show spectroscopic features that relate to that of the PSII active site, EXAFS data suggest that the adamantane core is too symmetrical and the Mn···Mn distance too long for it to be considered a structural model for the S_0-S_2 states.[48]

4.4.3.5. Open-Structure Homovalent Complexes with a $[Mn_4(\mu\text{-}O)_6]$ Core. An open-structure tetranuclear Mn(IV) complex, $[Mn_4(\mu\text{-}O)_6(bpy)_6]^{4+}$ (**163**), was first isolated by Girerd and co-workers from an acidified solution of $[Mn(bpy)Cl_3(H_2O)]$ (at pH ≈ 2).[357] Later, Dave and Czernuszewicz trapped this tetranuclear complex from the reaction of $[Mn_2O_2(bpy)_4]^{3+}$ (**19**) and $K_2Cr_2O_7$, although the dichromate counterion of the resulting complex makes it extremely insoluble in any common solvent.[358] Recently, Mènage and co-workers showed that this complex can be synthesized easily by the in situ reaction of Mn(II) salts with the ligand followed by the addition of a stoichiometric amount of $KMnO_4$ in acetate buffer at pH 4.5.[359] The core of this complex consists of three $[Mn_2(\mu\text{-}O)_2]$ units fused together exhibiting a "boat" or *cis*-conformation with respect to the plane of the central $[Mn_2O_2]$ core (shown in Figure 15). The average Mn···Mn distance is 2.75 Å. The manganese centers are strongly antiferromagnetically coupled to give rise to an $S = 0$ ground spin state. Consequently, no EPR signal was detected for this complex.[360] Magnetic susceptibility measurements were used to determine two strong antiferromagnetic Mn- - -Mn coupling interactions: $J = -134$ cm^{-1} for the central

$[Mn_2(\mu\text{-}O)_2]$ unit and $J = -88$ cm^{-1} for the two terminal $[Mn_2(\mu\text{-}O)_2]$ units. Cyclic voltammetry reveals irreversible features illustrating its inertness or instability toward redox processes by standard electrochemical or chemical routes.[360] However, the one-electron-reduced species, namely $[Mn^{III}Mn^{IV}_3O_6(bpy)_6]^{3+}$ (**164**), was obtained by cryogenic radiolytic reduction by exposure to γ-radiation (up to 6.5 Mrad) at 77 K in DMF.[361] The reduced complex exhibits an X-band multiline EPR signal that originates from a $S = {}^1/_2$ ground spin state at 77 K. The spectral width and intensity pattern of this hyperfine-structured signal are comparable to those of the PSII S_2 state signal. This species is unstable above 190 K, and therefore, structural analysis was not possible.

The structure of the all Mn(IV) analogue, $[Mn_4(\mu\text{-}O)_6(bpy)_6]^{4+}$, bears a strong resemblance to the proposed PSII EXAFS dimer-of-dimers model (Figure 15). However, the distance between the terminal Mn centers is much longer (6.28 Å) compared to a Mn···Mn distance of 3.4 Å as detected by EXAFS, and the complex lacks coordinated carboxylate ligands. On the basis of the oxidation states of the metal centers, this compound may be relevant to the S_3 or S_4 state of the enzyme active site.

4.4.3.6. Open-Structure Mixed-Valent Complexes. A heptadentate poly-pyridyl ligand, Htphpn, was employed by Armstrong and co-workers in attempts to synthesize tetranuclear manganese clusters relevant to the PSII active site.[170] The first isolated complex, $[\{Mn_2(tphpn)_2(OAc)(H_2O)\}_2O]^{4+}$ (**165**), formed when $Mn(OAc)_2$ was allowed to react with the deprotonated ligand (obtained by treatment with an equimolar amount of Et_3N) in methanol under ambient conditions.[362] The crystal structure in Figure 15 portrays that the complex comprises a pair of $Mn^{II}Mn^{III}$ moieties that are linked by a single oxo bridge between the Mn^{III} ions. The manganese centers are valence-trapped, as evidenced by the metal−ligand bond lengths. This was the first structurally analyzed tetranuclear species where a linear oxo group bridges the Mn^{III} centers and water molecules coordinate to Mn. The Mn^{II}···Mn^{III} distances are ~3.69 Å, whereas the Mn^{III} centers are ~3.53 Å apart from each other. Susceptibility measurements indicate that the antiferromagnetic interaction between the Mn^{III} centers is moderately strong whereas that between the Mn^{II} and Mn^{III} centers is weaker. Three quasi-reversible redox couples at $E_{1/2} = 0.83$, 1.05, and 1.35 V vs SCE, assigned to $II_2,III_2 \rightarrow II,III_3$; $II,III_3 \rightarrow III_4$; and $III_4 \rightarrow III_3IV$ couples, were observed in the cyclic voltammogram in acetonitrile, although oxidation of coordinated water cannot be ruled out. It should be mentioned here that the same complex was also reported by Suzuki et al.[363] They found that this tetranuclear species is unstable in ethanol and decomposes to form a Mn(II,III) dinuclear species, evident from the EPR spectrum.

An open chain Mn_4 complex, $[Mn_4O_2(tphpn)_2(OTf)_2(H_2O)_2]^{3+}$ (**166**), with the oxidation state assignment of $[Mn^{II}Mn^{III}Mn^{IV}Mn^{II}]$ was isolated when the above-mentioned reaction was attempted in the absence of acetate.[207] Either $Mn(ClO_4)_2$ or $Mn(OTf)_2$ salts can be used as the source of manganese for the synthesis of this compound. On the basis of the crystallographic data, the outer manganese atoms have been assigned as being in the +2 oxidation state, whereas the inner core contains a $[Mn^{III,IV}_2(\mu\text{-}O)_2]$ moiety with a Mn···Mn separation of ~2.72 Å. The crystal structure is shown in Figure 15. A water molecule and a triflate counterion are ligated to each Mn^{II} center. The water molecules are hydrogen bonded to the bridging oxide groups. The short O_{water}···O_{oxo} interaction (~2.6 Å) suggests that bond formation between these atoms may be promoted by an oxidation/deprotonation process to generate molecular oxygen. The manganese ions in this complex are found to be overall antiferromagnetically coupled, as indicated by the magnetic susceptibility studies. Uehara and co-workers reported that this compound shows a broad EPR signal at $g \approx 2$. They also found that substitution of the Mn^{2+} ions with Zn^{2+} ions causes a dramatic change in the EPR spectrum.[364] The resulting species exhibits a "16-line" hyperfine signal that is consistent with a $[Mn^{III,IV}_2O_2]^{3+}$ core (see section 4.4.1). This observation strongly supports the oxidation state assignment of valence-trapped [II,III,IV,II] for this complex.[364] Cyclic voltammograms of this mixed-valent Mn_4 complex and its Zn analogue show two quasi-reversible redox couples at 0.39 and 0.93 V vs SCE and 0.50 and 0.96 V vs SCE, respectively. These data indicate that the one-electron redox processes are associated with the central dinuclear Mn(III,IV) moiety, not with the Mn^{II} centers.

4.4.3.7. Dimer-of-Dimers Core. Chan and Armstrong showed that the aerial oxidation of **166** in acetonitrile yields a novel mixed-valent tetranuclear species, $[Mn_4O_4(tphpn)_2]^{4+}$ (**167**), where two $[Mn^{III,IV}_2(\mu\text{-}O)_2]^{3+}$ units are connected to each other by the alkoxide bridges, as shown in Figure 15.[365] This is a close analogue of the proposed EXAFS dimer-of-dimers model. The Mn···Mn separations in the dinuclear units and between two $[Mn_2O_2]$ units are ~2.65 and ~3.97 Å, respectively. The valent trapped dimanganese units show antiferromagnet coupling ($J = -101$ cm^{-1}) with $S = {}^1/_2$ state for each dinuclear unit, and two dinuclear units interact with each other ferromagnetically ($J = +38.8$ cm^{-1}) to give a triplet ($S = 1$) ground state.[366] This complex shows a broad parallel polarization EPR spectrum at liquid He temperature with a peak-to-peak width of 700 G, centered at $g \approx 6$ that resembles the PSII S_1 state EPR signal. The oxidation state assignments of the Mn centers are also in agreement with that of the S_1 state, making it a good spectroscopic model for the WO active site.[365] (See the note added in proof in section 7.)

Another complex with a dimer-of-dimers topology, $[Mn_4O_4(tmdp)_2(H_2O)_2]^{4+}$ (**168**), was reported by Uehara and co-workers, where they used a similar polydentate pyridyl-based ligand, Htmdp.[367] This complex contains two dimeric units, each containing two valence-trapped Mn^{III} and Mn^{IV} ions. In this complex, the alkoxide groups are monodentate and bind to the dimers alternatively, as opposed to the case of **167** (Figure 16), where the alkoxide groups are coordinated to both the dimeric units simultaneously. As a result, the shortest Mn···Mn separation

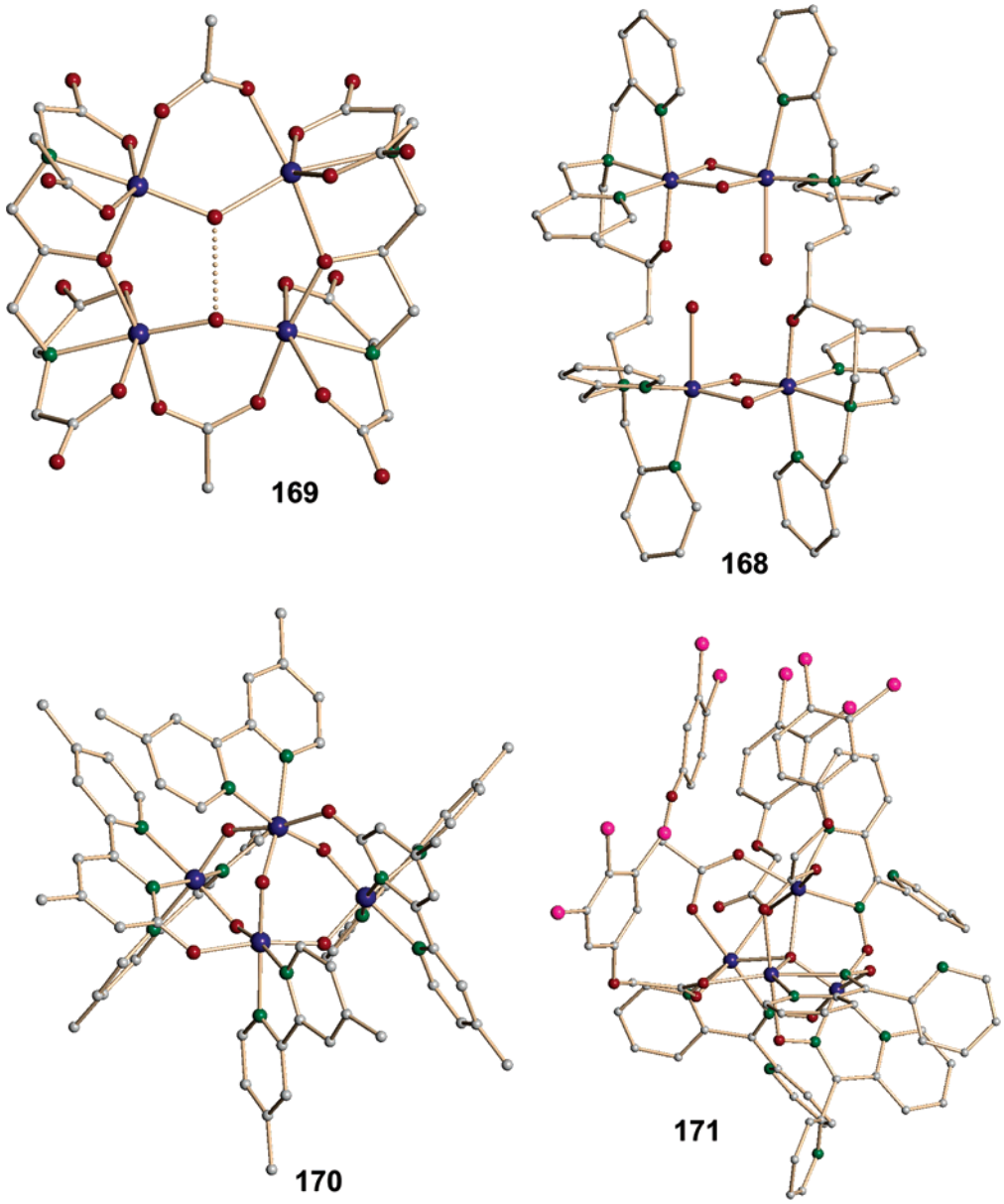

Figure 16. Crystal structures of selected tetranuclear manganese complexes portraying various core types. The Mn atoms are shown in blue, O atoms in red, N atoms in green, Cl atoms in pink, and C atoms in gray.

between the dinuclear units is 5.9 Å. The Mn···Mn distance within the dinuclear unit is ~2.65 Å. Water molecules occupy the sixth coordination sites of the Mn(III) centers. The intradimer interaction is antiferromagnetic in nature with $J = -145$ cm^{-1}, significantly higher than that for the tphpn dimer-of-dimers. The interdimer interaction is weakly ferromagnetic ($J = 0.2$ cm^{-1}), giving rise to a $S = 1$ spin ground state. Hydrogen bonding is believed to be responsible for the interdimer exchange interactions. Two broad EPR signals centered at $g \approx 4.5$ and $g \approx 2$ have been detected in frozen solution. A quasi-reversible redox response at 0.96 V (vs SCE) has been observed for this complex. The one-electron-oxidized [$Mn^{III}Mn^{IV}_3$] species, which can be generated by bulk electrolysis at +1.0 V, exhibits a 16-line EPR signal centered at $g \approx 2$, supporting the retention of the dimer-of-dimers core.[368]

Another tetranuclear complex, [$Mn^{III}_3Mn^{II}(\mu$-O)-(μ-OH)(μ-OAc)$_2$(tahpn)$_2$]$^{4-}$ (**169**), consisting of a dimer-of-dimers topology has been synthesized by Gorun and co-workers with the aid of a heptadentate tetracarboxylate ligand (tahpn).[369,370] This complex was synthesized by air oxidation of a pH ~ 7.0 aqueous mixture of an Mn^{II} source and the Ca or Ba salt of the ligand. Consequently, the complex crystallizes with either Ca^{2+} or Ba^{2+} as counterions. Calcium ion has been found to be essential for the catalytic activity of the water oxidase. At least one Ca^{2+} is believed to be linked to the Mn_4 cluster by a carboxylate at a distance of 3.3 Å (or larger than 3.6 Å).[36,61,108,109] This is the only tetranuclear complex reported that has a calcium ion present. The structure of the cation is shown in Figure 16. The Mn centers are valence-trapped in the molecule, as indicated by the existence of the Jahn−Teller distortion axes for Mn^{III} ions. The [Mn^{III}_2O(OAc)] unit is linked to the [$Mn^{II}Mn^{III}$(OH)-(OAc)] moiety through two alkoxide bridges provided by the ligands. A hydrogen-bonding interaction is present between the oxo and hydroxo groups to result in a short O···O interaction of 2.48−2.56 Å in these complexes. The distance between two Mn^{III} centers

in one dinuclear unit falls between 3.31 and 3.38 Å. The Mn^{II} and Mn^{III} centers are ~3.50−3.58 Å apart from each other in the other dinuclear unit. The Mn···Mn distances between two dimeric cores are ~3.71−3.83 Å. The Mn···Ca distances range from 4.89 to 6.17 Å. This complex was shown to decompose H_2O_2 to generate O_2 and, thus, is the first example of a biomimetic Mn_4/Ca model. The catalase-like activity of this complex and other related species has been reviewed recently by Pecoraro and co-workers.[371]

4.4.3.8. Open Structure with a Mn_4O_5 Core. The proposed PSII EXAFS dimer-of-dimers model by Klein and co-workers contains a $[Mn_4(\mu\text{-}O)_5]$ core. To date, there is only one complex known comprising a $\{Mn_4(\mu\text{-}O)_5\}$ moiety, $[Mn_4(\mu\text{-}O)_5(dmb)_4(dmbO)_2]^{4+}$ (**170**).[203] It has a rather open arrangement of four Mn atoms and five μ-oxo groups. This complex was synthesized by oxidizing a solution of $Mn(ClO_4)_2$ and ligand with 90% *tert*-butyl hydroperoxide. As evident in the crystal structure, shown in Figure 16, two of the six dmb ligands have also been oxidized selectively at the 6 position of the pyridine ring and are denoted as "dmbO". These two dmbO ligands bridge a pair of Mn atoms. Because of these manganese−aryloxo bonds, two of the Mn···Mn distances are slightly shorter (average 3.18 Å) than the other two (average 3.28 Å). The Mn and aryloxo−oxygen bond distances are longer than the Mn−oxo bonds (1.94 vs 1.77 Å). The Mn−O−Mn angles range from 126° to 132° for this compound. The manganese centers are antiferromagnetically coupled to give an $S = 0$ ground state. Consequently, the complex shows no perpendicular-mode EPR signal at low temperature. The Mn···Mn distances in this species rule it out as a close analogue of the PSII Mn_4 complex in the S_1 or S_2 state. However, as the recent EXAFS studies show significant elongation of the Mn···Mn separation in the S_3 state, indicating a possible structural rearrangement (see section 2.3 for details),[37] this complex may be structurally relevant to the higher Kok S states, namely S_3 or S_4. (See the note added in proof in section 7.)

4.4.3.9. Low-Valent Tetrahedral Structures. A tetranuclear manganese complex, $[Mn^{II}_3Mn^{IV}(\mu_4\text{-}O)(pko)_4(dcpaa)_4]$ (where dcpaa = 3,4-dichlorophenoxy acetic acid) (**171**), where valence-trapped Mn^{II} and Mn^{IV} centers are adjacent to each other has been reported by Kessissoglou and co-workers.[311] The central $[Mn_4(\mu_4\text{-}O)]^{8+}$ core has been described as a distorted Mn_4 tetrahedron, where all the Mn centers experience octahedral coordination environments (Figure 16). The μ_4-oxo group is at the center of the tetrahedron bridging all four metal centers. In contrast, in $[Mn_4O_4]$ cubane or $[Mn_4O_6]$ adamantane structures there are four μ_3-oxo groups and six μ-oxo groups, respectively, which bridge the manganese centers, occupying the apices of a tetrahedron. Mn···Mn separations fall in the range 3.18−3.61 Å. Variable temperature magnetic studies support the oxidation state assignment being [II,II,II,IV], which gives rise to a $S = 6$ ground spin state resulting from overall ferromagnetic couplings ($J = -4.15$, 48.4, 1.33 cm^{-1}). Several other tetrahedral $Mn^{II}_2Mn^{III}_2$ complexes supported by macrocyclic Schiff base ligands were reported earlier by McKee and co-workers.[372,373]

4.5. Theoretical Calculations

Not enough structural information is available for the WO active site to delineate a complete mechanistic pathway. The proposed mechanistic pathways were described in section 3. This section will highlight some of the theoretical studies and conclusions made therefrom. A tremendous effort has been made to understand the key steps in the entire catalytic cycle, that is, O−O bond formation, by using density functional theory (DFT). In an early study, methods other than DFT were used to calculate the energies of the key steps in this process.[374] The following conclusions were summarized: (i) The repulsive O···O interaction was surmised to be overcome by binding energies gained from Mn ions binding to the water molecules, (ii) transfer of protons is eased by stronger bases than water, and (iii) a single elementary four-electron oxidation step was unlikely. Soon after, many of the studies focused on complex geometries suggested by synthetic model chemistry. In this regard, dinuclear complexes belong to a class of minimal models being represented in many proposed reaction mechanisms, and as such, many calculations have focused on this particular unit. These studies by themselves do not afford a complete picture but provide clues concerning the entire cycle.[297,375−379] The peroxo bridged dinuclear complex, $[Mn^{IV}_2(\mu\text{-}O)_2(\mu\text{-}O_2)]^{2+}$ (**97**), that has been mentioned in section 4.4.1, has been examined by DFT methods though the existence of such species as a relevant intermediate has been questioned.[176] Hypothetical two-electron reduction of this complex has been shown to cause cleavage of the peroxo bond while the two-electron oxidation results in the formation of molecular oxygen.[376] Both transformations involve metal centered redox processes with the stability of the intermediate species being affected by the mode of coupling between the metal centers. The facile reductive cleavage of the peroxo bond in the Mn^{IV}_2 complex has been attributed to the Jahn−Teller effect, and the same principle explains the stability of the $[Mn^{III}_2(\mu\text{-}O)(\mu\text{-}O_2)]$ complex.[297] Interestingly, this provides some insight into the observed stability of peroxide in the synthetically isolated complex, $[Mn^{III}_3(\mu_3\text{-}O)(\mu\text{-}O_2)(OAc)(dien)_3]^{2+}$ (**99**). Intramolecular formation of O−O bonds in dinuclear complexes has also been investigated in the $[Mn_2(\mu\text{-}O)_2(NH_3)_6(H_2O)_2]^n$ (n = 2−5) family by DFT studies.[380] The MO picture that has emerged shows that one-electron oxidation of $[Mn_2(\mu\text{-}O)_2]^{4+}$ affects mainly the oxygen atom, consequently ruling out the formation of Mn^V species. The O−O bond in O_2^{3-} transiently forms ultimately dissociating dioxygen and a $Mn^{II,III}$ species. The first work on dinuclear model complexes was reported in 1992 where four dinuclear complexes (two di-μ-oxo, one tri-μ-oxo, one carboxylato-two-di-μ-oxo) were distorted to form O_2 bound complexes.[381] The formation of dioxygen through a peroxo intermediate was found to be energetically favorable, requiring two two-electron steps. It was found that an in-plane approach of two oxo groups is slightly less energeti-

cally demanding though they resulted in singlet oxygen release. A number of tetranuclear clusters guided by known inorganic models were also studied by the extended Hückel approach. These were (i) a $[Mn_4O_4]$ cubane-like core, (ii) $[Mn_2O_2]_2(\mu\text{-}O_2)_2$ dimer-of-dimers with a $\{\eta^2\text{-}\mu_4\text{-}O_2\}$ bound either in or out of the plane formed by the two coplanar $[Mn_2O_2]$ units, and (iii) a "planar -T" combination of two orthogonal $[Mn_2O_2]$ units with a Mn_3O_2 core and a $\{\eta^2\text{-}\mu_3\text{-}O_2\}$ bound to three Mn atoms. The least energetically demanding pathways were proposed for $[Mn_2O_2]_2$-$(\mu\text{-}O_2)$ and planar T models with the in-plane O−O approach. Overall it was found that coordination of oxo ligands to three Mn ions as opposed to two Mn ions was slightly favorable, bringing to light the objective of using a tetranuclear center along with a Ca^{2+} ion to perform the oxidation process. This opinion was voiced by researchers elsewhere.[382] In the latter work, universal force field techniques were utilized to minimize energies of two peroxo containing dinuclear subsets of dimer-of-dimers Mn aggregates. The metrical parameters agree well with those reported for peroxo species in the literature with the bound Cl^- ion reducing the effective charge on the attached metal site. The tetranuclear models with coordinated peroxo species are bound asymmetrically with Mn−O−O−Mn torsion angles ∼ 60°. Though only two Mn ions are proposed to be involved in the oxidation process, removal of two Mn ions is shown to be energetically unfavorable by ∼0.3 eV compared to the tetranuclear model.

The most current theoretical studies involving a Mn_3 model and also including Ca^{2+} and Cl^- ions are those of Siegbahn, who employs DFT techniques.[193,383] This model has been derived by systematically varying the positions of bridging water and hydroxides and calculating the corresponding O−H bond strengths that are correlated to trans effects and locations of the Jahn−Teller axis. The proposed mechanism using this strategy has been discussed above in section 3. One of the key highlights of the proposed steps involves the oxidation of a bridging oxygen (S_2 to S_3 conversion step) as opposed to a Mn ion and/or other ligands, forming a coordinated oxyl radical. The transition state for the O−O bond forming step was optimized, and an energy barrier of 15.1 kcal·mol^{-1} was reported, which is only slightly higher than the experimental barrier of 14 kcal·mol^{-1}. It was argued that the structure of their optimal Mn_3Ca cube is the only structure that provides the correct energetics for O−O bond formation. This structural motif is consistent with EPR and ENDOR data.[81] There is considerable doubt regarding the position of the fourth Mn ion. An attempt to address this problem has been made. Accurate values of the changes in Mn−Mn bond distances during the catalytic cycle were calculated.[193] However, the Mn···Mn bond separation is inaccurate in this model, as one of the Mn···Mn distances is longer in the S_1 and S_2 states by ∼0.05 Å compared to the case of the other pair. This has been rationalized by postulating that the Ca^{2+} is in closer proximity to this particular Mn···Mn distance, a feature that is not consistent with the EXAFS results.[60,384] This particular study, though lacking in the details of the steps leading to O−O bond formation,[17,193] has provided a structural entity that has been supported by other biophysical measurements.

4.6. Functional Analogues of Water Oxidase

Polynuclear manganese-oxo complexes described in section 4.4 have played an indispensable role in the search for a structural analogue for the WO active site. Though much progress has been made in this direction, attainment of functional behavior with structurally competent manganese clusters has not yet been achieved. However, a significant number of homogeneous catalysts and a few heterogeneous catalysts have been developed over the years for water oxidation. These systems have been recently reviewed elsewhere,[16,83,385] and thus, only a selected few that have direct implications in the WO function will be briefly discussed here.

The history of developing water oxidation catalysts goes all the way back to when Shilov and co-workers reported the activity of a colloidal MnO_2 system. In the presence of strong oxidants such as Ce^{4+}, MnO_4^-, $Ru(bpy)_3^{3+}$, or $Fe(bpy)_3^{3+}$, colloidal MnO_2 was shown to catalyze water oxidation.[386] Catalytic activity was enhanced by incorporating the manganese oxide particles into phospholipid membranes.[387,388] Later, the well studied dimanganese complex, $[Mn_2O_2(bpy)_4]^{3+}$ (**19**), potentially capable of splitting water, evolved oxygen from water on illumination in very low yield only when present as a solid or absorbed in kaolin clay.[389] There had been an earlier report of photolytic water oxidation on a silver−gold electrode surface by Calvin using the same dinuclear complex, **19**.[390] However, Cooper and Calvin immediately reported a correction, which stated that the apparent oxygen evolution was caused by a change of 0.4 °C in the temperature of the sample solution due to illumination during measurement, resulting in diffusion of atmospheric oxygen across the electrode membrane.[391]

Matsushita and co-workers demonstrated that mononuclear Mn(IV) Schiff base complexes with the formulation *trans*-$Mn^{IV}(ans)_2Cl_2$ (where ans = *N-alkyl*-3-nitrosalicylimide) are capable of generating oxygen in MeCN/water solution as well.[392,393] The liberation of dioxygen was monitored using an oxygen electrode and pyrogallol solution and was found to be at a maximum at neutral pH. A two-electron $Mn^{IV} \rightarrow Mn^{II}$ reduction process was suggested for delivering oxidizing equivalents required for water oxidation.[394] An *o*-phenylene-bridged Mn^{III}-porphyrin dimer (**172**) was later shown to catalyze electrochemical water oxidation with 5−17% efficiency at a potential of +1.2 to 2.0 V (vs Ag/Ag$^+$) in an acetonitrile/water mixture in the presence of *n*-Bu_4NOH as the supporting electrolyte.[395] A terminal Mn=O species was postulated as the reactive intermediate in this process.

The catalytic activity of a μ-oxo Ru^{III} dimer, $[(bpy)_2(H_2O)Ru^{III}ORu^{III}(OH_2)(bpy)_2]^{4+}$ (**173**) (and its derivatives), toward water oxidation in the presence of Ce(IV) has been studied extensively by Meyer among others[396−401] and has prompted a great deal of discussion in the photosynthetic research community. The

Ce^{4+} oxidizes **173** stepwise by four electrons (III,III → III,IV → IV,V → V,V) to generate a $Ru^{V}ORu^{V}$ species, in which the terminal aquo ligands are fully deprotonated to Ru=O moieties, as confirmed by resonance Raman studies. This (V,V) species is capable of converting water to O_2 between pH ∼ 1 and 7. However, the catalytic activity of **173** is thwarted greatly after only 10−25 turnovers because of oxidative degradation and anation induced by O_2 evolution.[174]

The $[Mn_4O_4]^{6+}$ cubane complex, **152**, has been shown to release two bridging oxo groups in the form of O_2 when irradiated with a laser beam at 355 nm (for details see section 4.4.3.3). This process accompanies a loss of a diphenylphosphinate ligand, which has been conjectured as a key step for the O−O bond formation. The resulting manganese complex has been put forward as a $[Mn_4O_2]^{6+}$ butterfly structure on the basis of the mass spectral data.[350,351] Such cubane to butterfly core conversion coupled with O_2 evolution was proposed in one of the earlier mechanisms.[178] However, this complex (**152**) is far from being a functional model, as it neither oxidizes water nor shows any catalytic behavior.

Brudvig and co-workers reported that when $[Mn^{II}(dpa)]^{-}$ (where dpa = dipicolinate) was added to a solution of oxone ($KHSO_5$), an oxygen atom transfer agent and powerful oxidant, a green solution resulted and dioxygen was generated catalytically below pH 3.5.[402] The green solution was surmised to be a Mn(III,IV) species on the basis of spectroscopic data. However, formation of MnO_4^{-} from the green species occurs concomitantly with O_2 evolution and causes termination of the catalytic process. The authors suggested that tridentate ligands capable of meridional coordination are required for oxygen evolution. Subsequently, they reported the catalytic activity of a structurally characterized dimanganese(III,IV) complex (**36**), supported by the planar ligand terpy in the presence of sodium hypochlorite as the oxidant.[254] On the basis of ^{18}O isotope labeling experiments, a dinuclear species containing a Mn^{V}=O moiety was proposed as the active intermediate. Such a terminal oxo-manganese species is also proposed to be involved in PSII water oxidation. A multimanganese system containing such a feature is yet to be synthesized.[17,79,175,176,181] Only a few monomeric Mn=O species that show no activity toward water oxidation have been reported with porphyrin and tetraamide ligands.[157,160,403−405] In the study by Brudvig and coworkers, water was suggested to be the source for the liberated oxygen, as $^{18}O_2$ was detected when $H_2{}^{18}O$ was used. A control experiment in the absence of the catalyst was reported to show a slower exchange rate of hypochlorite with water under the reaction conditions and thus excluded it as the possible source of oxygen. However, their recent studies using resonance Raman spectroscopy demonstrated that the O-atom exchange of OCl^{-} with water is rather fast ($t_{1/2}$ < 10 s) and thus may account for the labeled oxygen formed.[406] On the other hand, the exchange rate for oxone was found to be slower and thus was examined further in order to determine the oxygen source for generated O_2 in the system that employs **36**. In the presence of high concentrations of oxone and $H_2{}^{18}O$, a negligible amount of labeled product was formed, confirming oxone as the likely source for O_2. Lowering the ratio of oxone to **36** to 5:1 results in the increase of doubly labeled $^{36}O_2$ and mixed-labeled $^{34}O_2$. On the basis of these findings, two different mechanistic pathways involving a common Mn^{V}=O species that can exchange with water and then react with water or oxone to generate dioxygen were put forward (shown in Scheme 7). The formation of a Mn^{V}-oxo intermediate is proposed as the rate-limiting step. The authors claim this dinuclear Mn(III,IV) complex (**36**) as a functional model for PSII WO, although their studies provide no irrefutable evidence for water oxidation or for the existence of Mn^{V}=O intermediates. Recently, DFT and hybrid functional B3LYP calculations on the O−O bond formation step from water promoted by **36** (step I in Scheme 7) have been performed.[407] These studies favor a Mn^{IV}-oxyl radical as the reactive intermediate for O−O bond formation over a Mn^{V}-oxo formulation. A similar active species was also proposed for the O−O bond-forming step in the PSII WO active site.[14,17] Additionally, these calculations show that the energy barrier for O_2 formation with water is a few kilocalories per mole higher than that with oxone (∼23 vs 18 kcal/mol), which suggests that the oxygen formation from water is not energetically unfavorable. However, these studies do not include calculations on the oxone to oxygen conversion pathway (step III in Scheme 7). Also, they do not comment on the uniqueness of this particular system over other $Mn^{III/IV}Mn^{IV}$ diaquo complexes (for example, **62**) with other chelating ligands. Nonetheless, isolation and characterization or convincing transient observation of the Mn-oxo intermediate(s) for this process is extremely critical in order to discern the correct mechanism. (See the note added in proof in section 7.)

Scheme 7. Proposed Mechanism of O_2 Evolution by 36 (Adapted from Ref 406)

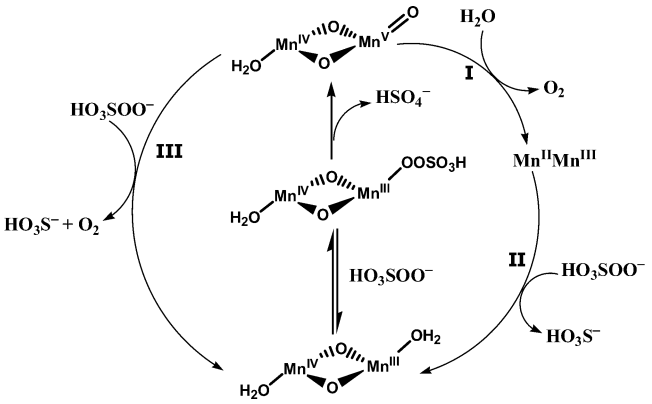

5. Conclusions and Future Perspective

A vast amount of time and effort has been devoted toward the synthesis and characterization of Mn-oxo complexes in order to better understand the structural and physicochemical properties of the WO site in PSII. Bioinorganic chemists' search for a synthetic analogue to accurately represent the Mn_4 active site

has been handicapped due to the absence of an adequate crystal structure of the enzyme at the desired resolution. Various biophysical studies (XAS, EPR, pulsed EPR, FTIR, and Raman) on the native enzyme have provided insightful perspectives regarding the mechanism of water oxidation and also have resulted in proposals of structural analogues of the tetramanganese cluster. The veracity of some of these biologically valid structural motifs has not yet been fully assessed; if indeed these species can be isolated in a peptide unassisted environment. This review focuses on the synthesis and properties of high-valent Mn-oxo chemistry during the period 1975−2003. The research presented here is the results of collaborative work in inorganic chemistry, biophysical chemistry, and protein crystallography. A major emphasis has been put toward complexes that have direct and/or indirect relevance to the PSII Mn_4 site. Though the major goal at the outset, that is, achieving a structural and functional analogue species, has not yet been realized, numerous examinations of synthetic strategies by many research groups have jointly led to the development of the rich chemistry that has few parallels in modern synthetic bioinorganic chemistry. Most of the compounds, ranging from dinuclear to tetranuclear Mn-oxo species, have been documented in this review. Higher nuclearity clusters (>4) form a large family of complexes that is beyond the scope of this present review, though structural segments imbedded in some of them bear similarities with the PSII WO active site.[13,218,408] Efforts have been made to summarize the recent spectroscopic studies (XAS, EPR and pulsed EPR, and FTIR) pertaining to the native enzyme and also to relevant synthetic complexes, which have enabled better understanding of the mechanism involved in the PSII catalytic O_2-evolving cycle. Theoretical calculations have also been mentioned wherever appropriate. All these data have helped in providing some aspects of the catalytic cycle, though we appear to be far from total elucidation of the mechanism. Functionally and/or spectroscopically viable analogue complexes have been claimed though the actual relevance of some of these with respect to the WO site is unclear currently. A lack of an agreed upon structural motif for the WO site at all S states has made these studies challenging and often speculative.

Recent crystal structures by Zouni et al.,[8] Kamiya and Shen,[9] and Ferreira et al.[10] of PSII WO at improved resolution have rekindled hopes among bioinorganic chemists of finally knowing the metal ion arrangement as well as the ligation environment of the Mn_4 cluster. In the most recent crystal structure, Ferreira et al. proposed a Mn_3Ca cubane core linked to a mono-oxo-bridged manganese center for the active site.[10] This remarkably different geometry suggested by the authors with only marginally improved resolution compared to those for the previous two crystal structures is surprising. Furthermore, the structural changes of this multicluster PSII assembly when exposed to an X-ray beam over a prolonged period of time during data collection should also be considered. An obvious path to resolve these issues would be to obtain a structure of a fully functional PSII crystal at a resolution where the exact positions of the Mn_4Ca core along with the surrounding ligands and cofactors can be accurately located. When such a structure indeed becomes available, the exploratory nature of the research that has characterized this area to date could be altered to a more direct target based approach. It is worthwhile to point out that the structure of the Mn_4Ca core involved in the above discussion represents a single intermediate in the entire catalytic cycle. The plethora of knowledge gained from the manganese coordination chemistry described herein will certainly be extremely useful to prepare a synthetic analogue PSII WO Mn_4 cluster for the dark adapted state as well as for the other intermediate S states, the structural identity of which is difficult to attain by X-ray diffraction methods. Until then, new studies and new synthetic challenges that further broaden the horizons of high-valent Mn-oxo chemistry need to be addressed.

6. Abbreviations

bbae	2-[bis(benzimidazol-2-ylmethyl)amino]ethanol
bbpe	1,2-bis(2,2′-bipyridine-6-yl)ethane
bbpmax	α,α′-bis(bis(2-pyridylmethyl)amino)-*m*-xylene
bhdmen	*N*,*N*-bis(2-hydroxybenzyl)-*N*′,*N*′-dimethylethylenediamine
bisimMe_2en	*N*,*N*′-dimethyl-*N*,*N*′-bis(2-imidazol-4-ylmethyl)ethane-1,2-diamine
bispicen	*N*,*N*′-bis(2-methylpyrid-2-yl)ethane
bispicMe_2en	*N*,*N*′-dimethyl-*N*,*N*′-bis(2-pyridylmethyl)ethane-1,2-diamine
bispicMe_2(−)-chxn	*N*,*N*′-dimethyl-*N*,*N*′-bis(2-pyridylmethyl)-(−)D-1,2-cyclohexanediamine
bpea	*N*,*N*-bis(2-pyridylmethyl)ethyldiamine
bped	*N*,*N*′-bis(2-methylpyrazyl)ethane-1,2-diamine
bpen	*N*,*N*′-bis((6-methylpyrid-2-yl)methyl)ethane-1,2-diamine
bpia	bis(picolyl)(*N*-methylimidazol-2-yl)amine
bpmpa	*N*,*N*′-bis((6-methylpyrid-2-yl)methyl)-*N*-2-pyridylmethylamine
bpmsed	*N*,*N*-bis(2-pyridylmethyl)-*N*′-salicyliden-1,2-diaminoethane
bpta	*N*,*N*-bis(2-pyridylmethyl)*tert*-butyldiamine
bpy	2,2′-bipyridine
cyclam	1,4,8,11-tetrazacyclotetradecane
cyclen	1,4,7,10-tetraazacyclododecane
dbmH	dibenzoylmethane
dien	diethylenetriamine
dmb	4,4′-dimethyl-2,2′-bipyridine
dtne	1,2-bis(1,4,7-triazacyclonon-1-yl)ethane
EPR	electron paramagnetic resonance
ENDOR	electron nuclear double resonance
ESEEM	electron spin−echo envelope modulation
EXAFS	extended X-ray absorption fine structure
H_3bsp	1,5-bis(salicylideneamino)-3-pentanol
$HB(pz)_3^-$	hydrotris(1-pyrazolyl) borate
Hdpm	dipivaloylmethane
Hhqn	8-hyrdoxyquinoline
Hhmp	2-(hydroxymethyl)pyridine
HIm	imidazole
Hpic	picolinic acid
H_2sal	salicylic acid
H_2salpn	*N*,*N*′-trimethylenebis(salicylidene)-1,3-diaminopropane

H_2saladpH	1,3-dihydroxy-2-methyl-2-(salicylidine amino)propane
Htmdp	1,5-bis[bis(2-pyridylmethyl)amino]-3-pentanol
Htphpn	*N*,*N*,*N*′,*N*′-tetrakis(2-pyridylmethyl)-2-hydroxypropane-1,3-diamine
H_2XDK	*m*-xylenediaminebis(Kemp's triacid imide)
Me_4dtne	1,2-bis(4,7-dimethyl-1,4,7-triazacyclonon-1-yl)ethane
Me_3tacn or tmtacn	1,4,7-trimethyl-1,4,7-triazacyclononane
mpdp	*m*-phenylenedipropionate
mpepma	methyl(2-(2-pyridyl)ethyl)(2-pyridylmethyl)amine
mpmpepa	((6-methyl-2-pyridyl)methyl)(2-(2-pyridyl)-ethyl)(2-pyridylmethyl)amine
N_3O-py	*N*,*N*′-bis(2-methylpyrid-2-yl)glycinate
5-NO_2-saldien	*N*,*N*′-bis(5-nitrosalicylidene)-1,7-diamino-3-azapentane
pbz	2-pyridylbenzimidazole
pc	phthalocyanine
pepma	(2-(2-pyridyl)ethyl)bis(2-pyridylmethyl)-amine
peppepma	(1-(2-pyridyl)ethyl)(2-(2-pyridyl)ethyl)(2-pyridylmethyl)amine
phen	1,10-phenanthroline
PhNIT	2-phenyl-4,4,5,5-tetramethyl-4,5-dihydro-1*H*-imidazolyl-1-oxy-3-oxide
phth	phthalate
pmap	bis[2-(2-pyridyl)ethyl]-2-pyridylmethyl
py	pyridine
pzH	pyrazole
saltren	salicylaldimine
tacn	1,4,7-triazacyclononane
tame	1,1,1-tris(aminomethyl)ethane
tahpn	1,3-diamino-2-hydroxypropane-*N*,*N*,*N*′,*N*′-tetraacetic acid
terpy	2,2′:6,2″-terpyridine
tmima	tris(1-methylimidazol-2-yl)methylamine
tmip	tris(*N*-methylimidazol-2-yl)phosphine
tpa	tris(2-methylpyridyl)amine
tpen	*N*,*N*,*N*′,*N*′-tetrakis(2-pyridylmethyl)-1,2-ethanediamine
tpp	*meso*-tetraphenyl porphinato dianion
tppn	*N*,*N*,*N*′,*N*′-tetrakis(2-pyridylmethyl)-1,3-propanediamine
tren	2,2′,2″-triaminotriethylamine
ttco	trispyrrolidine-1,4,7-triazacyclononane
XANES	X-ray absorption near edge spectroscopy
XAS	X-ray absorption spectroscopy
XES	X-ray emission spectroscopy

7. Note Added in Proof

Recently, Armstrong and co-workers reported that **167** undergoes a nonredox isomerization or shape-shifting process in solution (*J. Am. Chem. Soc.* **2004**, *126*, 9202). One-electron oxidation of **167** results in the formation of an adamantane-shaped complex, $[Mn_4O_4(tphpn)_2]^{5+}$. In addition, the one-electron reduced species of **167**, $[Mn_4O_4(tphpn)_2]^{3+}$, exhibits a multiline EPR signal around $g = 2$, which is strikingly similar to that of the S_0 state of the WO active site.

Recently, the second complex containing a $[Mn^{IV}{}_4O_5]^{6+}$ core, $[Mn^{IV}{}_4O_5(terpy)_4(H_2O)_2](ClO_4)_6$, has been reported by Brudvig and co-workers (*J. Am. Chem. Soc.* **2004**, *126*, 7345). This complex structurally resembles the proposed "dimer-of-dimers EXAFS model", although the dimanganese moieties are not stacked with each other. This complex has a linear Mn−O−Mn unit with a Mn···Mn separation of ∼3.5 Å and lacks carboxylate ligands.

Recently, Yagi and Narita reported that the reaction of **36** with Ce^{IV} salts as oxidant leads to the decomposition of **36** to form permanganate without evolving O_2 in aqueous solution; however, it produces O_2 from water catalytically when **36** was adsorbed on clay compounds (*J. Am. Chem. Soc.* **2004**, *126*, 8084).

8. References

(1) Photosynthetic water oxidation: Special Dedicated Issue; Nugent, J., Ed. *Biochim. Biophys. Acta* **2001**, *1503*, 1.
(2) Joliot, P.; Barbieri, G.; Chabaud, R. *Photochem. Photobiol.* **1969**, *10*, 309.
(3) Kok, B.; Forbush, B.; McGloin, M. *Photochem. Photobiol.* **1970**, *11*, 457.
(4) Rögner, M.; Dekker, J. P.; Boekema, E. J.; Witt, H. T. *FEBS Lett.* **1987**, *219*, 207.
(5) Dekker, J. P.; Boekema, E. J.; Witt, H. T.; Rögner, M. *Biochim. Biophys. Acta* **1988**, *936*, 307.
(6) Rhee, K.-H.; Morris, E. P.; Zheleva, D.; Hankamer, B.; Kühlbrandt, W.; Barber, J. *Nature (London)* **1997**, *389*, 522.
(7) Rhee, K.-H.; Morris, E. P.; Barber, J.; Kühlbrandt, W. *Nature (London)* **1998**, *396*, 283.
(8) Zouni, A.; Witt, H.-T.; Kern, J.; Fromme, P.; Krauβ, N.; Saenger, W.; Orth, P. *Nature (London)* **2001**, *409*, 739.
(9) Kamiya, N.; Shen, J.-R. *Proc. Natl. Acad. Sci. U.S.A.* **2003**, *100*, 98.
(10) Ferreira, K. N.; Iverson, T. M.; Maghlaoui, K.; Barber, J.; Iwata, S. *Science* **2004**, *303*, 1831.
(11) Yachandra, V. K. *Philos. Trans. R. Soc. London, Ser. B: Biol. Sci.* **2002**, *357*, 1347.
(12) Britt, R. D.; Peloquin, J. M.; Campbell, K. A. *Annu. Rev. Biophys. Biomol. Struct.* **2000**, *29*, 463.
(13) Sauer, K.; Yachandra, V. K. *Proc. Natl. Acad. Sci. U.S.A.* **2002**, *99*, 8631.
(14) Yachandra, V. K.; Sauer, K.; Klein, M. P. *Chem. Rev.* **1996**, *96*, 2927.
(15) Manchanda, R.; Brudvig, G. W.; Crabtree, R. H. *Coord. Chem. Rev.* **1995**, *144*, 1.
(16) Law, N. A.; Caudle, M. T.; Pecoraro, V. L. *Adv. Inorg. Chem.* **1998**, *46*, 305.
(17) Siegbahn, P. E. M. *Inorg. Chem.* **2000**, *39*, 2923.
(18) Carrell, T. G.; Tyryshkin, A. M.; Dismukes, G. C. *J. Biol. Inorg. Chem.* **2002**, *7*, 2.
(19) Barber, J. *Q. Rev. Biophys.* **2003**, *36*, 71.
(20) Shen, J.-R.; Qian, M.; Inoue, Y.; Burnap, R. L. *Biochemistry* **1998**, *37*, 1551.
(21) Gregor, W.; Britt, R. D. *Photosynth. Res.* **2000**, *65*, 175.
(22) Popelkova, H.; Wyman, A.; Yocum, C. *Photosynth. Res.* **2003**, *77*, 21.
(23) Diner, B. A.; Babcock, G. T. *Adv. Photosynth.* **1996**, *4*, 213.
(24) Olesen, K.; Andréasson, L.-E. *Biochemistry* **2003**, *42*, 2025.
(25) X-ray Absorption: Principles, Application, Techniques of EXAFS, SEXAFS and XANES; Koningsberger, D. C., Prins, R., Eds.; Wiley-Interscience: New York, 1988.
(26) Scott, R. A. In *Physical Methods in Bioinorganic Chemistry; Spectroscopy and Magnetism*; Que, L., Jr., Ed.; University Science Press: Menlo Park, CA, 2000; p 465.
(27) Robblee, J. H.; Cinco, R. M.; Yachandra, V. K. *Biochim. Biophys. Acta* **2001**, *1503*, 7.
(28) Kuzek, D.; Pace, R. J. *Biochim. Biophys. Acta* **2001**, *1503*, 123.
(29) Dau, H.; Iuzzolino, L.; Dittmer, J. *Biochim. Biophys. Acta* **2001**, *1503*, 24.
(30) Roelofs, T. A.; Liang, W.; Latimer, M. J.; Cinco, R. M.; Rompel, A.; Andrews, J. C.; Sauer, K.; Yachandra, V. K.; Klein, M. *Proc. Natl. Acad. Sci. U.S.A.* **1996**, *93*, 3335.
(31) Ono, T.; Noguchi, T.; Inoue, Y.; Kusunoki, M.; Matsushita, T.; Oyanagi, H. *Science* **1992**, *258*, 1335.
(32) Iuzzolino, L.; Dittmer, J.; Dörner, W.; Meyer-Klaucke, W.; Dau, H. *Biochemistry* **1998**, *37*, 17112.
(33) Goodin, D. B.; Yachandra, V. K.; Britt, R. D.; Sauer, K.; Klein, M. P. *Biochim. Biophys. Acta* **1984**, *767*, 209.
(34) Yachandra, V. K.; Guiles, R. D.; McDermott, A.; Britt, R. D.; Dexheimer, S. L.; Sauer, K.; Klein, M. P. *Biochim. Biophys. Acta* **1986**, *850*, 324.
(35) Cole, J.; Yachandra, V. K.; Guiles, R. D.; McDermott, A. E.; Britt, R. D.; Dexheimer, S. L.; Sauer, K.; Klein, M. P. *Biochim. Biophys. Acta* **1987**, *890*, 395.

(36) Latimer, M. J.; DeRose, V. J.; Yachandra, V. K.; Sauer, K.; Klein, M. P. *J. Phys. Chem. B* **1998**, *102*, 8257.
(37) Messinger, J.; Robblee, J. H.; Bergmann, U.; Fernandez, C.; Glatzel, P.; Visser, H.; Cinco, R. M.; McFarlane, K. L.; Bellacchio, E.; Pizarro, S. A.; Cramer, S. P.; Sauer, K.; Klein, M. P.; Yachandra, V. K. *J. Am. Chem. Soc.* **2001**, *123*, 7804.
(38) Visser, H.; Anxolabéhère-Mallart, E.; Bergmann, U.; Glatzel, P.; Robblee, J. H.; Cramer, S. P.; Girerd, J.-J.; Sauer, K.; Klein, M. P.; Yachandra, V. K. *J. Am. Chem. Soc.* **2001**, *123*, 7031.
(39) Dekker, J. P.; Van Gorkom, H. J.; Brok, M.; Ouwehand, L. *Biochim. Biophys. Acta* **1984**, *764*, 301.
(40) Dekker, J. P.; Van Gorkom, H. J.; Wensink, J.; Ouwehand, L. *Biochim. Biophys. Acta* **1984**, *767*, 1.
(41) Dekker, J. P.; Plijter, J. J.; Ouwehand, L.; Van Gorkom, H. J. *Biochim. Biophys. Acta* **1984**, *767*, 176.
(42) Gerken, S.; Brettel, K.; Schlodder, E.; Witt, H. T. *FEBS Lett.* **1987**, *223*, 376.
(43) Eckert, H.-J.; Wiese, N.; Bernarding, J.; Eichler, H. J.; Renger, G. *FEBS Lett.* **1988**, *240*, 153.
(44) Lavergne, J. *Biochim. Biophys. Acta* **1991**, *1060*, 175.
(45) Guiles, R. D.; Yachandra, V. K.; McDermott, A. E.; Cole, J. L.; Dexheimer, S. L.; Britt, R. D.; Sauer, K.; Klein, M. P. *Biochemistry* **1990**, *29*, 486.
(46) Robblee, J. H.; Messinger, J.; Cinco, R. M.; McFarlane, K. L.; Fernandez, C.; Pizarro, S. A.; Sauer, K.; Yachandra, V. K. *J. Am. Chem. Soc.* **2002**, *124*, 7459.
(47) Yachandra, V. K.; DeRose, V. J.; Latimer, M. J.; Mukerji, I.; Sauer, K.; Klein, M. P. *Science* **1993**, *260*, 675.
(48) DeRose, V. J.; Mukerji, I.; Latimer, M. J.; Yachandra, V. K.; Sauer, K.; Klein, M. P. *J. Am. Chem. Soc.* **1994**, *116*, 5239.
(49) Haumann, M.; Grabolle, M.; Neisius, T.; Dau, H. *FEBS Lett.* **2002**, *512*, 116.
(50) Popíšil, P.; Haumann, M.; Dittmer, J.; Solé, V. A.; Dau, H. *Biophys. J.* **2003**, *84*, 1370.
(51) Liang, W.; Roelofs, T. A.; Cinco, R. M.; Rompel, A.; Latimer, M. J.; Yu, W. O.; Sauer, K.; Klein, M. P.; Yachandra, V. K. *J. Am. Chem. Soc.* **2000**, *122*, 3399.
(52) Kirby, J. A.; Robertson, A. S.; Smith, J. P.; Thompson, A. C.; Cooper, S. R.; Klein, M. P. *J. Am. Chem. Soc.* **1981**, *103*, 5529.
(53) Kirby, J. A.; Goodin, D. B.; Wydrzynski, T.; Robertson, A. S.; Klein, M. P. *J. Am. Chem. Soc.* **1981**, *103*, 5537.
(54) Yachandra, V. K.; Guiles, R. D.; McDermott, A. E.; Cole, J. L.; Britt, R. D.; Dexheimer, S. L.; Sauer, K.; Klein, M. P. *Biochemistry* **1987**, *26*, 5974.
(55) McDermott, A. E.; Yachandra, V. K.; Guiles, R. D.; Cole, J. L.; Dexheimer, S. L.; Britt, R. D.; Sauer, K.; Klein, M. P. *Biochemistry* **1988**, *27*, 4021.
(56) George, G. N.; Prince, R. C.; Cramer, S. P. *Science* **1989**, *243*, 789.
(57) MacLachlan, D. J.; Hallahan, B. J.; Ruffle, S. V.; Nugent, J. H. A.; Evans, M. C. W.; Strange, R. W.; Hasnain, S. S. *Biochem. J.* **1992**, *285*, 569.
(58) Guiles, R. D.; Yachandra, V. K.; McDermott, A. E.; Britt, R. D.; Dexheimer, S. L.; Sauer, K.; Klein, M. P. *Prog. Photosynth. Res., Proc. Int. Congr. Photosynth., 7th* **1987**, *1*, 561.
(59) Guiles, R. D.; Zimmermann, J. L.; McDermott, A. E.; Yachandra, V. K.; Cole, J. L.; Dexheimer, S. L.; Britt, R. D.; Wieghardt, K.; Bossek, U.; et al. *Biochemistry* **1990**, *29*, 471.
(60) Cinco, R. M.; Holman, K. L. M.; Robblee, J. H.; Yano, J.; Pizarro, S. A.; Bellacchio, E.; Sauer, K.; Yachandra, V. K. *Biochemistry* **2002**, *41*, 12928.
(61) Penner-Hahn, J. E.; Fronko, R. M.; Pecoraro, V. L.; Yocum, C. F.; Betts, S. D.; Bowlby, N. R. *J. Am. Chem. Soc.* **1990**, *112*, 2549.
(62) Penner-Hahn, J. E.; Fronko, R. M.; Waldo, G. S.; Yocum, C. F.; Bowlby, N. R.; Betts, S. D. *Curr. Res. Photosynth., Proc. Int. Conf. Photosynth., 8th* **1990**, *1*, 797.
(63) Dau, H.; Andrews, J. C.; Roelofs, T. A.; Latimer, M. J.; Liang, W.; Yachandra, V. K.; Sauer, K.; Klein, M. P. *Biochemistry* **1995**, *34*, 5274.
(64) DeRose, V. J.; Latimer, M. J.; Zimmermann, J.-L.; Mukerji, I.; Yachandra, V. K.; Sauer, K.; Klein, M. P. *Chem. Phys.* **1995**, *194*, 443.
(65) Pizarro, S. A.; Visser, H.; Cinco, R. M.; Robblee, J. H.; Pal, S.; Mukhopadhyay, S.; Mok, H. J.; Sauer, K.; Wieghardt, K.; Armstrong, W. H.; Yachandra, V. K. *J. Biol. Inorg. Chem.* **2004**, *9*, 247.
(66) Dismukes, G. C.; Siderer, Y. *Proc. Natl. Acad. Sci. U.S.A.* **1981**, *78*, 274.
(67) Casey, J. L.; Sauer, K. *Biochim. Biophys. Acta* **1984**, *767*, 21.
(68) Zimmermann, J. L.; Rutherford, A. W. *Biochim. Biophys. Acta* **1984**, *767*, 160.
(69) Miller, A. F.; Brudvig, G. W. *Biochim. Biophys. Acta* **1991**, *1056*, 1.
(70) Koulougliotis, D.; Schweitzer, R. H.; Brudvig, G. W. *Biochemistry* **1997**, *36*, 9735.
(71) Boussac, A. *J. Biol. Inorg. Chem.* **1997**, *2*, 580.
(72) Lorigan, G. A.; Britt, R. D. *Photosynth. Res.* **2001**, *66*, 189.
(73) Haddy, A.; Dunham, W. R.; Sands, R. H.; Aasa, R. *Biochim. Biophys. Acta* **1992**, *1099*, 25.
(74) Boussac, A.; Girerd, J.-J.; Rutherford, A. W. *Biochemistry* **1996**, *35*, 6984.
(75) De Paula, J. C.; Beck, W. F.; Brudvig, G. W. *J. Am. Chem. Soc.* **1986**, *108*, 4002.
(76) Zimmermann, J. L.; Rutherford, A. W. *Biochemistry* **1986**, *25*, 4609.
(77) Hansson, O.; Aasa, R.; Vänngård, T. *Biophys. J.* **1987**, *51*, 825.
(78) Kim, D. H.; Britt, R. D.; Klein, M. P.; Sauer, K. *J. Am. Chem. Soc.* **1990**, *112*, 9389.
(79) Randall, D. W.; Sturgeon, B. E.; Ball, J. A.; Lorigan, G. A.; Chan, M. K.; Klein, M. P.; Armstrong, W. H.; Britt, R. D. *J. Am. Chem. Soc.* **1995**, *117*, 11780.
(80) Randall, D. W.; Chan, M. K.; Armstrong, W. H.; Britt, R. D. *Mol. Phys.* **1998**, *95*, 1283.
(81) Peloquin, J. M.; Campbell, K. A.; Randall, D. W.; Evanchik, M. A.; Pecoraro, V. L.; Armstrong, W. H.; Britt, R. D. *J. Am. Chem. Soc.* **2000**, *122*, 10926.
(82) Zheng, M.; Dismukes, G. C. *Inorg. Chem.* **1996**, *35*, 3307.
(83) Ruettinger, W.; Dismukes, G. C. *Chem. Rev.* **1997**, *97*, 1.
(84) Ioannidis, N.; Petrouleas, V. *Biochemistry* **2000**, *39*, 5246.
(85) Campbell, K. A.; Gregor, W.; Pham, D. P.; Peloquin, J. M.; Debus, R. J.; Britt, R. D. *Biochemistry* **1998**, *37*, 5039.
(86) Dexheimer, S. L.; Klein, M. P. *J. Am. Chem. Soc.* **1992**, *114*, 2821.
(87) Yamauchi, T.; Mino, H.; Matsukawa, T.; Kawamori, A.; Ono, T.-A. *Biochemistry* **1997**, *36*, 7520.
(88) Matsukawa, T.; Mino, H.; Yoneda, D.; Kawamori, A. *Biochemistry* **1999**, *38*, 4072.
(89) Mino, H.; Kawamori, A. *Biochim. Biophys. Acta* **2001**, *1503*, 112.
(90) Boussac, A.; Zimmermann, J. L.; Rutherford, A. W. *Biochemistry* **1989**, *28*, 8984.
(91) Boussac, A.; Zimmermann, J. L.; Rutherford, A. W.; Lavergne, J. *Nature* **1990**, *347*, 303.
(92) Szalai, V. A.; Kühne, H.; Lakshmi, K. V.; Brudvig, G. W. *Biochemistry* **1998**, *37*, 13594.
(93) Hallahan, B. J.; Nugent, J. H. A.; Warden, J. T.; Evans, M. C. W. *Biochemistry* **1992**, *31*, 4562.
(94) Lakshmi, K. V.; Eaton, S. S.; Eaton, G. R.; Frank, H. A.; Brudvig, G. W. *J. Phys. Chem. B* **1998**, *102*, 8327.
(95) Messinger, J.; Robblee, J.; Yu, W. O.; Sauer, K.; Yachandra, V. K.; Klein, M. P. *J. Am. Chem. Soc.* **1997**, *119*, 11349.
(96) Messinger, J.; Nugent, J. H. A.; Evans, M. C. W. *Biochemistry* **1997**, *36*, 11055.
(97) Åhrling, K. A.; Peterson, S.; Styring, S. *Biochemistry* **1997**, *36*, 13148.
(98) Geijer, P.; Peterson, S.; Åhrling, K. A.; Deák, Z.; Styring, S. *Biochim. Biophys. Acta* **2001**, *1503*, 83.
(99) Force, D. A.; Randall, D. W.; Lorigan, G. A.; Clemens, K. L.; Britt, R. D. *J. Am. Chem. Soc.* **1998**, *120*, 13321.
(100) Boussac, A.; Kuhl, H.; Ghibaudi, E.; Rögner, M.; Rutherford, A. W. *Biochemistry* **1999**, *38*, 11942.
(101) DeRose, V. J.; Yachandra, V. K.; McDermott, A. E.; Britt, R. D.; Sauer, K.; Klein, M. P. *Biochemistry* **1991**, *30*, 1335.
(102) Tang, X. S.; Diner, B. A.; Larsen, B. S.; Gilchrist, M. L., Jr.; Lorigan, G. A.; Britt, R. D. *Proc. Natl. Acad. Sci. U.S.A.* **1994**, *91*, 704.
(103) Debus, R. J.; Campbell, K. A.; Peloquin, J. M.; Pham, D. P.; Britt, R. D. *Biochemistry* **2000**, *39*, 470.
(104) Debus, R. J.; Campbell, K. A.; Gregor, W.; Li, Z.-L.; Burnap, R. L.; Britt, R. D. *Biochemistry* **2001**, *40*, 3690.
(105) Debus, R. J.; Campbell, K. A.; Pham, D. P.; Hays, A.-M. A.; Britt, R. D. *Biochemistry* **2000**, *39*, 6275.
(106) Campbell, K. A.; Force, D. A.; Nixon, P. J.; Dole, F.; Diner, B. A.; Britt, R. D. *J. Am. Chem. Soc.* **2000**, *122*, 3754.
(107) Debus, R. J.; Aznar, C.; Campbell, K. A.; Gregor, W.; Diner, B. A.; Britt, R. D. *Biochemistry* **2003**, *42*, 10600.
(108) Cinco, R. M.; Robblee, J. H.; Rompel, A.; Fernandez, C.; Yachandra, V. K.; Sauer, K.; Klein, M. P. *J. Phys. Chem. B* **1998**, *102*, 8248.
(109) Vrettos, J. S.; Stone, D. A.; Brudvig, G. W. *Biochemistry* **2001**, *40*, 7937.
(110) Noguchi, T.; Inoue, Y.; Tang, X.-S. *Biochemistry* **1999**, *38*, 10187.
(111) Noguchi, T.; Ono, T.-a.; Inoue, Y. *Biochim. Biophys. Acta* **1995**, *1228*, 189.
(112) Debus, R. J. *Biochim. Biophys. Acta* **2001**, *1503*, 164.
(113) Diner, B. A. *Biochim. Biophys. Acta* **2001**, *1503*, 147.
(114) Hays, A.-M. A.; Vassiliev, I. R.; Golbeck, J. H.; Debus, R. J. *Biochemistry* **1998**, *37*, 11352.
(115) Béck, W. F.; Brudvig, G. W. *Biochemistry* **1987**, *26*, 8285.
(116) Messinger, J.; Wacker, U.; Renger, G. *Biochemistry* **1991**, *30*, 7852.
(117) Lin, C.; Brudvig, G. W. *Photosynth. Res.* **1993**, *38*, 441.
(118) Kebekus, U.; Messinger, J.; Renger, G. *Biochemistry* **1995**, *34*, 6175.
(119) Riggs-Gelasco, P. J.; Mei, R.; Yocum, C. F.; Penner-Hahn, J. E. *J. Am. Chem. Soc.* **1996**, *118*, 2387.
(120) Messinger, J.; Seaton, G.; Wydrzynski, T.; Wacker, U.; Renger, G. *Biochemistry* **1997**, *36*, 6862.

(121) Sarrou, J.; Ioannidis, N.; Deligiannakis, Y.; Petrouleas, V. *Biochemistry* **1998**, *37*, 3581.
(122) Schansker, G.; Goussias, C.; Petrouleas, V.; Rutherford, A. W. *Biochemistry* **2002**, *41*, 3057.
(123) Ioannidis, N.; Sarrou, J.; Schansker, G.; Petrouleas, V. *Biochemistry* **1998**, *37*, 16445.
(124) Carey, P. R. *J. Biol. Chem.* **1999**, *274*, 26625.
(125) Spiro, T. G.; Czernuszewicz, R. S. *Methods Enzymol.* **1995**, *246*, 416.
(126) Kincaid, J. R. *Methods Enzymol.* **1995**, *246*, 460.
(127) Siebert, F. *Mikrochim. Acta, Suppl.* **1997**, *14*, 43.
(128) Vogel, R.; Siebert, F. *Curr. Opin. Chem. Biol.* **2000**, *4*, 518.
(129) Chu, H. A.; Hillier, W.; Law, N. A.; Babcock, G. T. *Biochim. Biophys. Acta* **2001**, *1503*, 69.
(130) Cua, A.; Stewart, D. H.; Reifler, M. J.; Brudvig, G. W.; Bocian, D. F. *J. Am. Chem. Soc.* **2000**, *122*, 2069.
(131) Noguchi, T.; Sugiura, M. *Biochemistry* **2000**, *39*, 10943.
(132) Kimura, Y.; Mizusawa, N.; Ishii, A.; Yamanari, T.; Ono, T. *Biochemistry* **2003**, *42*, 13170.
(133) Chu, H.-A.; Sackett, H.; Babcock, G. T. *Biochemistry* **2000**, *39*, 14371.
(134) Noguchi, T.; Sugiura, M. *Biochemistry* **2001**, *40*, 1497.
(135) Nakamoto, K. *Comp. Coord. Chem. Rev.* **1980**, 227.
(136) Nakamoto, K. *Infrared and Raman Spectra of Inorganic and Coordination Compounds, Part A: Theory and Applications in Inorganic Chemistry*, 5th ed.; Wiley: New York, 1997; p 387.
(137) Smith, J. C.; Gonzalez-Vergara, E.; Vincent, J. B. *Inorg. Chim. Acta* **1997**, *255*, 99.
(138) Kimura, Y.; Hasegawa, K.; Ono, T.-a. *Biochemistry* **2002**, *41*, 5844.
(139) Gerken, S.; Brettel, K.; Schlodder, E.; Witt, H. T. *FEBS Lett.* **1988**, *237*, 69.
(140) Junge, W.; Haumann, M.; Ahlbrink, R.; Mulkidjanian, A.; Clausen, J. *Philos. Trans. R. Soc. London, Ser. B: Biol. Sci.* **2002**, *357*, 1407.
(141) Berthomieu, C.; Hienerwadel, R.; Boussac, A.; Breton, J.; Diner, B. A. *Biochemistry* **1998**, *37*, 10547.
(142) Hienerwadel, R.; Boussac, A.; Breton, J.; Diner, B.; Berthomieu, C. *Biochemistry* **1997**, *36*, 14712.
(143) MacDonald, G. M.; Bixby, K. A.; Barry, B. A. *Proc. Natl. Acad. Sci. U.S.A.* **1993**, *90*, 11024.
(144) Kim, S.; Ayala, I.; Steenhuis, J. J.; Gonzalez, E. T.; Barry, B. A. *Biochim. Biophys. Acta* **1998**, *1364*, 337.
(145) Kim, S.; Barry, B. A. *Biophys. J.* **1998**, *74*, 2588.
(146) Ayala, I.; Kim, S.; Barry, B. A. *Biophys. J.* **1999**, *77*, 2137.
(147) Zhang, H.; Razeghifard, M. R.; Fischer, G.; Wydrzynski, T. *Biochemistry* **1997**, *36*, 11762.
(148) Tommos, C.; McCracken, J.; Styring, S.; Babcock, G. T. *J. Am. Chem. Soc.* **1998**, *120*, 10441.
(149) Miller, J. D.; Oliver, F. D. *J. Inorg. Nucl. Chem.* **1972**, *34*, 1873.
(150) Boucher, L. J.; Coe, C. G. *Inorg. Chem.* **1975**, *14*, 1289.
(151) Cooper, S. R.; Calvin, M. *J. Am. Chem. Soc.* **1977**, *99*, 6623.
(152) Dave, B. C.; Czernuszewicz, R. S. *Inorg. Chim. Acta* **1998**, *281*, 25.
(153) Dave, B. C.; Czernuszewicz, R. S. *Inorg. Chim. Acta* **1994**, *227*, 33.
(154) Sheats, J. E.; Czernuszewicz, R. S.; Dismukes, G. C.; Rheingold, A. L.; Petrouleas, V.; Stubbe, J.; Armstrong, W. H.; Beer, R. H.; Lippard, S. J. *J. Am. Chem. Soc.* **1987**, *109*, 1435.
(155) Cua, A.; Vrettos, J. S.; de Paula, J. C.; Brudvig, G. W.; Bocian, D. F. *J. Biol. Inorg. Chem.* **2003**, *8*, 439.
(156) Visser, H.; Dubé, C. E.; Armstrong, W. H.; Sauer, K.; Yachandra, V. K. *J. Am. Chem. Soc.* **2002**, *124*, 11008.
(157) Collins, T. J.; Powell, R. D.; Slebodnick, C.; Uffelman, E. S. *J. Am. Chem. Soc.* **1990**, *112*, 899.
(158) Workman, J. M.; Powell, R. D.; Procyk, A. D.; Collins, T. J.; Bocian, D. F. *Inorg. Chem.* **1992**, *31*, 1548.
(159) Smegal, J. A.; Schardt, B. C.; Hill, C. L. *J. Am. Chem. Soc.* **1983**, *105*, 3510.
(160) Groves, J. T.; Stern, M. K. *J. Am. Chem. Soc.* **1988**, *110*, 8628.
(161) Czernuszewicz, R. S.; Su, Y. O.; Stern, M. K.; Macor, K. A.; Kim, D.; Groves, J. T.; Spiro, T. G. *J. Am. Chem. Soc.* **1988**, *110*, 4158.
(162) Bell, C. F.; Waters, D. N. *J. Inorg. Nucl. Chem.* **1977**, *39*, 773.
(163) Kanno, H. *J. Raman Spectrosc.* **1987**, *18*, 301.
(164) Kusunoki, M. *Oxygen Evol. Syst. Photosynth., [Proc. Int. Symp. Photosynth. Water Oxid. Photosyst. 2 Photochem.]* **1983**, 165.
(165) Renger, G. *Photosynth. Oxygen Evol., [Symp.]* **1978**, 229.
(166) Raval, M. K.; Biswal, U. C. *Bioelectrochem. Bioenerg.* **1984**, *12*, 57.
(167) Critchley, C.; Sargeson, A. M. *FEBS Lett.* **1984**, *177*, 2.
(168) Govindjee; Kambara, T.; Coleman, W. *Photochem. Photobiol.* **1985**, *42*, 187.
(169) Kambara, T.; Govindjee. *Proc. Natl. Acad. Sci. U.S.A.* **1985**, *82*, 6119.
(170) Armstrong, W. H. *Manganese Redox Enzymes* **1992**, 261.
(171) Tommos, C.; Babcock, G. T. *Biochim. Biophys. Acta* **2000**, *1458*, 199.
(172) Westphal, K. L.; Tommos, C.; Cukier, R. I.; Babcock, G. T. *Curr. Opin. Plant Biol.* **2000**, *3*, 236.
(173) Tommos, C. *Philos. Trans. R. Soc. London, Ser. B: Biol. Sci.* **2002**, *357*, 1383.
(174) Binstead, R. A.; Chronister, C. W.; Ni, J.; Hartshorn, C. M.; Meyer, T. J. *J. Am. Chem. Soc.* **2000**, *122*, 8464.
(175) Hoganson, C. W.; Babcock, G. T. *Science* **1997**, *277*, 1953.
(176) Messinger, J.; Badger, M.; Wydrzynski, T. *Proc. Natl. Acad. Sci. U.S.A.* **1995**, *92*, 3209.
(177) Brudvig, G. W.; Crabtree, R. H. *Proc. Natl. Acad. Sci. U.S.A.* **1986**, *83*, 4586.
(178) Vincent, J. B.; Christou, G. *Inorg. Chim. Acta* **1987**, *136*, L41.
(179) Hoganson, C. W.; Babcock, G. T. *Metal Ions Biol. Syst.* **2000**, *37*, 613.
(180) Hoganson, C. W.; Lydakis-Simantiris, N.; Tang, X.-S.; Tommos, C.; Warncke, K.; Babcock, G. T.; Diner, B. A.; McCracken, J.; Styring, S. *Photosynth. Res.* **1995**, *46*, 177.
(181) Limburg, J.; Szalai, V. A.; Brudvig, G. W. *J. Chem. Soc., Dalton Trans.* **1999**, 1353.
(182) Force, D. A.; Randall, D. W.; Britt, R. D. *Biochemistry* **1997**, *36*, 12062.
(183) Haumann, M.; Junge, W. *Adv. Photosynth.* **1996**, *4*, 165.
(184) Haumann, M.; Junge, W. *Biochim. Biophys. Acta* **1999**, *1411*, 86.
(185) Rappaport, F.; Blanchard-Desce, M.; Lavergne, J. *Biochim. Biophys. Acta* **1994**, *1184*, 178.
(186) Schlodder, E.; Witt, H. T. *J. Biol. Chem.* **1999**, *274*, 30387.
(187) Nugent, J. H. A.; Rich, A. M.; Evans, M. C. W. *Biochim. Biophys. Acta* **2001**, *1503*, 138.
(188) Tommos, C.; Tang, X.-S.; Warncke, K.; Hoganson, C. W.; Styring, S.; McCracken, J.; Diner, B. A.; Babcock, G. T. *J. Am. Chem. Soc.* **1995**, *117*, 10325.
(189) Pecoraro, V. L. *Manganese Redox Enzymes* **1992**, 197.
(190) Pecoraro, V. L.; Baldwin, M. J.; Gelasco, A. *Chem. Rev.* **1994**, *94*, 807.
(191) Pecoraro, V. L.; Hsieh, W.-Y. *Metal Ions Biol. Syst.* **2000**, *37*, 429.
(192) Vrettos, J. S.; Limburg, J.; Brudvig, G. W. *Biochim. Biophys. Acta* **2001**, *1503*, 229.
(193) Siegbahn, P. E. M. *Q. Rev. Biophys.* **2003**, *36*, 91.
(194) Siegbahn, P. E. M.; Crabtree, R. H. *J. Am. Chem. Soc.* **1999**, *121*, 117.
(195) Baldwin, M. J.; Pecoraro, V. L. *J. Am. Chem. Soc.* **1996**, *118*, 11325.
(196) Caudle, M. T.; Pecoraro, V. L. *J. Am. Chem. Soc.* **1997**, *119*, 3415.
(197) Debus, R. J.; Barry, B. A.; Sithole, I.; Babcock, G. T.; McIntosh, L. *Biochemistry* **1988**, *27*, 9071.
(198) Metz, J. G.; Nixon, P. J.; Rogner, M.; Brudvig, G. W.; Diner, B. A. *Biochemistry* **1989**, *28*, 6960.
(199) Barry, B. A.; Babcock, G. T. *Proc. Natl. Acad. Sci. U.S.A.* **1987**, *84*, 7099.
(200) Ananyev, G. M.; Sakiyan, I.; Diner, B. A.; Dismukes, G. C. *Biochemistry* **2002**, *41*, 974.
(201) Renger, G. *Photosynth. Res.* **2003**, *76*, 269.
(202) Bhaduri, S.; Tasiopoulos, A. J.; Bolcar, M. A.; Abboud, K. A.; Streib, W. E.; Christou, G. *Inorg. Chem.* **2003**, *42*, 1483.
(203) Mukhopadhyay, S.; Staples, R. J.; Armstrong, W. H. *Chem. Commun.* **2002**, 864.
(204) Low, D. W.; Eichhorn, D. M.; Draganescu, A.; Armstrong, W. H. *Inorg. Chem.* **1991**, *30*, 877.
(205) Dave, B. C.; Czernuszewicz, R. S.; Bond, M. R.; Carrano, C. J. *Inorg. Chem.* **1993**, *32*, 3593.
(206) Marlin, D. S.; Bill, E.; Weyhermüller, T.; Rentschler, E.; Wieghardt, K. *Angew. Chem., Int. Ed.* **2002**, *41*, 4775.
(207) Chan, M. K.; Armstrong, W. H. *J. Am. Chem. Soc.* **1990**, *112*, 4985.
(208) Hagen, K. S.; Armstrong, W. H.; Hope, H. *Inorg. Chem.* **1988**, *27*, 967.
(209) Hagen, K. S.; Westmoreland, T. D.; Scott, M. J.; Armstrong, W. H. *J. Am. Chem. Soc.* **1989**, *111*, 1907.
(210) Mok, H. J.; Davis, J. A.; Pal, S.; Mandal, S. K.; Armstrong, W. H. *Inorg. Chim. Acta* **1997**, *263*, 385.
(211) Pal, S.; Chan, M. K.; Armstrong, W. H. *J. Am. Chem. Soc.* **1992**, *114*, 6398.
(212) Li, Q.; Vincent, J. B.; Libby, E.; Chang, H. R.; Huffman, J. C.; Boyd, P. D. W.; Christou, G.; Hendrickson, D. N. *Angew. Chem.* **1988**, *100*, 1799.
(213) Vincent, J. B.; Christmas, C.; Chang, H. R.; Li, Q.; Boyd, P. D. W.; Huffman, J. C.; Hendrickson, D. N.; Christou, G. *J. Am. Chem. Soc.* **1989**, *111*, 2086.
(214) Aromí, G.; Aubin, S. M. J.; Bolcar, M. A.; Christou, G.; Eppley, H. J.; Folting, K.; Hendrickson, D. N.; Huffman, J. C.; Squire, R. C.; Tsai, H.-L.; Wang, S.; Wemple, M. W. *Polyhedron* **1998**, *17*, 3005.
(215) Vincent, J. B.; Folting, K.; Huffman, J. C.; Christou, G. *Inorg. Chem.* **1986**, *25*, 996.
(216) Pal, S.; Olmstead, M. M.; Armstrong, W. H. *Inorg. Chem.* **1995**, *34*, 4708.
(217) Dubé, C. E.; Wright, D. W.; Bonitatebus, P. J., Jr.; Pal, S.; Armstrong, W. H. *J. Am. Chem. Soc.* **1998**, *120*, 3704.

(218) Mukhopadhyay, S.; Gandhi, B. A.; Kirk, M. L.; Armstrong, W. H. *Inorg. Chem.* **2003**, *42*, 8171.
(219) Wang, S.; Tsai, H.-L.; Hagen, K. S.; Hendrickson, D. N.; Christou, G. *J. Am. Chem. Soc.* **1994**, *116*, 8376.
(220) Wang, S.; Wemple, M. S.; Yoo, J.; Folting, K.; Huffman, J. C.; Hagen, K. S.; Hendrickson, D. N.; Christou, G. *Inorg. Chem.* **2000**, *39*, 1501.
(221) Mukhopadhyay, S.; Armstrong, W. H. *J. Am. Chem. Soc.* **2003**, *125*, 13010.
(222) Pal, S.; Armstrong, W. H. *Inorg. Chem.* **1992**, *31*, 5417.
(223) Aromí, G.; Bhaduri, S.; Artus, P.; Folting, K.; Christou, G. *Inorg. Chem.* **2002**, *41*, 805.
(224) Bossek, U.; Hummel, H.; Weyhermüller, T.; Wieghardt, K.; Russell, S.; van der Wolf, L.; Kolb, U. *Angew. Chem., Int. Ed. Engl.* **1996**, *35*, 1552.
(225) Hummel, H.; Bill, E.; Weyhermüller, T.; Wieghardt, K.; Davydov, R.; Russell, S.; van der Wolf, L. *J. Inorg. Biochem.* **1997**, *67*, 200.
(226) Vogt, L. H., Jr.; Zalkin, A.; Templeton, D. H. *Science* **1966**, *151*, 569.
(227) Vogt, L. H., Jr.; Zalkin, A.; Templeton, D. H. *Inorg. Chem.* **1967**, *6*, 1725.
(228) Ziolo, R. F.; Stanford, R. H.; Rossman, G. R.; Gray, H. B. *J. Am. Chem. Soc.* **1974**, *96*, 7910.
(229) Kipke, C. A.; Scott, M. J.; Gohdes, J. W.; Armstrong, W. H. *Inorg. Chem.* **1990**, *29*, 2193.
(230) Horner, O.; Anxolabéhère-Mallart, E.; Charlot, M.-F.; Tchertanov, L.; Guilhem, J.; Mattioli, T. A.; Boussac, A.; Girerd, J.-J. *Inorg. Chem.* **1999**, *38*, 1222.
(231) Baffert, C.; Collomb, M.-N.; Deronzier, A.; Pécaut, J.; Limburg, J.; Crabtree, R. H.; Brudvig, G. W. *Inorg. Chem.* **2002**, *41*, 1404.
(232) Triller, M. U.; Hsieh, W.-Y.; Pecoraro, V. L.; Rompel, A.; Krebs, B. *Inorg. Chem.* **2002**, *41*, 5544.
(233) Kitajima, N.; Osawa, M.; Tanaka, M.; Morooka, Y. *J. Am. Chem. Soc.* **1991**, *113*, 8952.
(234) Schardt, B. C.; Smegal, J. A.; Hollander, F. J.; Hill, C. L. *J. Am. Chem. Soc.* **1982**, *104*, 3964.
(235) Oberhausen, K. J.; O'Brien, R. J.; Richardson, J. F.; Buchanan, R. M.; Costa, R.; Latour, J. M.; Tsai, H. L.; Hendrickson, D. N. *Inorg. Chem.* **1993**, *32*, 4561.
(236) Arulsamy, N.; Glerup, J.; Hazell, A.; Hodgson, D. J.; McKenzie, C. J.; Toftlund, H. *Inorg. Chem.* **1994**, *33*, 3023.
(237) Goodson, P. A.; Hodgson, D. J. *Inorg. Chem.* **1989**, *28*, 3606.
(238) Goodson, P. A.; Oki, A. R.; Glerup, J.; Hodgson, D. J. *J. Am. Chem. Soc.* **1990**, *112*, 6248.
(239) Kitajima, N.; Singh, U. P.; Amagai, H.; Osawa, M.; Morooka, Y. *J. Am. Chem. Soc.* **1991**, *113*, 7757.
(240) Glerup, J.; Goodson, P. A.; Hazell, A.; Hazell, R.; Hodgson, D. J.; McKenzie, C. J.; Michelsen, K.; Rychlewska, U.; Toftlund, H. *Inorg. Chem.* **1994**, *33*, 4105.
(241) Nyholm, R. S.; Turco, A. *Chem. Ind.* **1960**, 74.
(242) Cooper, S. R.; Dismukes, G. C.; Klein, M. P.; Calvin, M. *J. Am. Chem. Soc.* **1978**, *100*, 7248.
(243) Plaksin, P. M.; Stoufer, R. C.; Mathew, M.; Palenik, G. J. *J. Am. Chem. Soc.* **1972**, *94*, 2121.
(244) Stebler, M.; Ludi, A.; Bürgi, H. B. *Inorg. Chem.* **1986**, *25*, 4743.
(245) Collins, M. A.; Hodgson, D. J.; Michelsen, K.; Towle, D. K. *J. Chem. Soc., Chem. Commun.* **1987**, 1659.
(246) Suzuki, M.; Senda, H.; Kobayashi, Y.; Oshio, H.; Uehara, A. *Chem. Lett.* **1988**, 1763.
(247) Towle, D. K.; Botsford, C. A.; Hodgson, D. J. *Inorg. Chim. Acta* **1988**, *141*, 167.
(248) Brewer, K. J.; Calvin, M.; Lumpkin, R. S.; Otvos, J. W.; Spreer, L. O. *Inorg. Chem.* **1989**, *28*, 4446.
(249) Oki, A. R.; Glerup, J.; Hodgson, D. J. *Inorg. Chem.* **1990**, *29*, 2435.
(250) Goodson, P. A.; Hodgson, D. J.; Glerup, J.; Michelsen, K.; Weihe, H. *Inorg. Chim. Acta* **1992**, *197*, 141.
(251) Frapart, Y.-M.; Boussac, A.; Albach, R.; Anxolabéhère-Mallart, E.; Delroisse, M.; Verlhac, J.-B.; Blondin, G.; Girerd, J.-J.; Guilhem, J.; et al. *J. Am. Chem. Soc.* **1996**, *118*, 2669.
(252) Schindler, S.; Walter, O.; Pedersen, J. Z.; Toftlund, H. *Inorg. Chim. Acta* **2000**, *303*, 215.
(253) Collomb, M.-N.; Deronzier, A.; Richardot, A.; Pécaut, J. *New J. Chem.* **1999**, *23*, 351.
(254) Limburg, J.; Vrettos, J. S.; Liable-Sands, L. M.; Rheingold, A. L.; Crabtree, R. H.; Brudvig, G. W. *Science* **1999**, *283*, 1524.
(255) Wieghardt, K.; Bossek, U.; Nuber, B.; Weiss, J.; Bonvoisin, J.; Corbella, M.; Vitols, S. E.; Girerd, J. J. *J. Am. Chem. Soc.* **1988**, *110*, 7398.
(256) Libby, E.; Webb, R. J.; Streib, W. E.; Folting, K.; Huffman, J. C.; Hendrickson, D. N.; Christou, G. *Inorg. Chem.* **1989**, *28*, 4037.
(257) Gohdes, J. W.; Armstrong, W. H. *Inorg. Chem.* **1992**, *31*, 368.
(258) Larson, E.; Lah, M. S.; Li, X.; Bonadies, J. A.; Pecoraro, V. L. *Inorg. Chem.* **1992**, *31*, 373.
(259) Law, N. A.; Kampf, J. W.; Pecoraro, V. L. *Inorg. Chim. Acta* **2000**, *297*, 252.
(260) Wieghardt, K.; Bossek, U.; Zsolnai, L.; Huttner, G.; Blondin, G.; Girerd, J. J.; Babonneau, F. *J. Chem. Soc., Chem. Commun.* **1987**, 651.
(261) Bossek, U.; Saher, M.; Weyhermüller, T.; Wieghardt, K. *J. Chem. Soc., Chem. Commun.* **1992**, 1780.
(262) Pal, S.; Gohdes, J. W.; Wilisch, W. C. A.; Armstrong, W. H. *Inorg. Chem.* **1992**, *31*, 713.
(263) Lal, T. K.; Mukherjee, R. *Inorg. Chem.* **1998**, *37*, 2373.
(264) Schäfer, K.-O.; Bittl, R.; Zweygart, W.; Lendzian, F.; Haselhorst, G.; Weyhermüller, T.; Wieghardt, K.; Lubitz, W. *J. Am. Chem. Soc.* **1998**, *120*, 13104.
(265) Bashkin, J. S.; Schake, A. R.; Vincent, J. B.; Chang, H. R.; Li, Q.; Huffman, J. C.; Christou, G.; Hendrickson, D. N. *J. Chem. Soc., Chem. Commun.* **1988**, 700.
(266) Reddy, K. R.; Rajasekharan, M. V.; Padhye, S.; Dahan, F.; Tuchagues, J. P. *Inorg. Chem.* **1994**, *33*, 428.
(267) Sarneski, J. E.; Didiuk, M.; Thorp, H. H.; Crabtree, R. H.; Brudvig, G. W.; Faller, J. W.; Schulte, G. K. *Inorg. Chem.* **1991**, *30*, 2833.
(268) Wieghardt, K.; Bossek, U.; Ventur, D.; Weiss, J. *J. Chem. Soc., Chem. Commun.* **1985**, 347.
(269) Ménage, S.; Girerd, J. J.; Gleizes, A. *J. Chem. Soc., Chem. Commun.* **1988**, 431.
(270) Nishida, Y.; Oshino, N.; Tokii, T. *Z. Naturforsch., B: Chem. Sci.* **1988**, *43*, 637.
(271) Vincent, J. B.; Folting, K.; Huffman, J. C.; Christou, G. *Biochem. Soc. Trans.* **1988**, *16*, 822.
(272) Bossek, U.; Wieghardt, K.; Nuber, B.; Weiss, J. *Inorg. Chim. Acta* **1989**, *165*, 123.
(273) Toftlund, H.; Markiewicz, A.; Murray, K. S. *Acta Chem. Scand.* **1990**, *44*, 443.
(274) Wu, F. J.; Kurtz, D. M., Jr.; Hagen, K. S.; Nyman, P. D.; Debrunner, P. G.; Vankai, V. A. *Inorg. Chem.* **1990**, *29*, 5174.
(275) Blackman, A. G.; Huffman, J. C.; Lobkovsky, E. B.; Christou, G. *J. Chem. Soc., Chem. Commun.* **1991**, 989.
(276) Hotzelmann, R.; Wieghardt, K.; Ensling, J.; Romstedt, H.; Gütlich, P.; Bill, E.; Flörke, U.; Haupt, H. J. *J. Am. Chem. Soc.* **1992**, *114*, 9470.
(277) Vincent, J. B.; Tsai, H.-L.; Blackman, A. G.; Wang, S.; Boyd, P. D. W.; Folting, K.; Huffman, J. C.; Lobkovsky, E. B.; Hendrickson, D. N.; Christou, G. *J. Am. Chem. Soc.* **1993**, *115*, 12353.
(278) Mahapatra, S.; Lal, T. K.; Mukherjee, R. *Inorg. Chem.* **1994**, *33*, 1579.
(279) Gultneh, Y.; Ahvazi, B.; Khan, A. R.; Butcher, R. J.; Tuchagues, J. P. *Inorg. Chem.* **1995**, *34*, 3633.
(280) Mandal, S. K.; Armstrong, W. H. *Inorg. Chim. Acta* **1995**, *229*, 261.
(281) Tanase, T.; Lippard, S. J. *Inorg. Chem.* **1995**, *34*, 4682.
(282) Corbella, M.; Costa, R.; Ribas, J.; Fries, P. H.; Latour, J.-M.; Öhrström, L.; Solans, X.; Rodríguez, V. *Inorg. Chem.* **1996**, *35*, 1857.
(283) Reddy, K. R.; Rajesekharan, M. V.; Sukumar, S. *Polyhedron* **1996**, *15*, 4161.
(284) Hage, R.; Gunnewegh, E. A.; Niël, J.; Tjan, F. S. B.; Weyhermüller, T.; Wieghardt, K. *Inorg. Chim. Acta* **1998**, *268*, 43.
(285) Bolm, C.; Meyer, N.; Raabe, G.; Weyhermüller, T.; Bothe, E. *Chem. Commun.* **2000**, 2435.
(286) Ruiz, R.; Sangregorio, C.; Caneschi, A.; Rossi, P.; Gaspar, A. B.; Real, J. A.; Muñoz, M. C. *Inorg. Chem. Commun.* **2000**, *3*, 361.
(287) Cañada-Vilalta, C.; Huffman, J. C.; Streib, W. E.; Davidson, E. R.; Christou, G. *Polyhedron* **2001**, *20*, 1375.
(288) Chen, C.; Zhu, H.; Huang, D.; Wen, T.; Liu, Q.; Liao, D.; Cui, J. *Inorg. Chim. Acta* **2001**, *320*, 159.
(289) Brunold, T. C.; Gamelin, D. R.; Stemmler, T. L.; Mandal, S. K.; Armstrong, W. H.; Penner-Hahn, J. E.; Solomon, E. I. *J. Am. Chem. Soc.* **1998**, *120*, 8724.
(290) Wieghardt, K.; Bossek, U.; Bonvoisin, J.; Beauvillain, P.; Girerd, J.-J.; Nuber, B.; Weiss, J.; Heinze, J. *Angew. Chem., Int. Ed.* **1986**, *98*, 1030.
(291) Duboc-Toia, C.; Hummel, H.; Bill, E.; Barra, A.-L.; Chouteau, G.; Wieghardt, K. *Angew. Chem., Int. Ed.* **2000**, *39*, 2888.
(292) Wieghardt, K.; Bossek, U.; Nuber, B.; Weiss, J.; Gehring, S.; Haase, W. *J. Chem. Soc., Chem. Commun.* **1988**, 1145.
(293) Bossek, U.; Weyhermüller, T.; Wieghardt, K.; Nuber, B.; Weiss, J. *J. Am. Chem. Soc.* **1990**, *112*, 6387.
(294) Li, X.; Kessissoglou, D. P.; Kirk, M. L.; Pecoraro, V. L.; Bender, C. J. *Inorg. Chem.* **1988**, *27*, 1.
(295) Kessissoglou, D. P. *Coord. Chem. Rev.* **1999**, *185−186*, 837.
(296) Bhula, R.; Gainsford, G. J.; Weatherburn, D. C. *J. Am. Chem. Soc.* **1988**, *110*, 7550.
(297) Delfs, C. D.; Stranger, R. *Inorg. Chem.* **2003**, *42*, 2495.
(298) Kessissoglou, D. P.; Kirk, M. L.; Lah, M. S.; Li, X.; Raptopoulou, C.; Hatfield, W. E.; Pecoraro, V. L. *Inorg. Chem.* **1992**, *31*, 5424.
(299) Tangoulis, V.; Malamatari, D. A.; Soulti, K.; Stergiou, V.; Raptopoulou, C. P.; Terzis, A.; Kabanos, T. A.; Kessissoglou, D. P. *Inorg. Chem.* **1996**, *35*, 4974.
(300) Tangoulis, V.; Malamatari, D. A.; Spyroulias, G. A.; Raptopoulou, C. P.; Terzis, A.; Kessissoglou, D. P. *Inorg. Chem.* **2000**, *39*, 2621.

(301) Hirotsu, M.; Kojima, M.; Yoshikawa, Y. *Bull. Chem. Soc. Jpn.* **1997**, *70*, 649.
(302) Hirotsu, M.; Kojima, M.; Mori, W.; Yoshikawa, Y. *Bull. Chem. Soc. Jpn.* **1998**, *71*, 2873.
(303) Kitajima, N.; Osawa, M.; Imai, S.; Fujisawa, K.; Moro-oka, Y.; Heerwegh, K.; Reed, C. A.; Boyd, P. D. W. *Inorg. Chem.* **1994**, *33*, 4613.
(304) Hirotsu, M.; Aoyagi, M.; Kojima, M.; Mori, W.; Yoshikawa, Y. *Bull. Chem. Soc. Jpn.* **2002**, *75*, 259.
(305) Yano, S.; Doi, M.; Tamakoshi, S.; Mori, W.; Mikuriya, M.; Ichimura, A.; Kinoshita, I.; Yamamoto, Y.; Tanase, T. *Chem. Commun.* **1997**, 997.
(306) Tanase, T.; Tamakoshi, S.; Doi, M.; Mikuriya, M.; Sakurai, H.; Yano, S. *Inorg. Chem.* **2000**, *39*, 692.
(307) Price, D. J.; Batten, S. R.; Berry, K. J.; Moubaraki, B.; Murray, K. S. *Polyhedron* **2003**, *22*, 165.
(308) Robin, M. B.; Day, P. *Adv. Inorg. Chem. Radiochem.* **1967**, *10*, 247.
(309) Yoshino, A.; Miyagi, T.; Asato, E.; Mikuriya, M.; Sakata, Y.; Sugiura, K.-i.; Iwasaki, K.; Hino, S. *Chem. Commun.* **2000**, 1475.
(310) Alexiou, M.; Dendrinou-Samara, C.; Karagianni, A.; Biswas, S.; Zaleski, C. M.; Kampf, J.; Yoder, D.; Penner-Hahn, J. E.; Pecoraro, V. L.; Kessissoglou, D. P. *Inorg. Chem.* **2003**, *42*, 2185.
(311) Afrati, T.; Dendrinou-Samara, C.; Raptopoulou, C. P.; Terzis, A.; Tangoulis, V.; Kessissoglou, D. P. *Angew. Chem., Int. Ed.* **2002**, *41*, 2148.
(312) Bhaduri, S.; Pink, M.; Christou, G. *Chem. Commun.* **2002**, 2352.
(313) Auger, N.; Girerd, J.-J.; Corbella, M.; Gleizes, A.; Zimmermann, J. L. *J. Am. Chem. Soc.* **1990**, *112*, 448.
(314) Sarneski, J. E.; Thorp, H. H.; Brudvig, G. W.; Crabtree, R. H.; Schulte, G. K. *J. Am. Chem. Soc.* **1990**, *112*, 7255.
(315) Reddy, K. R.; Rajasekharan, M. V.; Arulsamy, N.; Hodgson, D. J. *Inorg. Chem.* **1996**, *35*, 2283.
(316) Vincent, J. B.; Christou, G. *Adv. Inorg. Chem.* **1989**, *33*, 197.
(317) Ponomarev, V. I.; Atovmyan, L. O.; Bobkova, S. A.; Turté, K. I. *Dokl. Akad. Nauk SSSR* **1984**, *274*, 368.
(318) Armstrong, W. H.; Roth, M. E.; Lippard, S. J. *J. Am. Chem. Soc.* **1987**, *109*, 6318.
(319) Gorun, S. M.; Lippard, S. J. *Inorg. Chem.* **1988**, *27*, 149.
(320) Libby, E.; McCusker, J. K.; Schmitt, E. A.; Folting, K.; Hendrickson, D. N.; Christou, G. *Inorg. Chem.* **1991**, *30*, 3486.
(321) Wang, S.; Folting, K.; Streib, W. E.; Schmitt, E. A.; McCusker, J. K.; Hendrickson, D. N.; Christou, G. *Angew. Chem.* **1991**, *103*, 314.
(322) Libby, E.; Folting, K.; Huffman, C. J.; Huffman, J. C.; Christou, G. *Inorg. Chem.* **1993**, *32*, 2549.
(323) Wang, S.; Tsai, H.-L.; Folting, K.; Martin, J. D.; Hendrickson, D. N.; Christou, G. *J. Chem. Soc., Chem. Commun.* **1994**, 671.
(324) Wemple, M. W.; Coggin, D. K.; Vincent, J. B.; McCusker, J. K.; Strieb, W. E.; Huffman, J. C.; Hendrickson, D. N.; Christou, G. *J. Chem. Soc., Dalton Trans.* **1998**, 719.
(325) Cañada-Vilalta, C.; Huffman, J. C.; Christou, G. *Polyhedron* **2001**, *20*, 1785.
(326) Bouwman, E.; Bolcar, M. A.; Libby, E.; Huffman, J. C.; Folting, K.; Christou, G. *Inorg. Chem.* **1992**, *31*, 5185.
(327) Boskovic, C.; Folting, K.; Christou, G. *Polyhedron* **2000**, *19*, 2111.
(328) Pistilli, J.; Beer, R. H. *Inorg. Chem. Commun.* **2002**, *5*, 206.
(329) Kulawiec, R. J.; Crabtree, R. H.; Brudvig, G. W.; Schulte, G. K. *Inorg. Chem.* **1988**, *27*, 1309.
(330) Mikuriya, M.; Yamato, Y.; Tokii, T. *Chem. Lett.* **1991**, 1429.
(331) Mikuriya, M.; Yamato, Y.; Tokii, T. *Bull. Chem. Soc. Jpn.* **1992**, *65*, 2624.
(332) Chandra, S. K.; Chakravorty, A. *Inorg. Chem.* **1991**, *30*, 3795.
(333) Grillo, V. A.; Knapp, M. J.; Bollinger, J. C.; Hendrickson, D. N.; Christou, G. *Angew. Chem., Int. Ed. Engl.* **1996**, *35*, 1818.
(334) Sañudo, E. C.; Grillo, V. A.; Knapp, M. J.; Bollinger, J. C.; Huffman, J. C.; Hendrickson, D. N.; Christou, G. *Inorg. Chem.* **2002**, *41*, 2441.
(335) Christou, G. *Acc. Chem. Res.* **1989**, *22*, 328.
(336) Bashkin, J. S.; Chang, H. R.; Streib, W. E.; Huffman, J. C.; Hendrickson, D. N.; Christou, G. *J. Am. Chem. Soc.* **1987**, *109*, 6502.
(337) Hendrickson, D. N.; Christou, G.; Schmitt, E. A.; Libby, E.; Bashkin, J. S.; Wang, S.; Tsai, H.-L.; Vincent, J. B.; Boyd, P. D. W.; et al. *J. Am. Chem. Soc.* **1992**, *114*, 2455.
(338) Wang, S.; Tsai, H.-L.; Libby, E.; Folting, K.; Streib, W. E.; Hendrickson, D. N.; Christou, G. *Inorg. Chem.* **1996**, *35*, 7578.
(339) Wemple, M. W.; Adams, D. M.; Folting, K.; Hendrickson, D. N.; Christou, G. *J. Am. Chem. Soc.* **1995**, *117*, 7275.
(340) Aromí, G.; Wemple, M. W.; Aubin, S. J.; Folting, K.; Hendrickson, D. N.; Christou, G. *J. Am. Chem. Soc.* **1998**, *120*, 5850.
(341) Wemple, M. W.; Adams, D. M.; Hagen, K. S.; Folting, K.; Hendrickson, D. N.; Christou, G. *J. Chem. Soc., Chem. Commun.* **1995**, 1591.
(342) Wang, S.; Tsai, H.-L.; Streib, W. E.; Christou, G.; Hendrickson, D. N. *J. Chem. Soc., Chem. Commun.* **1992**, 1427.
(343) Aubin, S. M. J.; Dilley, N. R.; Wemple, M. W.; Maple, M. B.; Christou, G.; Hendrickson, D. N. *J. Am. Chem. Soc.* **1998**, *120*, 839.
(344) Cinco, R. M.; Rompel, A.; Visser, H.; Aromí, G.; Christou, G.; Sauer, K.; Klein, M. P.; Yachandra, V. K. *Inorg. Chem.* **1999**, *38*, 5988.
(345) Ruettinger, W. F.; Campana, C.; Dismukes, G. C. *J. Am. Chem. Soc.* **1997**, *119*, 6670.
(346) Ruettinger, W. F.; Ho, D. M.; Dismukes, G. C. *Inorg. Chem.* **1999**, *38*, 1036.
(347) Ruettinger, W. F.; Dismukes, G. C. *Inorg. Chem.* **2000**, *39*, 1021.
(348) Carrell, T. G.; Bourles, E.; Lin, M.; Dismukes, G. C. *Inorg. Chem.* **2003**, *42*, 2849.
(349) Maneiro, M.; Ruettinger, W. F.; Bourles, E.; McLendon, G. L.; Dismukes, G. C. *Proc. Natl. Acad. Sci. U.S.A.* **2003**, *100*, 3707.
(350) Ruettinger, W.; Yagi, M.; Wolf, K.; Bernasek, S.; Dismukes, G. C. *J. Am. Chem. Soc.* **2000**, *122*, 10353.
(351) Yagi, M.; Wolf, K. V.; Baesjou, P. J.; Bernasek, S. L.; Dismukes, G. C. *Angew. Chem., Int. Ed.* **2001**, *40*, 2925.
(352) Wieghardt, K.; Bossek, U.; Gebert, W. *Angew. Chem.* **1983**, *95*, 320.
(353) Dubé, C. E.; Wright, D. W.; Armstrong, W. H. *J. Am. Chem. Soc.* **1996**, *118*, 10910.
(354) Sivaraja, M.; Philo, J. S.; Lary, J.; Dismukes, G. C. *J. Am. Chem. Soc.* **1989**, *111*, 3221.
(355) Baumgarten, M.; Philo, J. S.; Dismukes, G. C. *Biochemistry* **1990**, *29*, 10814.
(356) Dubé, C. E.; Sessoli, R.; Hendrich, M. P.; Gatteschi, D.; Armstrong, W. H. *J. Am. Chem. Soc.* **1999**, *121*, 3537.
(357) Philouze, C.; Blondin, G.; Ménage, S.; Auger, N.; Girerd, J.-J.; Vigner, D.; Lance, M.; Nierlich, M. *Angew. Chem.* **1992**, *104*, 1634.
(358) Dave, B. C.; Czernuszewicz, R. S. *New J. Chem.* **1994**, *18*, 149.
(359) Dunand-Sauthier, M.-N. C.; Deronzier, A.; Piron, A.; Pradon, X.; Ménage, S. *J. Am. Chem. Soc.* **1998**, *120*, 5373.
(360) Philouze, C.; Blondin, G.; Girerd, J.-J.; Guilhem, J.; Pascard, C.; Lexa, D. *J. Am. Chem. Soc.* **1994**, *116*, 8557.
(361) Blondin, G.; Davydov, R.; Philouze, C.; Charlot, M.-F.; Styring, T.; Akermark, B.; Girerd, J.-J.; Boussac, A. *J. Chem. Soc., Dalton Trans.* **1997**, 4069.
(362) Chan, M. K.; Armstrong, W. H. *J. Am. Chem. Soc.* **1989**, *111*, 9121.
(363) Suzuki, M.; Sugisawa, T.; Senda, H.; Oshio, H.; Uehara, A. *Chem. Lett.* **1989**, 1091.
(364) Suzuki, M.; Senda, H.; Suenaga, M.; Sugisawa, T.; Uehara, A. *Chem. Lett.* **1990**, 923.
(365) Chan, M. K.; Armstrong, W. H. *J. Am. Chem. Soc.* **1991**, *113*, 5055.
(366) Kirk, M. L.; Chan, M. K.; Armstrong, W. H.; Solomon, E. I. *J. Am. Chem. Soc.* **1992**, *114*, 10432.
(367) Suzuki, M.; Hayashi, Y.; Munezawa, K.; Suenaga, M.; Senda, H.; Uehara, A. *Chem. Lett.* **1991**, 1929.
(368) Kawasaki, H.; Kusunoki, M.; Hayashi, Y.; Suzuki, M.; Munezawa, K.; Suenaga, M.; Senda, H.; Uehara, A. *Bull. Chem. Soc. Jpn.* **1994**, *67*, 1310.
(369) Stibrany, R. T.; Gorun, S. M. *Angew. Chem.* **1990**, *102*, 1195.
(370) Gorun, S. M.; Stibrany, R. T.; Lillo, A. *Inorg. Chem.* **1998**, *37*, 836.
(371) Wu, A. J.; Penner-Hahn, J. E.; Pecoraro, V. L. *Chem. Rev.* **2004**, *104*, 903.
(372) McKee, V.; Tandon, S. S. *J. Chem. Soc., Chem. Commun.* **1988**, 1334.
(373) McCrea, J.; McKee, V.; Metcalfe, T.; Tandon, S. S.; Wikaira, J. *Inorg. Chim. Acta* **2000**, *297*, 220.
(374) Krishtalik, L. I. *Bioelectrochem. Bioenerg.* **1990**, *23*, 249.
(375) McGrady, J. E.; Stranger, R. *J. Am. Chem. Soc.* **1997**, *119*, 8512.
(376) McGrady, J. E.; Stranger, R. *Inorg. Chem.* **1999**, *38*, 550.
(377) Delfs, C. D.; Stranger, R. *Inorg. Chem.* **2000**, *39*, 491.
(378) Delfs, C. D.; Stranger, R. *Inorg. Chem.* **2001**, *40*, 3061.
(379) Zhao, X. G.; Richardson, W. H.; Chen, J. L.; Li, J.; Noodleman, L.; Tsai, H. L.; Hendrickson, D. N. *Inorg. Chem.* **1997**, *36*, 1198.
(380) Aullón, G.; Ruiz, E.; Alvarez, S. *Chem.—Eur. J.* **2002**, *8*, 2508.
(381) Proserpio, D. M.; Hoffmann, R.; Dismukes, G. C. *J. Am. Chem. Soc.* **1992**, *114*, 4374.
(382) Proserpio, D. M.; Rappé, A. K.; Gorun, S. M. *Inorg. Chim. Acta* **1993**, *213*, 319.
(383) Himo, F.; Siegbahn, P. E. M. *Chem. Rev.* **2003**, *103*, 2421.
(384) Yachandra, V. K.; Klein, M. P. *Adv. Photosynth.* **1996**, *3*, 337.
(385) Yagi, M.; Kaneko, M. *Chem. Rev.* **2001**, *101*, 21.
(386) Shafirovich, V. Y.; Shilov, A. E. *Kinet. Katal.* **1979**, *20*, 1156.
(387) Knerel'man, E. I.; Luneva, N. P.; Shafirovich, V. Y.; Shilov, A. E. *Kinet. Katal.* **1988**, *29*, 1350.
(388) Luneva, N. P.; Knerel'man, E. I.; Shafirovich, V. Y.; Shilov, A. E. *J. Chem. Soc., Chem. Commun.* **1987**, 1504.
(389) Ramaraj, R.; Kira, A.; Kaneko, M. *Chem. Lett.* **1987**, 261.
(390) Calvin, M. *Science* **1974**, *184*, 375.
(391) Cooper, S. R.; Calvin, M. *Science* **1974**, *185*, 376.
(392) Matsushita, T.; Fujiwara, M.; Shono, T. *Chem. Lett.* **1981**, 631.

(393) Fujiwara, M.; Matsushita, T.; Shono, T. *Polyhedron* **1985**, *4*, 1895.
(394) Matsushita, T.; Spencer, L.; Sawyer, D. T. *Inorg. Chem.* **1988**, *27*, 1167.
(395) Naruta, Y.; Sasayama, M.-a.; Sadaki, T. *Angew. Chem.* **1994**, *106*, 1964.
(396) Gersten, S. W.; Samuels, G. J.; Meyer, T. J. *J. Am. Chem. Soc.* **1982**, *104*, 4029.
(397) Gilbert, J. A.; Eggleston, D. S.; Murphy, W. R., Jr.; Geselowitz, D. A.; Gersten, S. W.; Hodgson, D. J.; Meyer, T. J. *J. Am. Chem. Soc.* **1985**, *107*, 3855.
(398) Raven, S. J.; Meyer, T. J. *Inorg. Chem.* **1988**, *27*, 4478.
(399) Geselowitz, D.; Meyer, T. J. *Inorg. Chem.* **1990**, *29*, 3894.
(400) Chronister, C. W.; Binstead, R. A.; Ni, J.; Meyer, T. J. *Inorg. Chem.* **1997**, *36*, 3814.
(401) Schoonover, J. R.; Ni, J.; Roecker, L.; White, P. S.; Meyer, T. J. *Inorg. Chem.* **1996**, *35*, 5885.
(402) Limburg, J.; Brudvig, G. W.; Crabtree, R. H. *J. Am. Chem. Soc.* **1997**, *119*, 2761.
(403) Groves, J. T.; Lee, J.; Marla, S. S. *J. Am. Chem. Soc.* **1997**, *119*, 6269.
(404) Collins, T. J.; Gordon-Wylie, S. W. *J. Am. Chem. Soc.* **1989**, *111*, 4511.
(405) MacDonnell, F. M.; Fackler, N. L. P.; Stern, C.; O'Halloran, T. V. *J. Am. Chem. Soc.* **1994**, *116*, 7431.
(406) Limburg, J.; Vrettos, J. S.; Chen, H.; de Paula, J. C.; Crabtree, R. H.; Brudvig, G. W. *J. Am. Chem. Soc.* **2001**, *123*, 423.
(407) Lundberg, M.; Blomberg, M. R. A.; Siegbahn, P. E. M. *Inorg. Chem.* **2004**, *43*, 264.
(408) Tasiopoulos, A. J.; Abboud, K. A.; Christou, G. *Chem. Commun.* **2003**, 580.
(409) Goodson, P. A.; Hodgson, D. J.; Michelsen, K. *Inorg. Chim. Acta* **1990**, *172*, 49.
(410) Gohdes, J. W. Ph.D. Dissertation, University of California, Berkeley, 1991.

CR0206014